EXPERIMENTAL AND THEORETICAL STUDY ON STABILITY OF HIGH EXPANSION FOAM USED FOR LNG VAPOR RISK MITIGATION

A Dissertation

by

PRATIK KRISHNAN

Submitted to the Office of Graduate and Professional Studies of
Texas A&M University
in partial fulfillment of the requirements for the degree of

DOCTOR OF PHILOSOPHY

Chair of Committee,	Zhengdong Cheng
Co-Chair of Committee,	Mahmoud El-Halwagi
Committee Members,	Nagamangala Anand
	Hung-Jen Wu
Head of Department,	M. Nazmul Karim

May 2019

Major Subject: Chemical Engineering

ABSTRACT

Liquefaction of natural gas is an effective way to easily store and transport natural gas. A spill of liquefied natural gas (LNG) can result in the formation of a vapor cloud, which can migrate downwind near the ground because of a density greater than air. This cloud has the potential to ignite, and presents an asphyxiation hazard as well. The National Fire Protection Association (NFPA) recommends the use of high expansion (HEX) foam to mitigate the vapor risk due to cryogenic LNG.

This dissertation studies the effects of forced convection and thermal radiation on HEX foam breakage. A lab-scale foam generator was used to produce HEX foam and carry out experiments to evaluate the rate of foam breakage, the amount of liquid drained from foam, the vaporization rate of the cryogenic liquid, and the temperature profile in the foam. In addition, zirconium phosphate (ZrP) nanoplates were utilized to improve the stability of HEX foam. A heat transfer model was also developed to estimate HEX foam height that should be applied.

The results indicated that forced convection and thermal radiation can significantly affect foam breakage rates. Therefore, accounting for these effects provides a better estimate for the amount of foam that needs to be applied for effective vapor risk mitigation. Nanoplates could be used to improve HEX foam stability and showed lower foam breakage rates. The heat transfer model predicted the height of the HEX foam that needs to be applied for outgoing vapors to be neutrally buoyant.

DEDICATION

To my immediate family, for their encouragement and support,

To Sweta, Attai, Prabha chitti and family, for being there for me during difficult times,

To Fara, Jerry and Connor, for including me in their family and making me feel loved,

To Purvali, for being such an amazing friend,

And most of all, To Cort, for constant support and patience, we finally did it!

ACKNOWLEDGEMENTS

I would like to express sincere gratitude to Dr. Sam Mannan for providing guidance and support through my research. I would also like to thank my committee chair Dr. Zhengdong Cheng for collaborating on this research work and providing insightful comments, Dr. Mahmoud El-Halwagi for serving on my committee as co-chair, and other committee members, Dr. Hung-Jen Wu for helping me through my Masters research and serving on this committee, and Dr. N.K. Anand for teaching me the fundamentals of CFD and taking time to serve on this committee.

I would also like to express thanks to Anas Al-Rabbat for help performing my experiments, exfoliating the nanoplates as well as with the image analysis and Dr. Bin Zhang who gave some input for designing the experiments. I would also like to thank Dali Huang for help with performing some experiments as well as Lecheng Zhang and Minxiang Zeng for help with exfoliating the nanoplates. I would also like to recognize my friends and colleagues at the MKOPSC and the staff for making my time at Texas A&M University a great experience. I would also like to thank my family for their patience and support.

CONTRIBUTORS AND FUNDING SOURCES

This work was supported by Dr. Sam Mannan and a dissertation committee consisting of Dr. Zhengdong Cheng, Dr. Mahmoud El-Halwagi, and Dr. Hung-Jen Wu of the Department of Chemical Engineering and Dr. N.K. Anand of the Department of Mechanical Engineering.

The experiments performed towards this research were designed, and conceptualized by Pratik Krishnan, with some input from Dr. Bin Zhang. As the equipment was bulky, all experiments were performed jointly by Pratik Krishnan and Anas Al-Rabbat under the guidance of Dr. Sam Mannan and Dr. Zhengdong Cheng of the Department of Chemical Engineering. In addition, the experiments with liquid nitrogen require two students for safety (possibility of asphyxiation), in case there is any incident, as highlighted in our Project Safety Analysis (PSA). The data was primarily analyzed by Pratik Krishnan and the image analysis was done by Anas Al-Rabbat. All other work conducted for the dissertation was completed by the student independently.

This work was sponsored by the Mary Kay O'Connor Process Safety Center, Texas A&M University.

NOMENCLATURE

BLEVE	Boiling Liquid Expanding Vapor Explosion
CEI	Chemical Explosion Index
CFD	Computational Fluid Dynamics
CFM	Cubic Feet per Minute
CMC	Critical Micelle Concentration
GC-MS	Gas Chromatography-Mass Spectrometry
GIS	Geographic Information System
HAZID	Hazard Identification
HEX	High Expansion
LFL/UFL	Lower/Upper Flammability Limit
LN_2	Liquid Nitrogen
LNG	Liquefied Natural Gas
LOPA	Layer of Protection Analysis
MKOPSC	Mary Kay O'Connor Process Safety Center
NFPA	National Fire Protection Association
NIH	National Institutes of Health
SEM	Scanning Electron Microscopy
SIMPLE	Semi-Implicit Method for Pressure Linked Equations
TBA	Tetrabutylammonium hydroxide
TEM	Transmission Electron Microscopy
ZrP	Zirconium Phosphate

TABLE OF CONTENTS

Page

LIST OF FIGURES

Page

LIST OF TABLES

Page

1 INTRODUCTION*

1.1 Background

The Unites States Energy Information Administration (US EIA) estimates that natural gas consumption will increase by nearly 40 percent over the next few decades. This is primarily because it is a cleaner source of energy compared to oil or coal and produces lower amounts of carbon dioxide, sulfur oxide and nitrogen oxide per unit of energy produced, as seen in Figure 1 [1-3]. This has been aided by advances in fracking technology, which have enabled its extraction from shale reserves previously considered as economically infeasible [4].

In 2015, EIA reported that over 40% of the electric power capability was provided by natural gas [3]. Contributions by different energy sources to meet the electric power demand may be seen in Figure 2. The amount of power produced by natural gas has been consistently increasing since 1996.

*Parts of this section have been reprinted with permission from: "Improving the stability of HEX foam used for LNG vapor risk mitigation using exfoliated zirconium phosphate nanoplates", Krishnan, P., Al-Rabbat, A., Zhang, B., Huang, D., Zhang, L., Zeng, M., Mannan, M.S., Cheng, Z., 2019, Process Safety and Environmental Protection, 123, 48-58, Copyright 2019 by Krishnan *et al.* [5] and "Effects of forced convection and thermal radiation on HEX foam used for LNG vapor risk mitigation", Krishnan, P., Zhang, B., Al-Rabbat, A., Cheng Z., Mannan, M.S., Journal of Loss Prevention in Process Industries, 2018, 55, 423-436, Copyright 2018 by Krishnan *et al.* [6]

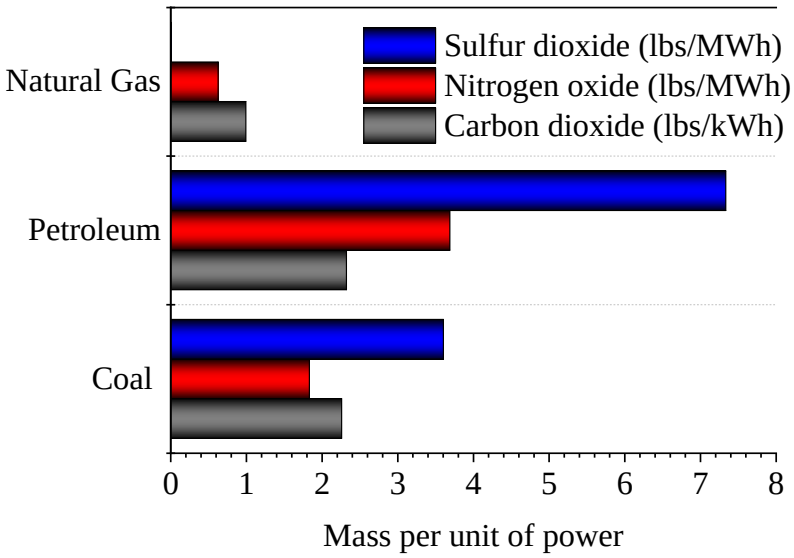

Figure 1: Comparison of carbon dioxide, sulfur dioxide and nitrogen oxide emissions due to electric power generation from natural gas, coal and petroleum

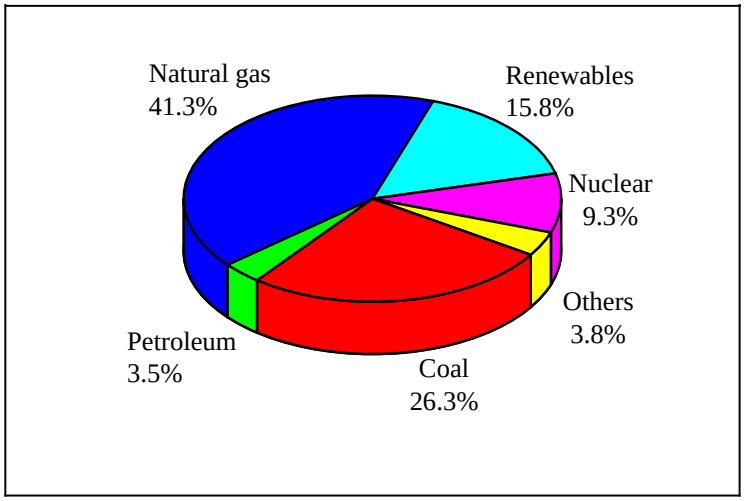

Figure 2: Electric power industry capability by energy source in the US in 2015

Pipelines may not always be the best form of transportation of natural gas, especially over long distances [1]. Liquefaction of natural gas can be an effective way of storing and transporting it because its volume is nearly 600 times lower in its liquid form. Exports of liquefied natural gas (LNG) from the US are expected to increase in the future, as shown in Figure 3 [1].

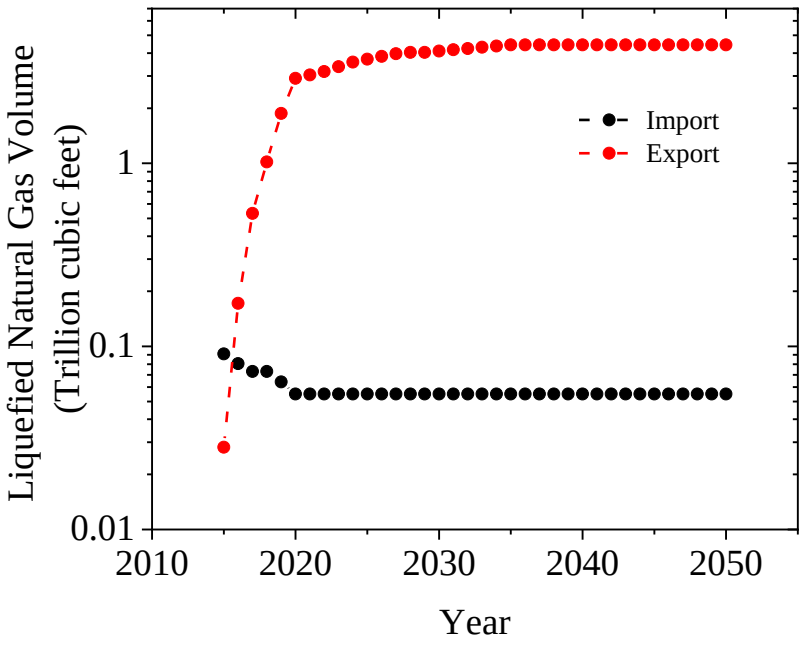

Figure 3: Projected increase in the import and export of LNG from the US

1.2 LNG properties and hazards

1.2.1 Properties of LNG

Liquefied natural gas (LNG) is a cryogenic liquid condensed from natural gas. Natural gas is mainly composed of methane with small quantities of lighter hydrocarbons including ethane, propane and butane [7]. Table 2 summarizes some of the key properties of methane, which is the principal component of natural gas. The boiling point of LNG is nearly -160 ^{o}C and varies depending on its composition. This low boiling point makes it a cryogenic liquid. It is clear from Table 1 that the density of methane at 20 ^{o}C is nearly 600 times the density of liquid methane. This property allows ease of storage and transportation of large quantities of natural gas when converted to its liquid form. When LNG vapor concentration is between 5 to 15%, it may be flammable. It should be noted that this depends on the composition of the vapors.

Table 1: Important properties of Methane [7-9]

Salient properties of Methane	
Molecular weight	16
Boiling Point (^{o}C)	-161.5
Density of liquid at boiling point (kg/m^3)	422.5
Density of vapor at boiling point (kg/m^3)	1.81
Density of vapor at 20 ^{o}C (kg/m^3)	0.67
Heat of combustion (MJ/kg)	50
LFL-UFL	5-15%
Latent heat of vaporization (kJ/kg)	509.5
Heat capacity of gas at 0 ^{o}C (kJ/m^3 K)	1.52
Specific heat at constant pressure (kJ/kg K)	2.2

1.2.2 LNG hazards

While some of the properties of LNG make it useful, they also present a potential to cause harm. Therefore, hazards of LNG must be well understood. Several possible hazards are briefly summarized here [7, 10].

Freeze burns

As the boiling point of LNG is very low, it is considered to be a cryogenic liquid. Therefore, any direct contact with a leak of LNG or pool can result in a freeze burn [11].

Asphyxiation hazard

If an LNG spill occurs, its cryogenic nature causes it to expand and convert to its vapor form. These LNG vapors may act as a simple asphyxiant displacing oxygen, reducing its concentration and potentially presenting danger to personnel [12].

Jet fire

A jet fire generally occurs when liquid leaks under pressure and catches fire. They may produce extremely large heat fluxes but typically have shorter ranges (<50 m) [7]. Therefore, it is a greater threat to plant personnel but not the public. If leaked liquid turns into vapor on leaving a hole, without forming a pool, immediate ignition causes jet fires while delayed ignition may result in a flash fire or explosion [13].

Flash fire

A flash fire generally lasts for a short duration, generally in the order of tens of seconds. It can be dangerous for people in the vicinity of the fire but the radiative heat reaching nearby objects is unlikely to be high [14].

Pool fire

A pool fire occurs when a pool of LNG catches fire. Larger fires may be smoky. LNG pool fires may pose the highest hazard in case of an LNG spill [7]. Their effects are generally localized but tend to last longer. During the release of LNG, immediate ignition results in a pool fire [15]. If the some of it has vaporized, a flash fire occurs which spreads to the pool causing a pool fire.

BLEVE

BLEVE is an abbreviation for boiling liquid expanding vapor explosion. In case a vessel containing flammable liquid is exposed to fire, the liquid in the vessel vaporizes, increasing the pressure. The liquid may eventually stop vaporizing due to an increased vapor pressure but its temperature continues to rise. The high temperature may compromise the structural integrity of the vessel. If the vessel ruptures, the liquid under high pressure and temperature is suddenly exposed to atmospheric pressure. This causes the rupture to be catastrophic, resulting in a BLEVE [16]. This scenario is generally neglected for LNG as hydrocarbon tanks remain at atmospheric pressure during a fire [7].

Fire ball

Fire balls are approximately spherical in shape and occur due to burning vapor that rises or flashing liquid [17]. The released vapor is dominated by buoyancy forces rather than momentum forces involved for BLEVEs resulting in lower durations for an incident [7].

Vapor Cloud Explosions (VCE)

An LNG leak absorbs heat from its surroundings and evaporates because of its cryogenic nature [18]. This vapor can mix with air and disperse. As the density of cold LNG vapors is greater than air, it behaves as a dense gas. This mixture disperses over time and can ignite. The flame may travel to the source through the vapor [7]. There are two broad classifications of VCEs: Deflagrations and Detonations. Deflagrations occur when the flame propagates through the unreacted fuel-air mixture at velocities lower than the speed of sound while detonations involve flame propagation at supersonic velocities [19]. Detonations are generally violent and can cause significant damage. While detonations generally require high energy ignition sources, it is possible for deflagrations to transition into detonations. Deflagrations depend on the fuel reactivity, congestion and confinement and lower peak overpressures when compared to detonations. As methane is classified as a fuel with low reactivity, detonations are considered to be uncommon, especially when congestion is low.

Rapid Phase Transition (RPT)

When LNG leaks over water or a warmer fluid, it can explode due to very fast evaporation to its vapor phase even without ignition. RPTs occur because of the cryogenic nature of LNG, which is vaporized when it comes in contact with warmer fluids such as water. The sudden evolution of vapor creates localized overpressures [20]. The occurrence of RPTs depends on the temperature of the fluid, penetration depth and composition [7].

Rollover

Rollover occurs when layers of different densities and heat capacities suddenly mix inside an LNG tank. This may happen when LNG of different compositions are mixed causing stratification [21]. When the lower layer heats up and becomes lighter or a heavier layer is added on top of a light layer. Hydrostatic pressure of the upper layer can inhibit evaporation of lighter components from the lower layer which then becomes warmer and less dense. Over time, the densities come closer together, making the interface unstable causing sudden mixing. The process of rapid mixing results in heat exchange generating a large amount of vapor, which suddenly increases pressure, which may cause sudden discharge from valves or vents.

1.3 LNG incidents

Despite its advantages, a leak of liquefied natural gas (LNG) can result in the formation of a vapor cloud which can migrate downwind near ground level, exhibiting dense gas behavior as the density of methane at low temperatures is higher than atmospheric air. This vapor cloud presents the danger of asphyxiation to any population in its vicinity and also has the potential to ignite.

There are several documented instances of LNG-related incidents, which are summarized in Table 2 [22-26]. An incident in 2004 at an LNG facility in Skikda, Algeria claimed 27 lives and resulted in over 70 injuries [27]. Another incident occurred in Plymouth, Washington, in 2014, in which an LNG tank was pierced by debris and resulted in an LNG leak and injured 5 workers [28, 29].

Table 2: List of select LNG-related incidents and their consequences (Reprinted with permission from [6])

Ship / Facility Name	Location	Year	Effect on human life
East Ohio Gas LNG Tank	Cleveland, OH	1944	128-133 deaths
LNG Import Facility	Canvey Island, UK	1965	1 person burned
LNG export facility	Arzew, Algeria	1977	1 worker frozen to death
Columbia Gas LNG import	Cove Point, MD	1979	1 killed, 1 injured
LNG export facility	Bontang, Indonesia	1983	3 workers died
Skikda I	Algeria	2004	27 killed, 72-74 injured
Atlantic LNG (Train 2)	Port Fortin, Trinidad	2006	1 person injured
LNG Facility	Plymouth, WA	2014	5 workers injured

1.4 HEX foam for LNG risk mitigation

The National Fire Protection Association suggests the use of high expansion (HEX) foam to mitigate the vapor risk of an LNG spill [30]. HEX foam forms a vapor barrier containing the hazardous cryogen. In case there is a fire, the bubbles will help suffocate the flames and prevent re-ignition [31]. HEX foam is also gaining more attention as they tend to be biodegradable, making them environment friendly [32, 33].

In case of an LNG spill, as LNG is a cryogenic liquid, it absorbs heat from the surroundings and forms a vapor cloud. There are multiple heat transfer mechanisms involved including conduction from the ground, convection due to wind and radiation from the sun or potential fires which can affect the rate of LNG vaporization. These are depicted in Figure 4. Application of HEX foam helps block the heat due to convection and thermal radiation. This is called the “blocking effect” of foam [34]. Due to gravity, liquid from the foam drains and may contribute to additional vaporization of LNG. This is called as the “boil-off effect” of the foam and is significant immediately after foam application, before an ice layer is formed [35]. These two effects may be combined together and called as the “blanketing effect” of foam which determines the net vaporization rate of LNG [34]. As the vapors of LNG pass through the foam layers, they exchange heat and become warmer reducing their density. This is known as the “warming effect” of foam and allows for ease of dispersion of LNG vapors [9].

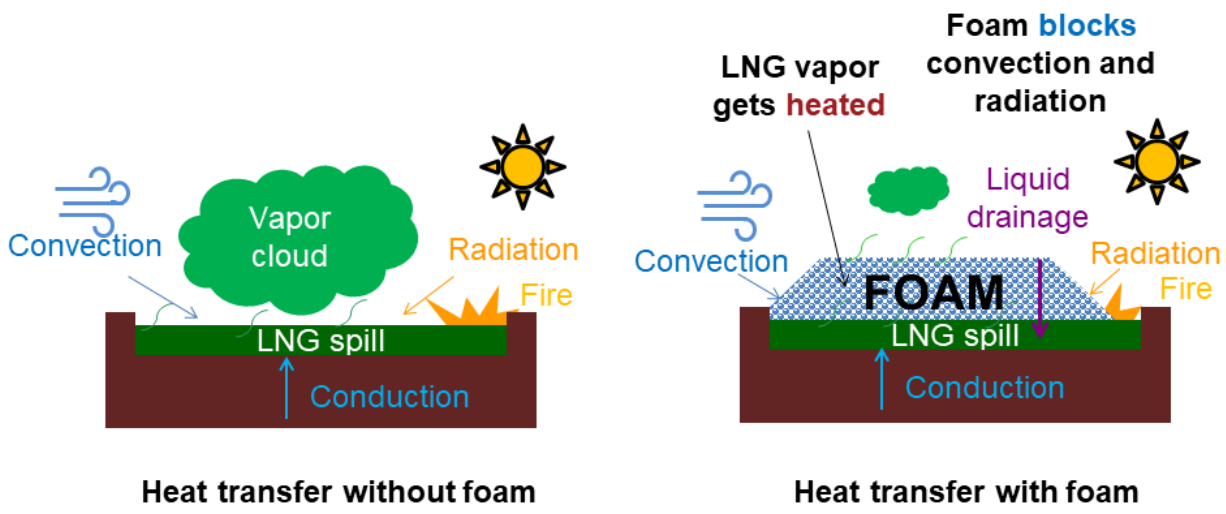

Figure 4: Heat transfer mechanisms involved during foam application

While foam can block convection and thermal radiation, these heat transfer mechanisms can ameliorate foam breakage, altering the amount of foam that needs to be applied to ensure effective vapor dispersal. They may also affect the liquid drained from foam, which contributes to LNG vaporization.

Zhang *et al.* performed experiments to study the effectiveness of foam in shielding a cryogenic liquid (liquid nitrogen) pool from heat transfer due to forced convection and thermal radiation [34]. They estimated heat fluxes with and without foam for a spill of a cryogenic liquid. The values of heat fluxes were reported under forced convection (Wind speed = 1.8 ± 0.3 m/s) and thermal radiation (Radiation intensity = 170 ± 4 W/m^2).

Assuming that the same heat fluxes are present in the case of LNG, it is possible to calculate the mass of LNG vaporized with and without foam application. This helps in understanding the effectiveness of foam application on LNG. These values are extrapolated for different pool sizes and shown in Figure 5.

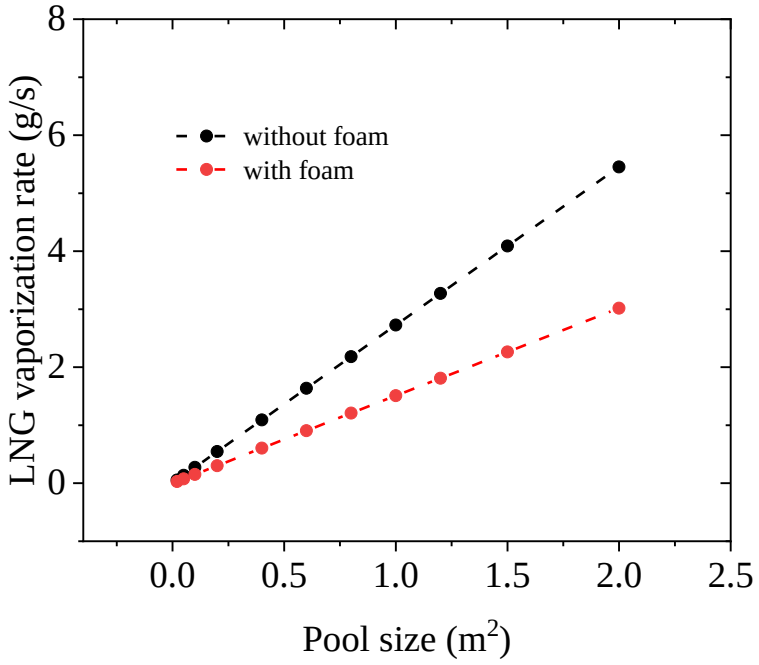

Figure 5: LNG vaporization rate for different pool sizes based on heat fluxes by Zhang *et al.* [34]

In addition, it is possible to estimate the hazard distance for each case based on the DOW's CEI [36]. This is illustrated in Figure 6.

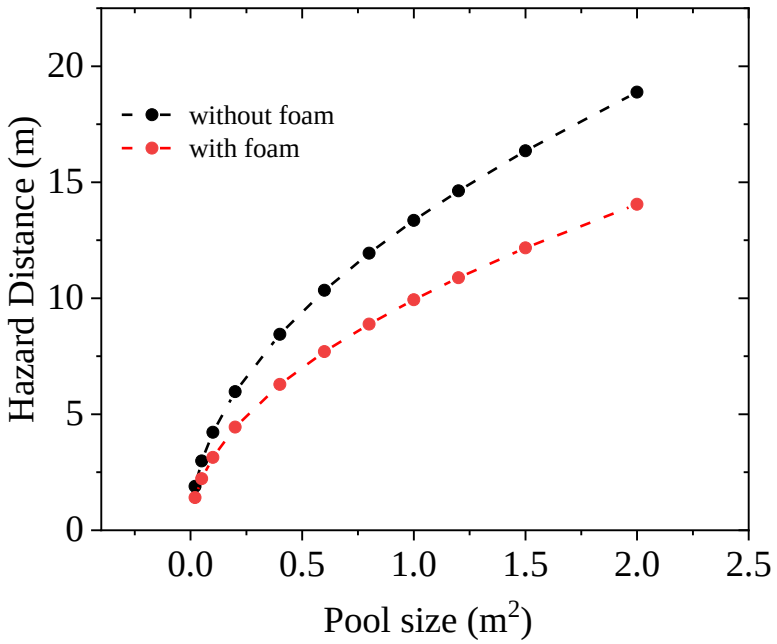

Figure 6: Hazard distance for different pool sizes based on heat fluxes by Zhang *et al.* [34]

It is clear from these plots that foam can reduce the vaporization rate of a cryogenic liquid and consequently the hazard distance. However, it should be noted that this is not the only reason foam is applied. Application of foam also helps in vapor dispersion, which reduces the downwind concentration by making the vapors more buoyant [37]. In case of an LNG fire, foam application also allows fire fighters to reduce the size of the fire as well as the radiative heat, allowing them to go near and extinguish it with dry chemical [10]. The effectiveness of foam application depends on the application rate and should be determined by experiments under controlled conditions [30].

1.5 LNG research overview

A comprehensive literature review was performed to identify gaps in previous LNG research and then establish the objectives. A brief overview has been provided here and includes some of the previous LNG research projects undertaken by the Mary Kay O'Connor Process Safety Center (MKOPSC) and of research specific to the use of high expansion (HEX) foam, especially for liquefied natural gas (LNG) vapor risk mitigation. This is followed by a review of some research studying HEX foam stability, research involving use of nanoparticles to improve foam stability, and research involving modeling of foam application on LNG.

1.5.1 LNG research at the MKOPSC

The Mary Kay O'Connor Process Safety Center (MKOPSC) at Texas A&M University has invested a significant amount of time and resources working in LNG research. LNG research topics include the release of LNG (loss of containment), pool spreading and vaporization of LNG, dispersion of LNG vapors, fire scenarios resulting from LNG release as well as mitigation techniques to reduce its vapor risk. A short summary of select research is provided here.

LNG release

The effects of release variables on potential consequences from LNG spillage were studied based on models from the Federal Energy Regulatory Commission (FERC) [38]. This study concluded that hole size and ullage pressure affect the pool size, spill duration and the dispersion process. Underwater release of LNG was studied to understand the underlying phenomena [39]. It was found that an underwater release of LNG results in the formation of buoyant vapor instead of a pool of LNG, even when the release depth is shallow.

LNG pool spreading

LNG pool spreading on land was modeled incorporating momentum, friction, and heat transfer effects [40]. This model was validated and found that in the early stages of pool development, momentum effects were dominant while the other effects became more significant later on.

LNG pool spreading on water and subsequent vaporization were studied by carrying out experiments [41]. The vaporization rate was found to be high initially and reduced once the pool stopped spreading.

LNG vaporization

Cryogenic liquid vaporization was studied by performing small- and medium-scale experiments using liquid nitrogen, a safer analog of LNG [42]. The study concluded that heat transfer from a concrete substrate to a liquid nitrogen pool could be characterized well using simple conduction models. It also showed that convection could play a significant role in cryogenic vaporization.

The influence of different heat transfer mechanisms including convection and radiation on cryogenic liquid vaporization rate was studied through experiments in the lab [43].
These experiments proved that forced convection can play a crucial role in determining the vaporization rate of the cryogenic liquid.

Cryogenic liquid vaporization on ice was studied through small-scale experiments using liquid nitrogen [44]. The vaporization mass flux was found to depend on the release rate of the cryogenic liquid and ice temperature and independent of amount of liquid spilled.

Film boiling was simulated using a Computational Fluid Dynamics (CFD) model, to estimate the vaporization rate of cryogenic liquids such as LNG in case of a spill [45]. This study may help researchers understand the physics of film boiling.

LNG vapor dispersion

A study of the most uncertain parameters in LNG source-term and dispersion modeling was carried out [46]. A case study including a general procedure considering the uncertainty in variables was demonstrated using fuzzy sets and Monte Carlo approaches. This approach showed better agreement with experiments than traditional methods.

A CFD software, ANSYS CFX® was employed to study LNG vapor dispersion to determine the exclusion zone in case of an LNG release [47]. The results were validated using medium-scale experiments which measured downwind gas concentrations.

CFD was also used to study several parameters such as release rate, pool shape and area, wind velocity and direction for LNG vapor dispersion [48]. This work also provided a methodology to evaluate LNG release over water and concrete.

Field experiments were performed to study the effects of foam application on LNG vapor dispersion [49]. The experimental results indicated that foam increased the temperature of the LNG vapors, thereby increasing their buoyancy.

The effects of obstacles on LNG vapor dispersion were studied using CFD [50]. It was shown that height, width and shape of the obstacles can play a key role in determining the vapor concentration.

LNG fire scenarios

Several outdoor experiments with LNG pool fires were conducted to determine profiles of radiant heat flux, fire height and their change with HEX foam application [51]. The results from this study show that expansion foam can be beneficial and reduce the flame height and radiant heat flux.

Radiative characteristics of LNG pool fires were studied using small-scale experiments and provided information on measurement of mass burning rates as well as use of correlations to predict the characteristics of an LNG pool fire [52]. These experiments showed that energy received on the liquid surface is entirely used for evaporation and is not transmitted to the surroundings.

Field experiments were performed to study the effectiveness of HEX foam in controlling an LNG pool fire [53]. It was found that foam controls the fire by blanketing the pool fire, thereby reducing radiation to the pool.

LNG vapor risk mitigation

A study involving Foamglas® PFS™ as a passive mitigation system for LNG pool fires was performed [54]. This material has a density lower than LNG and acts as floating barrier and successfully reduced 90% of the radiant heat. While Foamglas® PFS™ was found to effectively

suppress pool fires, it does not provide heat to warm the vapor to make it buoyant [10]. In addition, it may not be effective under freezing conditions.

The use of water curtain as a mitigation technique in case of LNG spills was studied. Its effectiveness in dispersing LNG vapor clouds was analyzed through experiments [55, 56]. Experimental results confirmed that water curtains can control the movement of vapor clouds, reducing vapor concentration. The water sprays lowered LNG concentration, pushed the vapor upward and also provided some heat to the vapor cloud. Different types of water sprays were employed, which produced droplets of different sizes and provided different coverage. The entrainment of air depended on the type of water spray, and this affected its ability to warm up a vapor cloud. The effectiveness of the water curtain was also found to depend on weather conditions such as wind speed and solar flux. The rate of evaporation of LNG was found to depend on the amount of heat obtained from the spill surface. Additional experiments showed that the water curtain is able to control ground level LNG vapor concentration but unable to do so at higher levels [57].

Experiments were performed to study the effect of HEX foam application on cryogenic liquid spills [34]. This study showed that the HEX foam can block the effects of convection and radiation through the foam, while liquid drainage contributed to additional vaporization. Results showed 70% reduction in heat transfer to the pool through convection and radiation.

An in-house foam generator was used to study the interaction between a cryogenic liquid and HEX foam [35]. It was found that the temperature increased immediately after foam application and that the boil-off effect due to liquid drainage was small and did not last long.

In addition, other research related to LNG have been conducted previously. A risk assessment of LNG terminals was conducted using a combination of Bayesian estimation and layer of protection analysis (LOPA) [58]. This work demonstrated a new methodology to update data using Bayesian estimation used in LOPA with the help of a case study. A risk management strategy for LNG road transport was performed by identifying hazards using HAZID, bow-tie analysis for preventative and mitigative measures and identifying scenarios that lead to incidents [59]. The new challenges of incorporating LNG export terminals into existing networks were studied using PHAST® and GIS [60].

1.5.2 HEX foam application on LNG

There is a dearth of literature available that specifically relates to research related to HEX foam application on LNG. A lot of pioneering research has been carried out by the MKOPSC to understand the ability of HEX foam to mitigate the vapor risk of LNG and is included in detail here.

Standards for HEX foam application were established by the National Fire Protection Association (NFPA). The NFPA guidelines were first reviewed to understand the industrial application of HEX foam for LNG vapor risk mitigation.

NFPA 11A includes standards for installing, designing, operating, testing and maintaining HEX foam systems [30]. HEX foam is recommended to control fires involving LNG and for vapor dispersion. HEX foam is defined as foam that has an expansion ratio between 200 and 1000 [31]. HEX foam was found to control LNG spill fires and in reducing vapor concentrations downwind in confined areas. The design of the HEX foam system depends on the individual sites. The application rates are determined based on standard evaluation tests of HEX foam systems shown in NFPA11 A-1-10.5(d) along with increases by a factor based on initial vaporization rates and hazard configuration. NFPA 471 includes standards for recommended practices for responding to hazardous materials incidents and also recommends HEX foam to mitigate LNG spill hazards [35].

A brief historical overview of previous research on HEX foam application on LNG is presented here.

An effort to study the effectiveness of HEX foam as a mitigation method was carried out in Louisiana in the 1960s [61]. This study used low expansion foam and did not find it to be effective. However, subsequent tests in LNG facilities in France and Japan found that HEX was effective with an expansion ratio close to 500 being optimum. When foam was applied on an

LNG spill, it formed an ice layer and floated. Nearly three to six feet was found to be a reasonable depth to control LNG pool fires.

A study in the 1970's by University Engineers involved testing the effectiveness of HEX foam in mitigating the vapor risk of LNG [10, 62, 63]. They performed experiments by filling LNG in a pit (~110 m^2) to simulate an LNG spill scenario and applying HEX foam (expansion ratio = 500) over it. The resulting LNG vapor cloud was found to be much smaller than the one formed without the HEX foam. They also observed the formation of a frozen layer of foam at the interface with LNG. Vapors of LNG which passed through the foam layers were found to rise as they were warmed sufficiently, reducing their probability of ignition. The temperature profile before and after application of HEX foam was studied. It was also found that the application of HEX foam decreased radiant heat even with a lower pressure and flow rate of water when compared with just a water curtain system while at the same pressure as a water curtain, the HEX foam system provided around 30% heat reduction.

In 1996, Takeno *et al.* also performed experiments to study the ability of HEX foam to increase the temperature of vaporized cryogenic liquids [9]. For their experiments, they substituted LNG with liquid nitrogen, which has a similar boiling point and a small difference in heat capacities. They also highlighted previous work, which described the ability of HEX foam to decrease LNG vaporization rates by reducing the effects of convection and thermal radiation, controlling the growth of fires by cutting of oxygen supply to the fuel and raising the temperature of vaporized gas. There were two categories of experiments performed by Takeno *et al.* [9]. The first set of experiments were large-scale tests to study the temperature profile of the vaporized gas as it

moves through HEX foam. Their experiments corroborated the ability of HEX foam to raise the temperature of dispersed gas. They also reported the solidification of HEX foam resulting in the formation of honeycomb-like structures as well as the formation of flow passages for the cryogenic vapor. They used two different methods of HEX foam dispersion; in the first, they applied HEX foam and left it standing while in the second, they reapplied additional HEX foam to maintain a constant height. The second set of experiments were lab-scale tests to estimate the vaporization rate of the cryogenic liquid by measuring the variation in weight of the liquid. They dispersed the liquid nitrogen into their container and then filled the liquid nitrogen gently.

In addition to these experiments, Takeno *et al.* also modeled the heat transfer phenomena and performed basic calculations using heat balances [9]. They concluded that over 90% of the heat provided by HEX foam was used to increase the temperature of the vaporized gas while the rest was used to vaporize additional liquid.

As the NFPA recommends that foam application rates be determined by tests, experiments involving HEX foam and LNG spills were conducted by BP and Texas A&M Emergency Services Training Institute in 2006 and found that 10 L/min/m^2 is an effective rate for Expandol HEX foam concentrate used in a Turbex foam generator (three times the ideal condition) [10]. The fire control time, defined as the time required for a 90% reduction in thermal radiation, was also found to reduce with increasing foam application rates.

Two pits were considered, one 45 m^2 area with 2.64 m depth and another with 65 m^2 area with 1.32 m depth, filled to a height of 6 inches. The deeper pit had more concrete, which is at a higher temperature and therefore took longer to reduce the thermal radiation with HEX foam. The foam generator location and the wind direction were also important factors that affect the time required for achieving foam of sufficient depth. Foam will float on the pool and therefore, additional foam application can help reduce heat due to thermal radiation. Dikes should be designed considering the use of HEX foam in case of spills.

HEX foam provides an insulation shielding the pool surface to a certain extent from pool fires and also warms the rising LNG vapors, aiding in vapor dispersion. A pool fire controlled by HEX foam application may be extinguished using dry chemical. HEX foam was found to not only reduce the density of rising vapors by making them warmer but also contribute to decreasing the amount of vapor generated. HEX foam was found to reduce heat flux by 90%.

Experiments were also carried out to test the effectiveness of Foamglas® PFS™, which is a type of cellular glass that is non-flammable and can be molded into different shapes and sizes [54]. It has been previously used for insulation of pipelines as well as in storage tanks. It is suggested as an alternative method for mitigating LNG fires. Solid Foamglas® PFS™ has a density lower than LNG, allowing it to float on LNG in case of a spill. This acts as an insulating barrier on the LNG surface. Some of its favorable properties include its non-flammable nature, its structure being stable at high temperatures, not absorbing any LNG and being waterproof. One advantage of this type of mitigation system does not require a large quantity of water and foam solution. The results of this study indicated that Foamglas® PFS™ did not provide sufficient heat to warm LNG vapor and therefore was not good for control of LNG vapor dispersion. In addition, under

freezing conditions, if it rains, such a system may not get activated. Recommendations were made to install both HEX foam and Foamglas® PFS™ systems for effective LNG vapor mitigation.

In 2009, field experiments were conducted to estimate the vaporization rate of LNG, temperature profile through foam layers, concentration of vapor above foam and effective foam depth to study the effectiveness of foam in vapor dispersion [64]. Foam application on LNG pool fires was also studied to determine the vaporization rate of LNG, temperature profile through foam layers and heat flux profile. In addition, a theoretical model was made to study the heat transfer in the fire pit, vaporization rate estimation as well as radiant heat calculation.

The objectives were to estimate minimum foam depth for effective vapor dispersion, concentration of outgoing vapors, temperature profiles through the foam layers, and the vaporization rates after foam application. The field tests were of two types, small-scale tests for estimating foam breakage rates over an LNG pool and medium-scale tests for evaluating the vapor dispersion effectiveness of foam application on LNG spills. The small-scale tests helped identify the formation of ice-tube passages along vapor path. The foam breakage rates were also estimated which helped determine the minimum effective foam depth. The medium-scale tests allowed the measurement of temperature profiles through the foam layers, showing the effectiveness of HEX foam in LNG vapor dispersion. A minimum effective foam depth 0.64 m was determined for LNG vapor risk mitigation. However, for practical applications, a safety margin was recommended. HEX foam was also found to reduce the LFL distance by 80% and the thermal hazard distance by 52%.

In 2014, experiments were carried out to study the “blanketing effect” of HEX foam when applied on cryogenic liquid spills [34]. Liquid nitrogen was used as a safer alternative to LNG for these experiments. “Blanketing effect” was defined as a combination of “boil-off” effect, which is the additional vaporization caused due to liquid drained from foam and the “blocking effect”, which involves HEX foam blocking forced convection and thermal radiation, thereby reducing the vaporization rate of the cryogenic liquid. A 70% net reduction of heat due to forced convection and thermal radiation was observed due to HEX foam application.

An improved research-scale foam generator was constructed to produce foam, on a lab-scale, which can be used for tests which simulate HEX foam application on LNG to mitigate its vapor risk and for non-firefighting foam used for chemical, biological or nuclear decontamination [65]. This foam generator produced HEX foam with expansion ratios nearly between 300 and 900. The foam generator design was based on the NFPA standard with some modifications to address some drawbacks of industrial-scale generators.

Experiments with an in-house foam generator allowed based on the NFPA standards were carried out to quantitatively study the boil-off effect of foam in 2016 [35]. The temperature profile through the foam layers were also studied along with the foam breakage rate and vaporization rate of the cryogenic liquid (liquid nitrogen).

Experiments producing decontamination foam for application on non-polar hazardous bio-chemicals were carried out by the MKOPSC [66]. Previous work addresses the application of foam on polar hazardous chemicals which quickly dissolve and react with the foam. In this work,

the application of decontamination foam on a derivative of cysteine called N-(tert-Butoxycarbonyl)-Lcysteine methyl ester (TCME) was studied using a GC-MS to estimate the extent of reaction.

In 2016, a heat transfer and evaporation model of LNG covered by HEX foam was developed. For this model development small-scale tests involving liquid nitrogen were carried out [67]. They observed that three distinct layers, a layer of frozen ice, a layer of frozen foam and liquid HEX foam were formed. A heat transfer and evaporation model was developed to estimate the mass evaporation rate of the cryogenic liquid and compared with experimental results. There were several drawbacks of this model including: neglecting the effects of forced convection and thermal radiation on foam breakage, calculating only vaporization rates of the cryogenic liquid, uncertainty in assumed physical properties (used liquid nitrogen instead of LNG without accounting for how it would differ if LNG is used). It might be more useful to carry out an overall heat transfer model, including effects of foam breakage and the temperature profile through the foam, which will account for heat transfer to the LNG vapors ("Warming effect of foam") and help estimate how much foam needs to be applied for effective vapor dispersion.

In 2018, Yang *et al.* studied the effect of operating parameters of the foam generator, collection containers and time on foam stability [68]. They studied the effects of these parameters on stability deviation using Taguchi analysis. They concluded that the influence of collection container and collection time cannot be ignored. Solution pressure was found to impact the foam stability the most while the influence of air volume was much lower. In addition, they concluded that the amount to solution that reaches the mesh screen, which depends on the solution pressure,

nozzle and screen type, foam solution and distance between nozzle and screen, should match the air volume for improved foam stability.

1.5.3 Foam stability studies

Foams are colloidal dispersions in which the dispersed phase is gas and the dispersion medium is liquid [69]. Liquid fraction of the foam is used to classify it as low, medium or high expansion. Expansion ratio is defined as the ratio of foam volume to liquid volume. When the liquid fraction is low, the foam has high expansion

ratio. These types of foam are referred to as high expansion (HEX) foam. HEX foam generally has an expansion ratio higher than 200 [31].

Foams mainly consist of water, foam concentrate, and may include some form of particle stabilizers [70]. The particle stabilizer may either be a surfactant or a solid particle. The role of a particle stabilizer in foam is to reduce the surface tension between gas and liquid phase, and there exists an ideal concentration of surfactant called the critical micelle concentration (CMC) at which the surfactant would best perform its function without any excess surfactant or a deficiency in surfactant [71].

Foams are thermodynamically unstable because foam bubbles have high interfacial energy [72]. As a result, bubbles coarsen with time and eventually disappear. The rates of decay of different types of foam will vary depending on the type of foam, its composition and presence of stabilizers.

Some foam may be so unstable that they are stable only for a few seconds while there are others that can last for several days or months. Foam destabilization mechanisms may include liquid drainage, Ostwald ripening, evaporation, coalescence, and external disturbances [72]. All these mechanisms can contribute to making foam less stable, ultimately resulting in its breakage.

Liquid drainage is the liquid that gets drained out of the foam due to gravity. The loss of liquid from foam can significantly affect its effectiveness [32]. If more liquid drains out of the foam, it can significantly increase the rate of vaporization of LNG.

Ostwald ripening is the coarsening of bubbles due to the diffusion of air from one bubble to another over time to attain thermodynamic equilibrium. Smaller bubbles tend to lose gas and become smaller and eventually disappear while larger bubbles grow over time. This eventually increases the average size of bubbles [70].

Evaporation due to convection and radiation can decrease the critical liquid fraction of bubbles in the upper layers of the foam. Carrier and Colin found that when the liquid fraction drops below a critical value, bubbles tend to break [73]. Li *et al.* also performed experiments verifying the influence of environmental humidity on foam stability and found that change in humidity can significantly alter foam stability [74]. Thus, it is possible for evaporation to affect the stability of foam.

Coalescence can also influence the rate of foam breakage. Coalescence occurs when the film separating two bubbles breaks. This can be a cooperative process resulting in a series of rupture of

many bubbles [70, 73]. Coalescence observed in foam may be different from that observed in isolated thin films and its mechanism is not very well understood.

External disturbances include both forced convection and thermal radiation. Zhang *et al.* found that foam application can significantly reduce the heat flux due to forced convection and thermal radiation which contribute to vaporizing cryogenic liquids [34].

A schematic combining these factors resulting in foam breakage is shown in Figure 7.

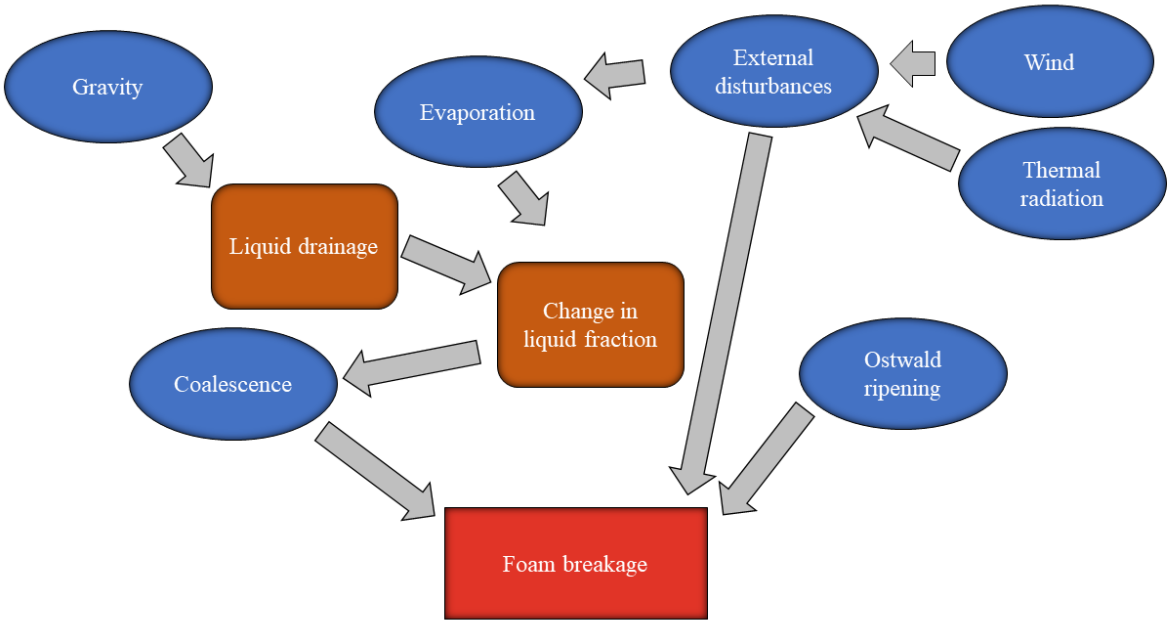

Figure 7: Schematic showing the mechanism of foam breakage (Reprinted with permission from [6])

1.5.4 Nanoparticles as foam stabilizers

The use of nanoparticles as foam stabilizers has gained interest. There are several previous efforts to improve the stability of foam using nanoparticles. Binks *et al.* studied the use of silica nanoparticles to stabilize foam solely, without the addition of surfactants [75]. Zhang *et al.* studied the stabilization of foam with laponite clay nanoparticles and observed a synergistic effect when mixtures of laponite particles and certain nonionic surfactants were used to produce aqueous foam [76].

Zirconium Phosphate as nanoparticles

Zirconium Phosphate (ZrP) is a layered inorganic material with a hexagonal shape whose chemical formula is $Zr(HPO_4)_2*H_2O$. The applications of layered ZrP range from fuel cells, gas sensors, lubricant additives, and flame retardancy [77-80]. Exfoliating the ZrP nanoplates further allows more applications such as pickering foams, stabilizing pickering emulsions and liquid crystals [81]. With pickering emulsion of oil-water phase mixtures, exfoliated ZrP nanoplates are considered to be used to stabilize liquid-gas foam.

An SEM image before the exfoliation process was taken and is shown in Figure 8, along with a TEM image of an exfoliated ZrP molecule. This helped analyze the structure of the ZrP nanoplates before and after exfoliation.

(a) (b)

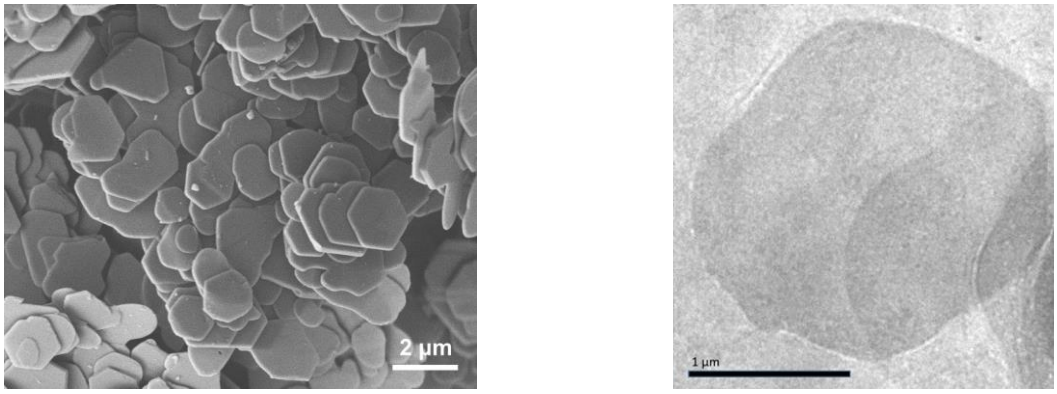

Figure 8: (a) SEM image of ZrP nanoplates before exfoliation. (b) TEM image of a monolayer ZrP nanoplates (exfoliated with TBA) (Reprinted with permission from [5])

Guevara *et al.* and Zhang studied the effect of adding exfoliated zirconium phosphate (ZrP) nanoparticles to improve foam stability [33, 71]. Guevara *et al.* developed foam stabilized with high aspect ratio ZrP nano-sheets exfoliated with PA [33]. SEM images showed the adsorption of these nano-sheets on the air-water interface. Foam stability was measured by studying foam breakage and liquid drainage rates.

Zhang performed experiments to identify the use of Zirconium Phosphate (ZrP) exfoliated with propyl amine as a foam stabilizer to improve the performance of HEX foam [71]. It was identified that several properties of nanoparticles may affect its ability to contribute to foam stability including hydrophobicity, size, shape, aspect ratio, and concentration [71]. The

experiments concluded that foam stability, measured by the foam breakage rate, increased with the addition of exfoliated ZrP nanoplates. ZrP stabilized foam even under extreme conditions of low temperature and high salinity. It was found that in the pickering foam formed by adding ZrP nanoplates to the foam, there was a reduction in liquid drainage rate and increase in surface stability. The vaporization rate of liquid nitrogen, which was used as a safe cryogenic substitute for LNG, was found to be modestly lower for foam with ZrP nanoplates. It was also hypothesized that the ZrP nanoplates, modify the surface of the foam, reducing liquid drainage. There are limitations to the use of this experimental setup. In this study, experiments were conducted on the benchtop on a relatively small-scale. The foam was produced by shaking and is therefore not bound to be of uniform size. Therefore, additional studies on a larger scale, with the use of a foam generator are required before drawing conclusions.

The studies by Guevara *et al.* and Zhang found that these particles may be contributing to enhanced foam stability due to the particles reducing gas diffusion between bubbles, controlling Ostwald ripening and coalescence and also potentially lower liquid drainage by acting as a physical barrier to liquid flow [33, 71]. This phenomenon is illustrated in Figure 9.

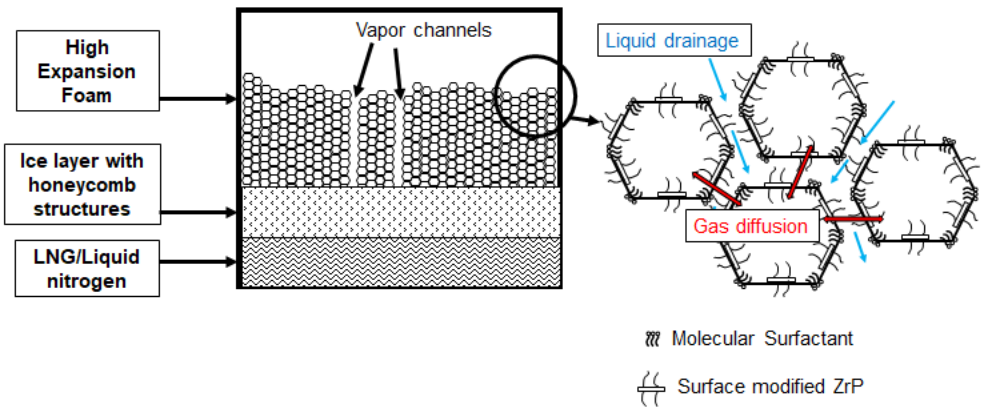

Figure 9: Schematic showing how foam stability was enhanced using exfoliated ZrP nanoplates (Reprinted with permission from [5])

1.5.5 Modeling of foam application on LNG

There have been previous efforts to develop heat transfer models but they have several drawbacks. Takeno *et al.* proposed a simple model by performing a heat balance on the system [9]. However, this model has several drawbacks including assuming steady state, an average temperature of foam, a fixed vaporization rate and a fixed height of foam. In 2016, Ye *et al.* developed a heat transfer model for LNG covered by HEX foam [67]. However, this model too has several drawbacks. It calculates only the vaporization rates of the cryogenic liquid, but it might be more useful to have a model predict the amount of foam that needs to be applied.

1.6 Gaps and objectives

Liquefaction of natural gas enables ease of storage and transportation. However, the leak of LNG can present many hazards outlined previously, including, vapor cloud explosion and asphyxiation hazard. The NFPA has suggested the use of high expansion (HEX) foam for LNG vapor risk mitigation but its effectiveness depends on application the application rate and should be determined by experiments under controlled conditions [30].

Based on the literature review, it is evident that most experiments conducted previously have neglected the effects of forced convection and thermal radiation on foam breakage. Zhang *et al.* conducted some experiments at one wind speed and one radiation intensity and recommended additional work over different wind speeds and radiation intensities, along with a study of liquid drainage rate which can help determine the vaporization rate of the cryogenic liquid [34]. While foam can block convection and thermal radiation, these heat transfer mechanisms can ameliorate foam breakage, altering the amount of foam that needs to be applied to ensure effective vapor dispersal. They may also affect the liquid drained from foam, which contributes to LNG vaporization.

In addition, some experiments performed previously show the ability of exfoliated ZrP nanoplates in stabilizing HEX foam. However, these small-scale benchtop experiments involved shaking test tubes to form foam which may introduce significant variability between experiments, producing foam of varying expansion ratios and also introduce non-uniformity in bubble size [33, 71]. Therefore, additional studies on a larger scale, with the use of a foam with a

uniform bubble size is necessary before drawing conclusions. Also, the mechanism through which the nanoplates stabilize the foam is not well understood.

A heat transfer model will help predict the amount of foam that needs to be applied in case of an incident and develop guidelines based on the underlying physics of the system. While there have been previous efforts to develop heat transfer models but they have several drawbacks.
All these gaps highlight a need for an experimental and theoretical study on stability of HEX foam used for LNG vapor risk mitigation.

Therefore, the following objectives were proposed based on these gaps:

1) Study the effects of forced convection and thermal radiation on HEX foam breakage
2) Study the effect of addition of exfoliated ZrP nanoplates to HEX foam
3) Develop a heat transfer model to predict the amount of HEX foam that needs to be applied

Therefore, this dissertation focuses on quantifying the effects of forced convection and thermal radiation on foam breakage, understanding the role of liquid drainage rate on foam vaporization and analyzing the temperature profile through the foam. This will help estimate the amount of foam that needs to be applied for effective vapor risk mitigation. This work also explores the ability of exfoliated zirconium phosphate (ZrP) nanoplates in stabilizing HEX foam, which can help reduce the duration over which foam needs to be applied. It also includes the development of a heat transfer model to estimate the amount of foam that needs to be applied in case of an LNG spill.

2 EFFECTS OF FORCED CONVECTION AND THERMAL RADIATION ON HEX FOAM*

2.1 Introduction

The National Fire Protection Association (NFPA) suggests the use of high expansion (HEX) foam for an liquefied natural gas (LNG) spill [30]. There are several mechanisms that can affect the vaporization rate of LNG in the presence of foam [34]. The foam blocks the effect of both forced convection and thermal radiation on LNG vaporization and is called as the "blocking effect" of foam. Liquid from the foam can drain over time and can increase the rate of vaporization of LNG. This is termed as the "boil-off effect" of foam. Over time, an ice layer forms since the temperature of the cryogenic liquid is far lower than the freezing point of water. This acts as a physical barrier preventing direct contact of foam with LNG. However, as this ice is porous, it allows vapor to pass through. The "blocking effect" and "boil-off effect" are combined together and termed as the "blanketing effect" of foam which highlights the net effect of foam addition and determines the vaporization rate of LNG [34]. In addition, the vapors that pass through the foam layers exchange heat with the foam as they pass through, increasing their temperature. This increases the density of vapors leaving the foam making them more buoyant, which makes their dispersion easier. This is termed as the "warming effect" of foam.

*Parts of this section have been reprinted with permission from: "Effects of forced convection and thermal radiation on HEX foam used for LNG vapor risk mitigation", Krishnan, P., Zhang, B., Al-Rabbat, A., Cheng Z., Mannan, M.S., Journal of Loss Prevention in Process Industries, 2018, 55, 423-436, Copyright 2018 by Krishnan *et al.* [6]

Zhang *et al.* (2014) performed experiments which revealed the existence of the "blocking effect" of HEX foam [34]. A 70% net reduction of heat due to forced convection and thermal radiation was observed due to foam application. Experiments were previously conducted at one wind speed and one radiation intensity and recommended additional work over different wind speeds and radiation intensities, along with a study of liquid drainage rate which can help determine the vaporization rate of the cryogenic liquid [34]. While foam can block convection and thermal radiation, these heat transfer mechanisms can ameliorate foam breakage, altering the amount of foam that needs to be applied to ensure effective vapor dispersal. They may also affect the liquid drained from foam, which contributes to LNG vaporization.

In this work, experiments were carried out with HEX foam with forced convection and thermal radiation to estimate the foam breakage rate and liquid drainage rate from foam. In addition, experiments were also carried out to understand the effects of forced convection and thermal radiation on foam breakage when foam is applied over a cryogenic liquid. The foam breakage rate, vaporization rates of the cryogen as well as the temperature profile of the vapors through the foam layers were measured. This study aims to understand the effects of convection and radiation on foam breakage, and the liquid drainage from HEX foam to minimize vaporization of the cryogen and to ensure effective vapor dispersal.

2.2 Materials and methods

The foam concentrate used in this work was C2 HEX foam concentrate by Chemguard. The foam solution was prepared as prescribed by the foam manufacturer (2%). Refrigerated liquid nitrogen (N_2) (> 99.998%) was purchased from Praxair.

A foam generator apparatus was designed at the Mary Kay O'Connor Process Safety Center by Harding and Zhang based on the NFPA standard along with some modifications [30, 65]. These modifications allow lower foam flow rates for experiments in the laboratory, enhanced safety without depending on pressurized air, easier shutdown procedure, smaller pressurized volume negating the requirement of a solenoid valve and a deflector plate for directing the foam to the required location.

2.2.1 Estimation of foam breakage rate

Foam height was estimated by taking photographs of the foam container over specific intervals of time and analyzing them using an image processing software developed by the NIH known as ImageJ. The foam breakage rate was estimated by calculating the rate of change of foam height.

2.2.2 Mesh setup to measure liquid drainage

To measure liquid drainage, foam was placed in a container below which a mesh was placed as shown in Figure 10. As the liquid drained from the foam through this mesh setup, a weighing balance (Scale WPT/4 300 C7, RadWag, Poland, Maximum capacity = 300 kg, readability = 0.1 kg) measured the weight of the falling liquid with time.

(a)

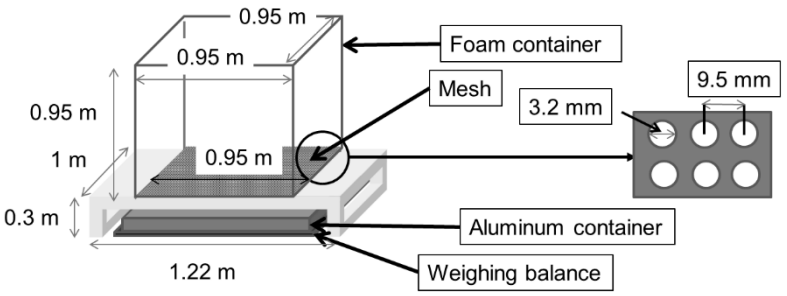

(b)

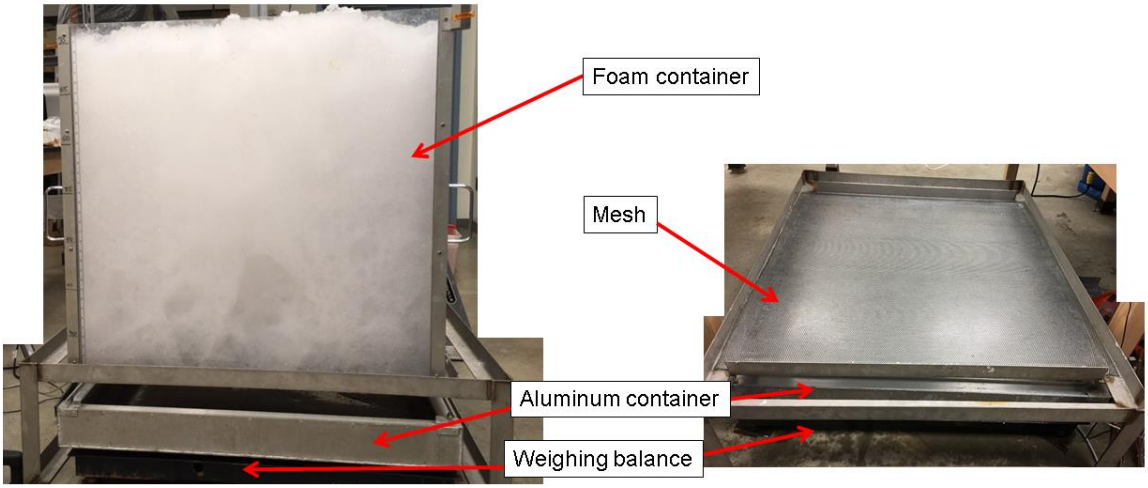

Figure 10 : Mesh setup to measure liquid drainage a) schematic with dimensions (not to scale) b) images of the actual setup (Reprinted with permission from [6])

Using the in-house foam generator, foam was generated and experiments were carried out in the presence of wind induced forced convection and thermal radiation.

2.2.3 Wind tunnel setup for experiments under forced convection

A wind tunnel was constructed to minimize lateral losses and create a unidirectional space that can be upscaled to practice, based on Zhang *et al.* and is shown in Figure 11 [34]. A screen was added in the wind tunnel to homogenize the flow over the cross-sectional area and to avoid large eddies. Although the screen introduced a pressure drop, which limited the magnitude of wind speeds possible, it ensured that the flow was less turbulent [82]. Wind was generated using a fan (Global Industrial, Oscillating Pedestal Fan, 30 Inch Diameter, 1/3HP, 8775CFM). The wind speeds were measured using an anemometer (Omega Engineering, CFMMasterII, 0.4-35 m/s ± 3%) at the extreme ends of the foam container and the average of 30 readings is reported as the average wind velocity. The wind speed was varied by changing the position of the fan and using a transformer to vary the input voltage.

(a)

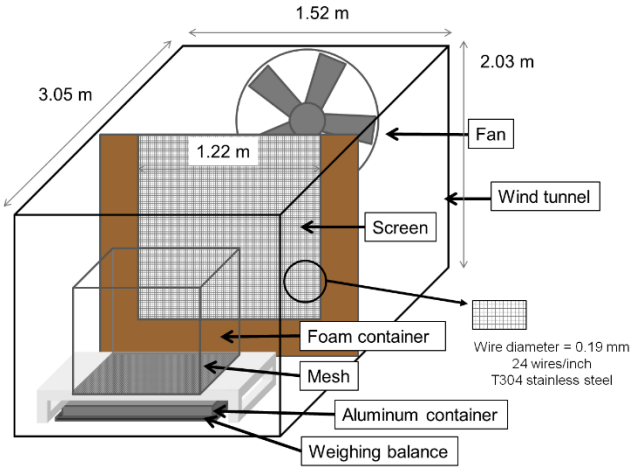

(b)

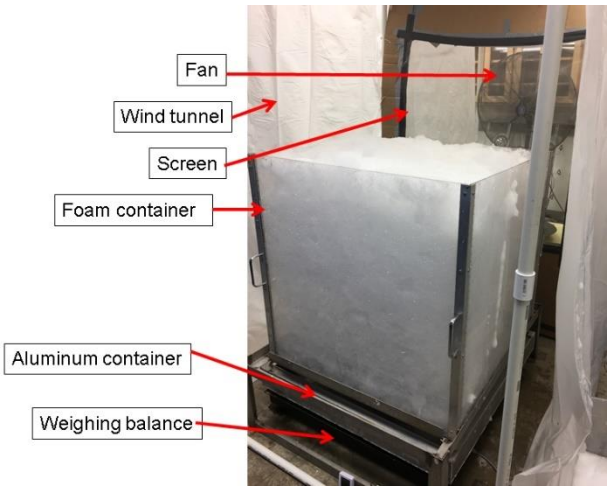

Figure 11: Wind tunnel setup a) schematic with dimensions (not to scale) b) image of actual setup (Reprinted with permission from [6])

2.2.4 Bulb panel setup for experiments under thermal radiation

The bulb panel setup included a frame that was made from slotted angles to which lamp holders (HDX, 150-Watt Incandescent Clamp Light) were attached and is shown in Figure 12. Nine light

bulbs (Philips, 125W, 120V, BR40, Heat Lamp Reflector) were used to produce radiation of required intensities, simulating solar radiation. The thermal radiation intensities were measured with a sensor (Tenmars, TM-206) that can detect up to 2,000 W/m^2 (±10 W/m^2 or ±5%, whichever is greater). The values obtained over a specific area were averaged and reported. The radiation intensities are varied using a transformer to vary the input voltage.

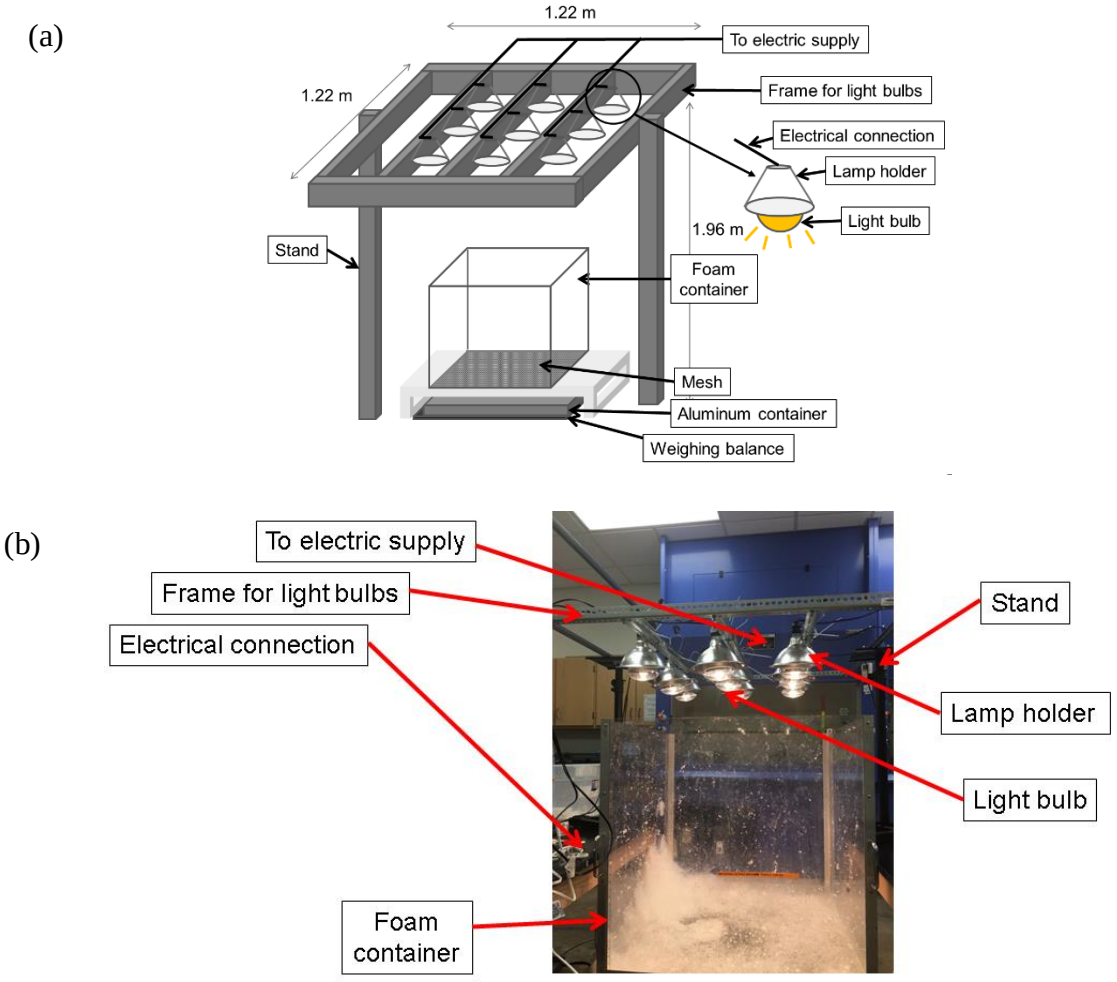

Figure 12: Bulb panel setup a) schematic with dimensions (not to scale) b) image of actual setup (Reprinted with permission from [6])

2.2.5 Setup for experiments with cryogenic liquid

A spill of a cryogenic liquid such as LNG contained in a dike was simulated by filling an aluminum container with liquid nitrogen. Liquid nitrogen was used for the experiments as it is not flammable, has similar heat transfer properties as LNG, and has been previously used for lab-scale tests [9, 34, 35].

The setup used for the cryogenic liquid tests is shown in Figure 13, similar to that employed by Zhang *et al.* [35]. The main features of this setup include a weighing balance, an outer aluminum container with trenches to hold a transparent foam container, an inner aluminum container (not shown in figure) to hold the liquid nitrogen. A saturated solution of calcium chloride (83-87%, McMaster Carr) was prepared and added in the trenches to create a liquid seal, blocking the flow of liquid nitrogen vapors through it, and allowing a freezing point depression due to the presence of salt.

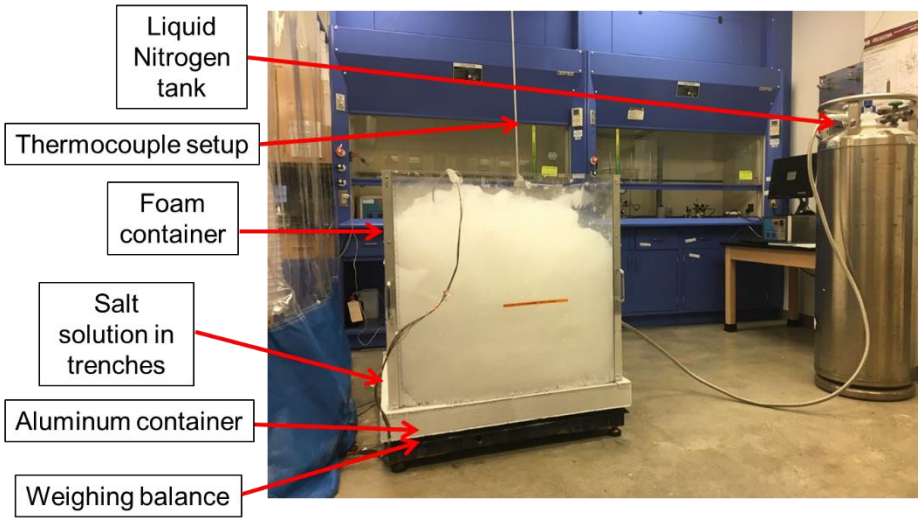

Figure 13: Image showing setup for experiments with liquid nitrogen (Reprinted with permission from [6])

Approximately 35 kilograms of liquid nitrogen was filled in each experiment through a circular perforation made on the side of the foam container. Foam was filled about 5 minutes after all the liquid nitrogen was filled in the container. Images were captured to record the foam height using a recording device and analyzed using ImageJ. The temperatures of the foam and outgoing vapor were measured using six thermocouples (Type T, TJC300 series, Omega Engineering) with a distance of 0.18 m between adjacent thermocouples. The thermocouple setup has a unique design and was first used by Zhang *et al.* [35]. It allows the measurement of the foam and vapor temperature simultaneously using an upward thermocouple, which is largely influenced by the foam temperature and a downward thermocouple, which is predominantly affected by the temperature of the outgoing vapor.

The temperature and humidity of the room during all experiments were also recorded. The temperature of the room was mostly between 21-22^{o}C and the relative humidity generally varied between 20-50% (AcuRite Indoor Temperature and Humidity Monitor, Temperature - ± 0.3°C, % RH - ± 2%).

2.3 Results

2.3.1 Expansion ratio of HEX foam

To determine the expansion ratio of foam, experiments were carried out by filling the foam container placed on the weighing balance and measuring the weight of the foam added. By estimating the volume of the foam in the container and the weight, the expansion ratio was calculated. The average expansion ratio was 420 ± 35.

2.3.2 Foam breakage rate and liquid drainage measurement

Foam breakage rate helps estimate when foam needs to be applied to replenish an existing layer of foam, to ensure that the outgoing vapor of the cryogenic liquid is lighter than air, for better vapor dispersal. The foam breakage rate is calculated by measuring the foam height over time and then calculating the rate of change of foam breakage. Liquid drainage from foam can affect the rate of LNG vaporization from a spill as it determines the boil-off effect from foam. If the liquid drainage from foam is too high, then the amount of vapor generated due to foam application may be significantly higher. Therefore, this work aims to study the effect of this liquid drainage on the LNG vaporization. Experiments were carried out with the mesh setup to estimate the liquid drained from foam under varying conditions of forced convection and thermal radiation.

2.3.3 Foam breakage and liquid drainage without forced convection or thermal radiation

Change in foam height with time for experiments without forced convection and thermal radiation is illustrated in Figure 14. These experiments are used as a control in this study, to measure the variation between experiments with and without forced convection and thermal radiation. The foam breakage rate was estimated by fitting the change in foam height with time data and estimating the slope of the graph. This experiment was repeated three times to ensure reproducibility of the experimental results and the average slope is shown in Table 3.

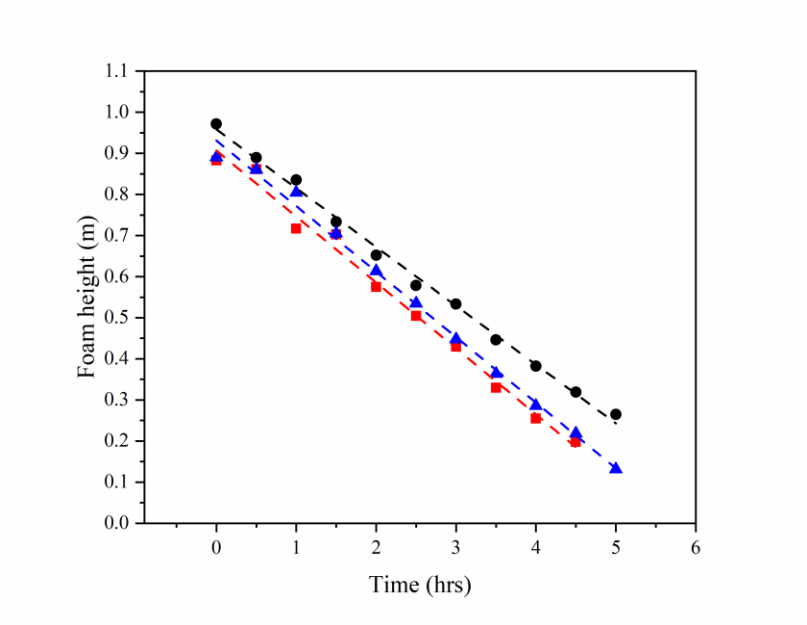

Figure 14: Change in foam height without forced convection or radiation (three experiments under the same condition) (Reprinted with permission from [6])

Table 3: Foam breakage rates without forced convection or radiation (three experiments under the same condition) (Reprinted with permission from [6])

Experiment	Foam breakage rate	R^2
1	0.143 ± 0.003	0.996
2	0.160 ± 0.005	0.991
3	0.159 ± 0.004	0.995
Average	**0.154 ± 0.004**	

The foam applied on the mesh drained liquid over time and the amount of liquid drained was measured using a weighing balance. The liquid drainage rate is the amount of liquid drained over a specific interval of time. The liquid drainage rates for these experiments were also quite consistent and are show in Figure 15. The consistency of these results indicates that the experiments are reproducible.

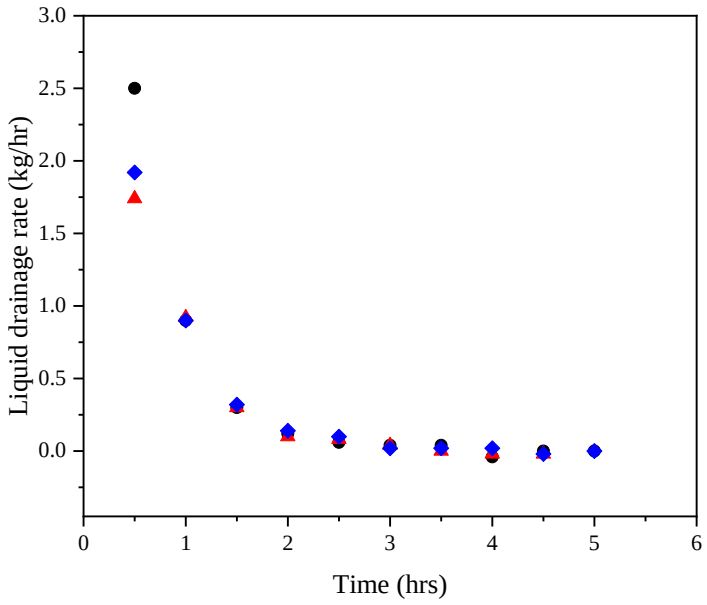

Figure 15: Liquid drainage rate without forced convection or radiation (three experiments under the same condition) (Reprinted with permission from [6])

2.3.4 Foam breakage and liquid drainage under forced convection

Average wind speeds in the wind tunnel were determined using an anemometer. The values measured are shown in Table 4.

Table 4: Measured average wind speeds (Reprinted with permission from [6])

Experiment	Measured average wind speed (m/s)
1	0.4 ± 0.01
2	0.9 ± 0.08
3	1.3 ± 0.06
4	1.9 ± 0.5
5	2.1 ± 0.7
6	2.4 ± 0.5
7	2.5 ± 0.4

Experiments with forced convection showed how the foam height reduced with time and this is illustrated in Figure 16, which helped determine the foam breakage rate under different wind speeds.

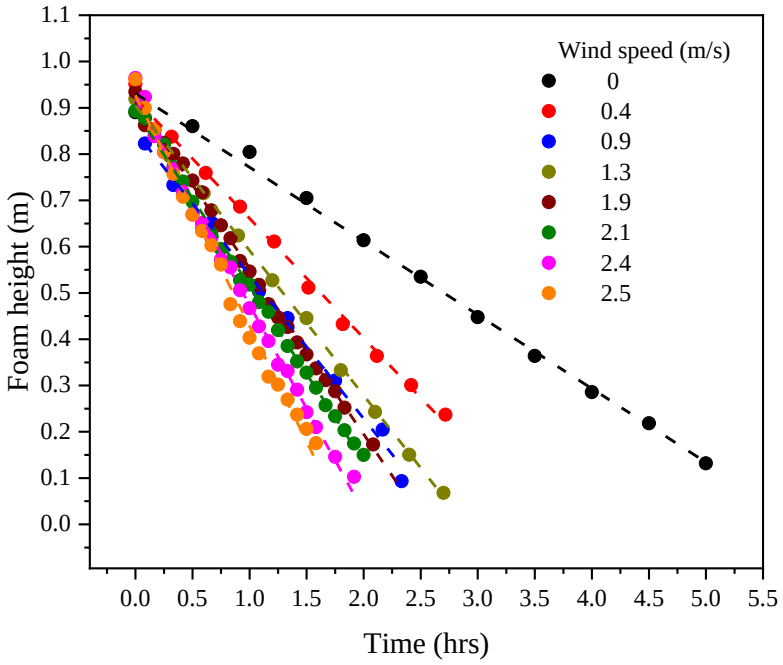

Figure 16: Change in foam height under forced convection (Reprinted with permission from [6])

The foam breakage rate was estimated by adding a linear fit to the plot of change in foam height with time and calculating the slope for each fit. The foam breakage rate at different wind speeds is shown in Figure 17 and shows the variation of foam breakage rate with wind speed. Increasing the wind speed can significantly alter the foam breakage rate. When compared with no forced convection, the maximum breakage rate at 2.5 m/s was found to be 0.5 m/hr, which is more than three times faster than the foam breakage without forced convection. In addition, the values for these slopes along with the standard deviations and R^2 are shown in Table 5. This provides an

estimate of foam breakage rates under different wind speeds, which should be accounted for when foam is applied to ensure vapor dispersal.

Table 5: Foam breakage rates at different wind speeds (Reprinted with permission from [6])

Average wind speed (m/s)	Foam breakage rate (m/hr)	R^2
0	0.159 ± 0.004	0.993
0.4	0.258 ± 0.004	0.997
0.9	0.309 ± 0.009	0.993
1.3	0.313 ± 0.003	0.999
1.9	0.359 ± 0.004	0.997
2.1	0.368 ± 0.004	0.996
2.4	0.447 ± 0.007	0.995
2.5	0.500 ± 0.010	0.993

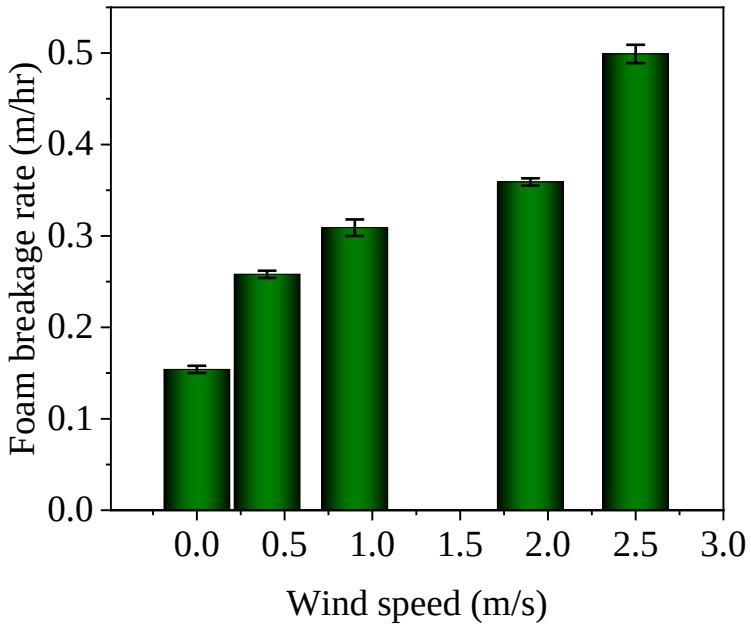

Figure 17: Comparison of foam breakage rates with different average wind speeds (adapted from [6])

The liquid drainage rate under forced convection was also obtained from the mesh setup. The liquid drainage rate as a function of time was plotted and is shown in Figure 18.

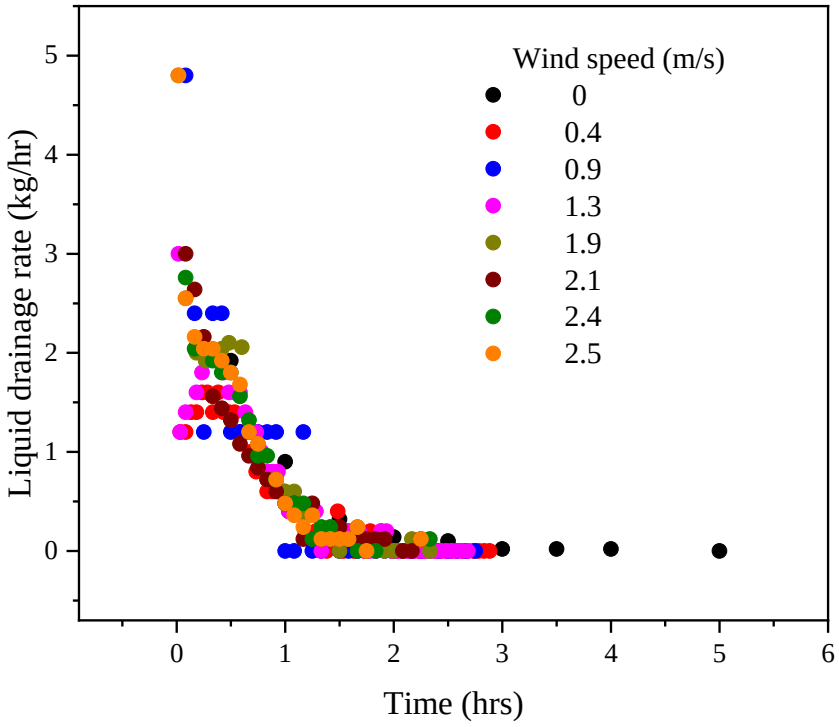

Figure 18: Liquid drainage rates under forced convection (Reprinted with permission from [6])

It is easily observed that the liquid drainage rate in all cases is quite similar. This possibly indicates that the water being drained from the upper layers of the foam might be retained by the lower layers, maintaining a uniform liquid drainage rate independent of wind speed. It is important to note that the water drainage may be affected by several factors including the initial height of the foam, the humidity, and the evaporation of water in the presence of forced convection [32, 55, 57, 74].

2.3.5 Foam breakage and liquid drainage under thermal radiation

Different radiation intensities were measured using a radiation sensor. As the radiation intensities varied with height, the foam breakage and liquid drainage from the top (~1 m) to nearly 0.8 m were estimated and used for data analysis. Ten readings of radiation intensities between these heights were averaged and are reported in Table 6. All these readings were taken at different equally spaced positions between the above-mentioned heights.

Table 6: Measured average radiation intensities (Reprinted with permission from [6])

Experiment No.	Measured average radiation intensity (W/m^2)
1	60 ± 12
2	140 ± 25
3	200 ± 33
4	270 ± 50

Experiments with different intensities of thermal radiation showed are illustrated in Figure 19. Since the foam breakage was measured as the foam height reduced from nearly 1 m to 0.8 m, to maintain close to uniform radiation intensity, the time period for such measurements was shorter than the experiments with forced convection and without forced convection and radiation.

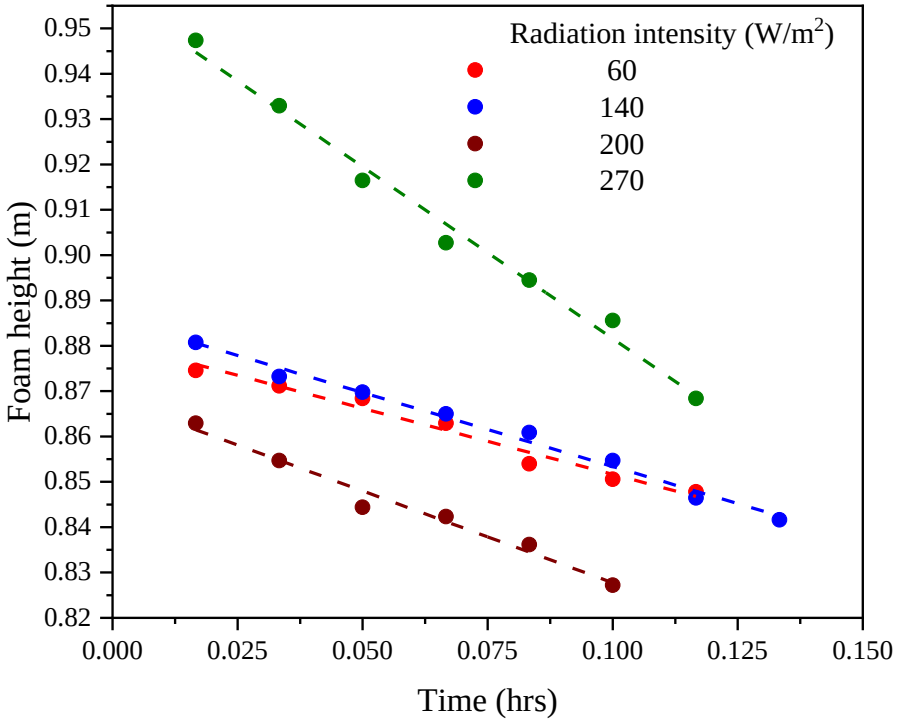

Figure 19: Change in foam height under thermal radiation (Reprinted with permission from [6])

The effect of increasing radiation intensity on foam breakage rate is illustrated in Figure 20. The foam breakage rates estimated in these experiments are the initial rate of foam breakage and not steady-state rates. These results clearly demonstrate the effect radiation has on foam breakage, highlighting that increasing the radiation intensity increases foam breakage. The values of foam breakage rates along with the standard deviations and R^2 are shown in Table 7.

Table 7: Foam breakage rates at different radiation intensities (Reprinted with permission from [6])

Radiation intensity (W/m^2)	Foam breakage rate (m/hr)	R^2
4	0.159 ± 0.004	0.993
60	0.29 ± 0.02	0.974
140	0.33 ± 0.01	0.990
200	0.41 ± 0.02	0.985
270	0.76 ± 0.04	0.989

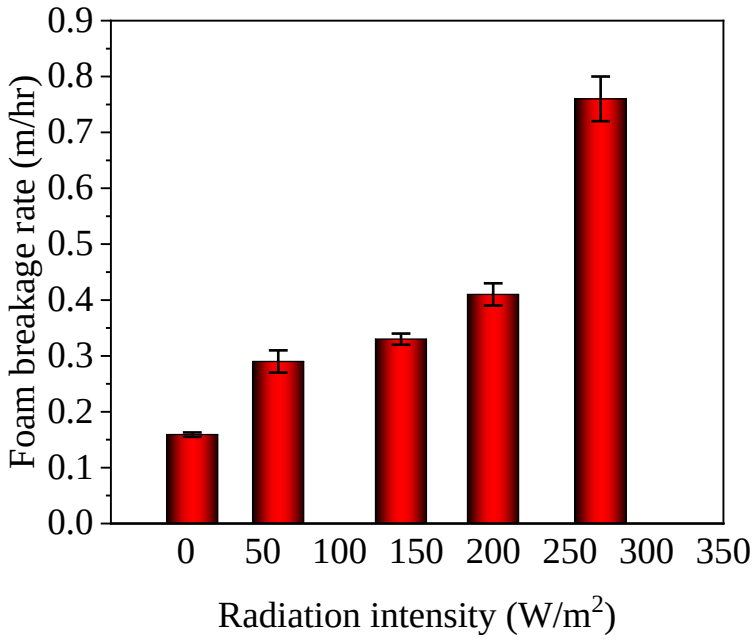

Figure 20: Comparison of foam breakage rate with different average radiation intensities (adapted from [6])

The average initial liquid drainage rate at each radiation intensity over the short time interval is shown in Table 8. It should be noted that the standard deviation was high in these calculations as there were limited data points available for these experiments. Therefore, no quantitative conclusions may be drawn from this data set, although there appears to be a trend of higher liquid drainage rate at higher radiation intensities.

Table 8: Average initial liquid drainage rates at different radiation intensities (Reprinted with permission from [6])

Radiation intensity (W/m^2)	Liquid drainage rate (kg/hr)
60	1.7 ± 0.2
140	2.8 ± 0.9
200	3.4 ± 0.8
270	3.7 ± 0.7

2.3.6 Experiments with liquid nitrogen

2.3.6.1 Foam breakage rate with liquid nitrogen

Change in foam height with liquid nitrogen, for all three cases, without forced convection or radiation, with forced convection and with radiation are shown in Figure 21.

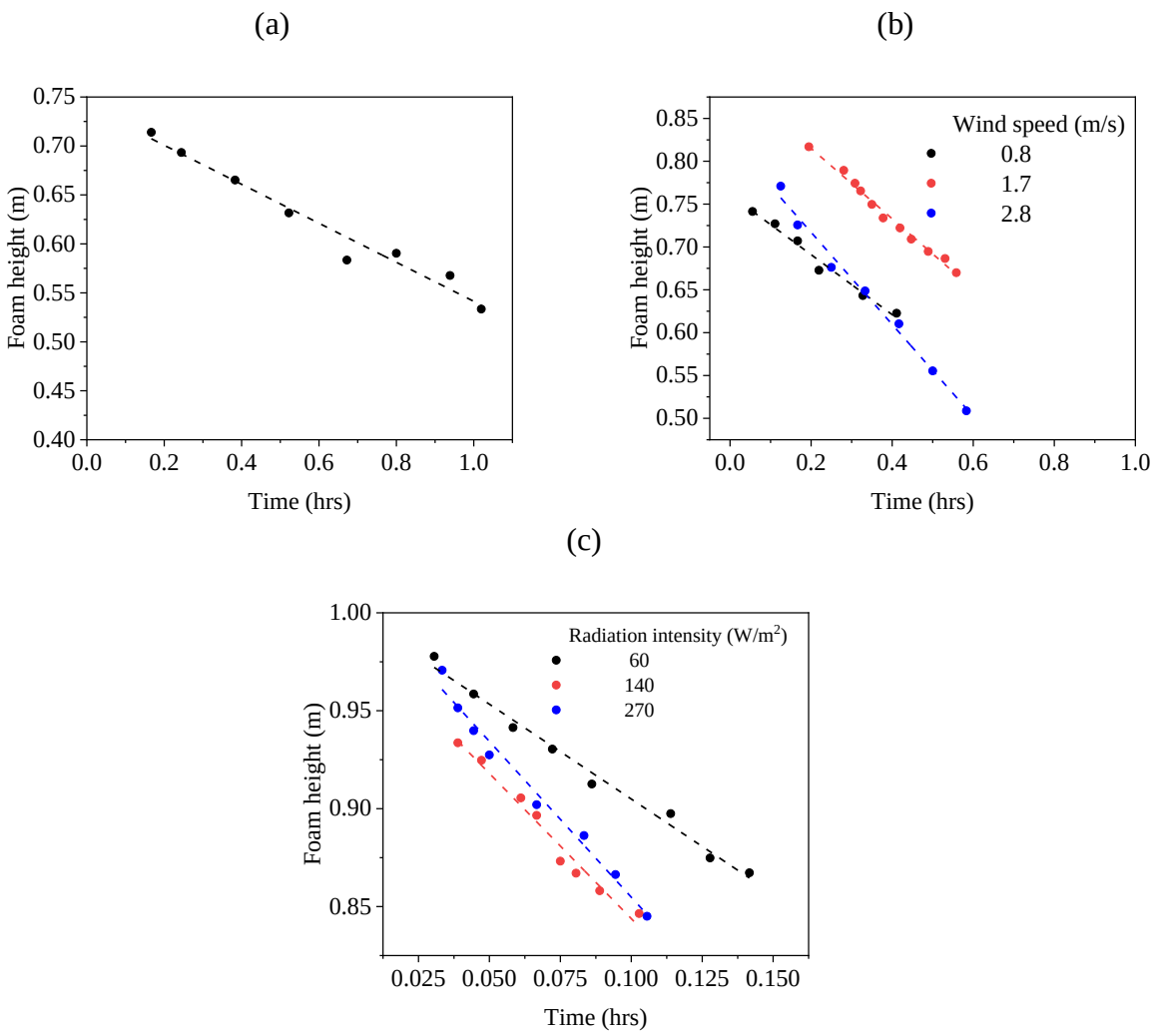

Figure 21: Change in foam height with liquid nitrogen under a) without forced convection or radiation b) forced convection and c) thermal radiation (Reprinted with permission from [6])

It can be clearly observed that the foam breakage with liquid nitrogen is more rapid in all three cases, by estimating the foam breakage rates and is shown in Table 9. This can be attributed to the effect of cryogenic liquid interaction with the foam.

Table 9 : Comparison of foam breakage rates with and without liquid nitrogen (Reprinted with permission from [6])

Experimental condition	Wind speed (m/s)	Radiation intensity (W/m^2)	Foam breakage rate (m/hr)
without LN_2	-	-	0.159 ± 0.004
with LN_2	-	-	0.199 ± 0.015
without LN_2	0.9 ± 0.08	-	0.309 ± 0.009
with LN_2	0.8 ± 0.09	-	0.350 ± 0.024
without LN_2	1.9 ± 0.5	-	0.359 ± 0.004
with LN_2	1.7 ± 0.2	-	0.410 ± 0.015
without LN_2	2.5 ± 0.4	-	0.500 ± 0.010
with LN_2	2.8 ± 0.2	-	0.537 ± 0.026
without LN_2	-	60 ± 12	0.291 ± 0.021
with LN_2	-	60 ± 12	0.968 ± 0.044
without LN_2	-	140 ± 25	0.327 ± 0.014
with LN_2	-	140 ± 25	1.482 ± 0.096
without LN_2	-	270 ± 50	0.758 ± 0.036
with LN_2	-	270 ± 50	1.591 ± 0.084

2.3.6.2 Vaporization rate of liquid nitrogen

Vaporization rate of liquid nitrogen without forced convection or radiation

The vaporization rate of liquid nitrogen was measured by recording the variation in weight of the container over time. The vaporization rate without forced convection and thermal radiation is shown in Figure 22(a). The liquid drainage rate from foam, which was previously measured using the mesh setup, is also shown in the same Figure and illustrates how the liquid drainage rate influences the rate of vaporization of the cryogenic liquid. Once the liquid drainage rate falls below 2 kg/hr, the vaporization rate stabilizes and is primarily influenced by conduction through the container. The steady-state vaporization rate is similar to that obtained by Zhang *et al.*, which was close to 11 kg/hr [35]. The steady-state vaporization rate of liquid nitrogen without foam was nearly 22 ± 3 kg/hr.

Vaporization rate of liquid nitrogen under forced convection

The vaporization rate with forced convection is shown in Figure 22 (b-d) along with liquid drainage from the foam under similar conditions. This graph also illustrates that once the liquid drainage rate falls below 2 kg/ hr in the three cases, it does not significantly contribute to the vaporization rate of the cryogenic liquid.

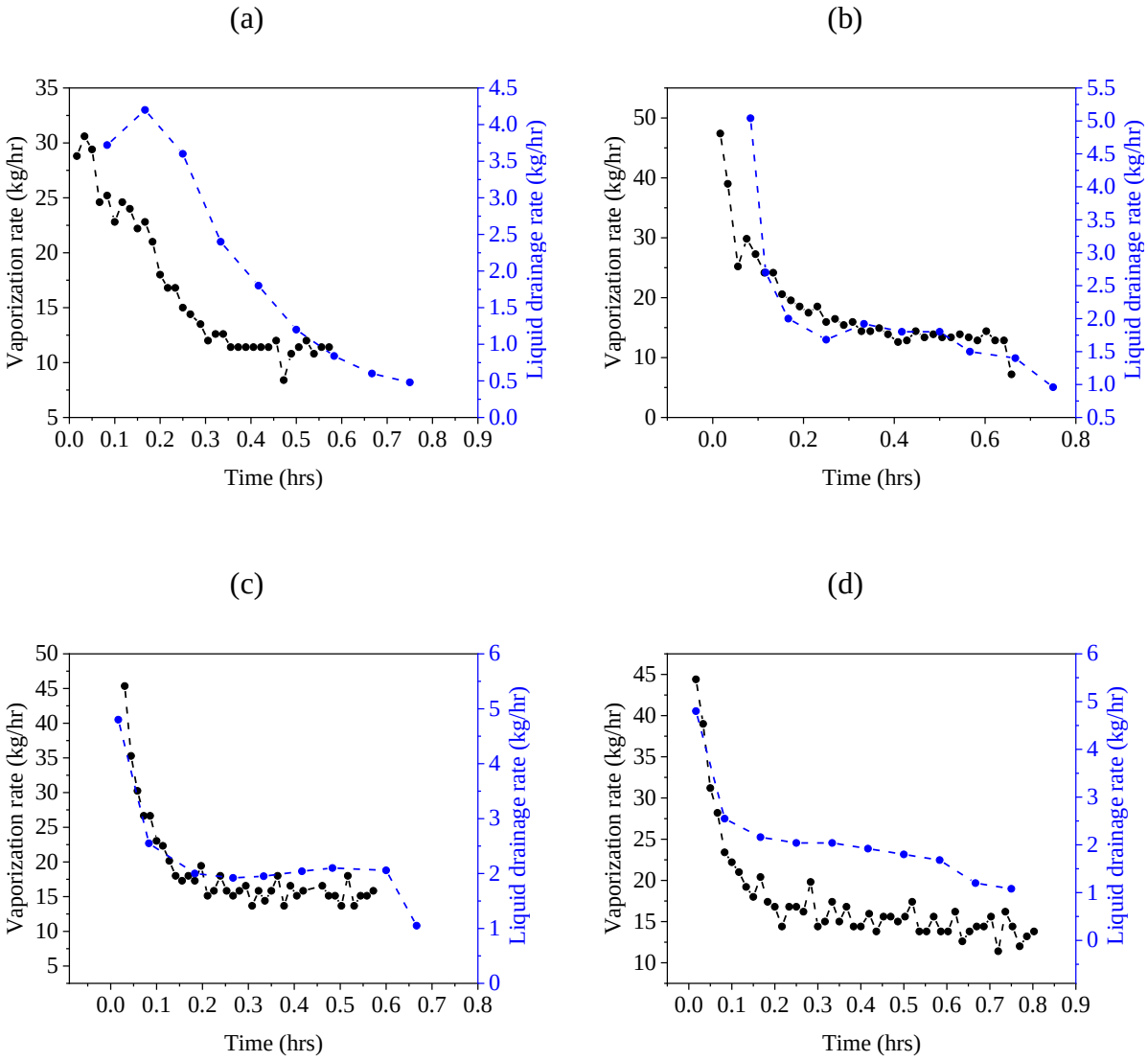

Figure 22: (a) Vaporization rate of liquid nitrogen and liquid drainage rate without forced convection or radiation (b-d) Vaporization rate under forced convection with wind speeds = 0.8, 1.7 and 2.8 m/s respectively and liquid drainage rate with forced convection with wind speeds = 0.9, 1.9 and 2.5 m/s respectively (Reprinted with permission from [6])

Vaporization rate of liquid nitrogen with thermal radiation

As the radiation data was collected only for the foam breakage until the foam height reached 0.8 m, it was not possible to obtain the steady-state vaporization rate. The initial vaporization rate with time is shown in Figure 23.

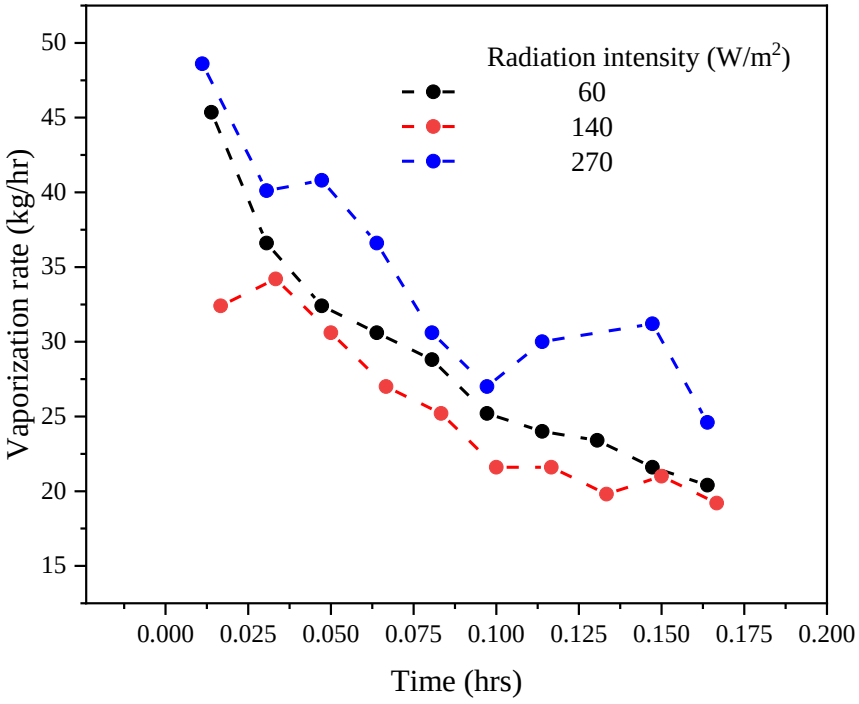

Figure 23: Vaporization rate of liquid nitrogen under thermal radiation (Reprinted with permission from [6])

2.3.6.3 Temperature profile with liquid nitrogen

The temperature profile was measured in these experiments to explain the ability of the foam to exchange heat with the outgoing vapor of the cryogenic liquid and decrease its density, thereby ensuring effective vapor dispersal.

The temperature profile without forced convection and thermal radiation has been studied by Zhang *et al.* [35]. The temperature profiles under forced convection and thermal radiation, for one case each, are shown in Figure 24 and Figure 25 respectively.

The unique design of the thermocouple setup allows the measurement of the foam and vapor temperature simultaneously. The upward thermocouple is mainly affected by the foam temperature, and the downward thermocouple primarily indicates the temperature of the outgoing vapor. As the vapor rises up through the foam, heat is transferred from the foam to the vapor, increasing its temperature and decreasing its density.

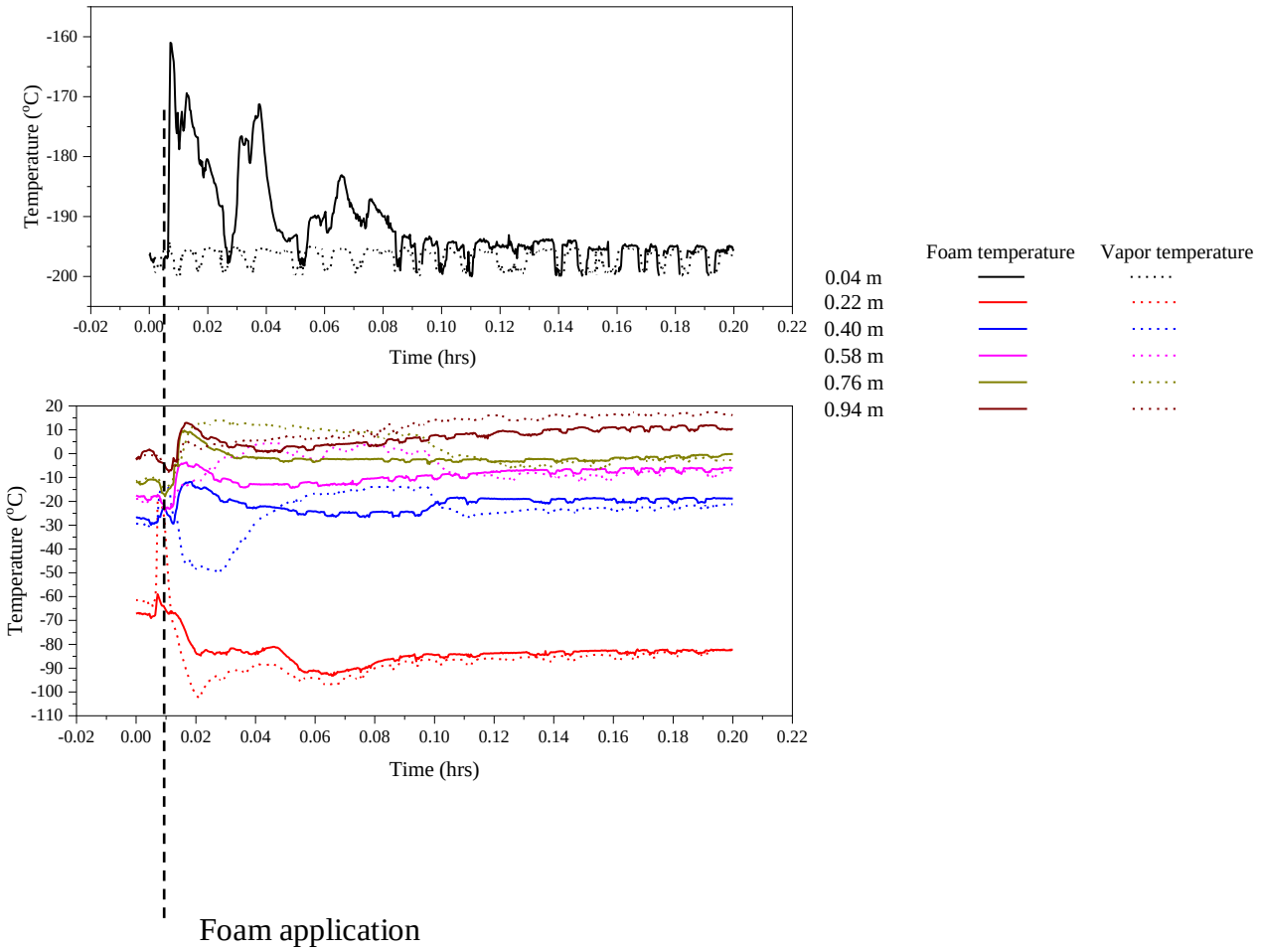

Figure 24: Temperature profile under forced convection (wind speed = 2.7 m/s) (Reprinted with permission from [6])

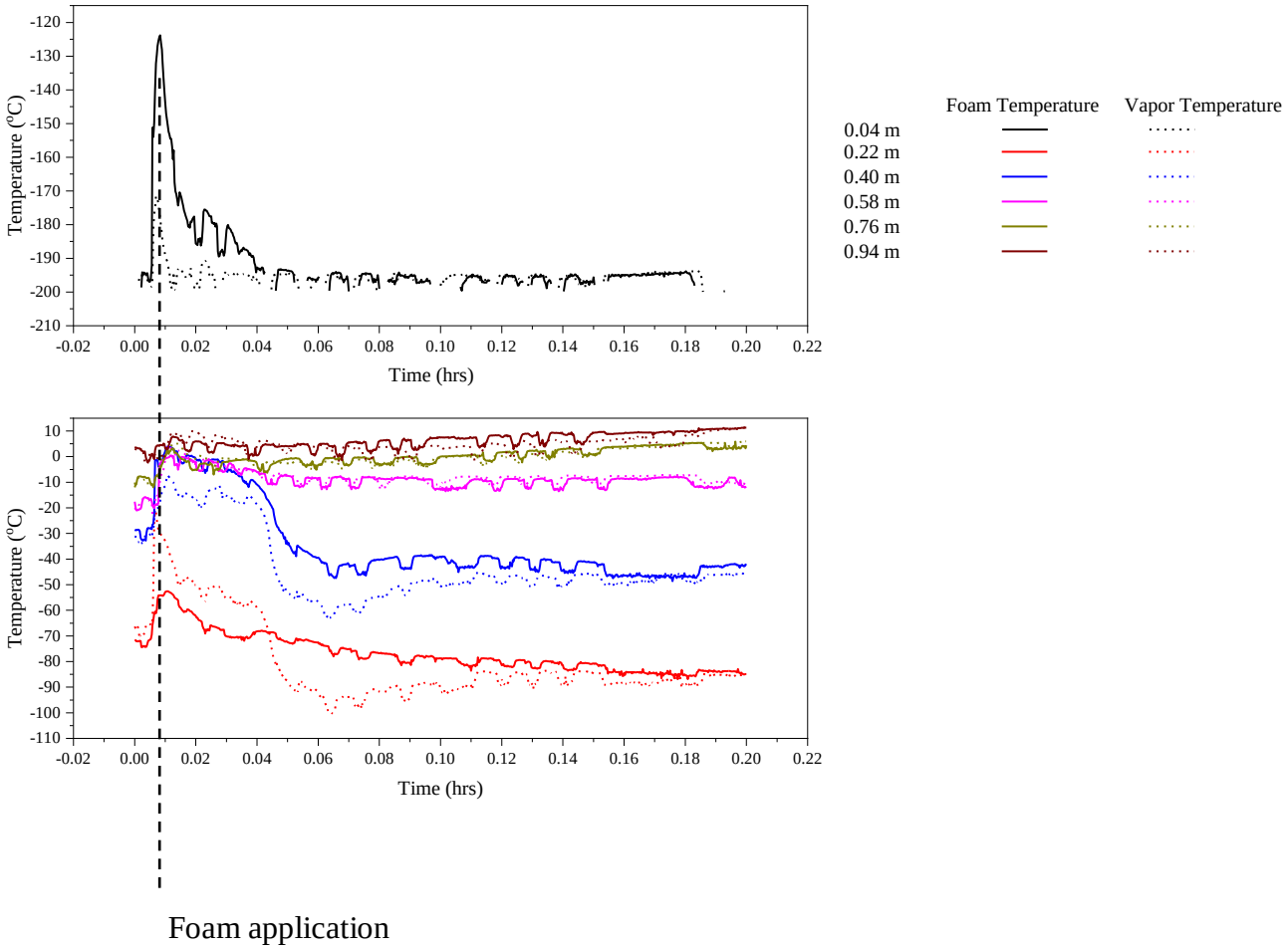

Figure 25: Temperature profile under thermal radiation (radiation intensity = 140 W/m^2) (Reprinted with permission from [6])

2.3.7 Mechanism of foam breakage

It is clear from the results obtained that forced convection and thermal radiation influence the rates of foam breakage. However, identifying the mechanisms which affect foam breakage and liquid drainage will give a better understanding of how forced convection and thermal radiation

affect foam breakage. Pugh has listed out the phenomena destabilizing the foam [72]. These may include liquid drainage, Ostwald ripening, evaporation, coalescence, and external disturbances. All these mechanisms can contribute to making foam less stable and ultimately causing its breakage. While all these phenomena can destabilize foam, it is important to estimate their effect on foam breakage to identify factors that may be controlled to minimize foam breakage. It is important to note that several factors may be dependent on each other and may exhibit synergistic effects. Forced convection and thermal radiation may be contributing to evaporation of the liquid from the foam which in turn reduces the liquid fraction. This may contribute to an increase in the rate of coalescence. While this mechanism is likely to dominate, a more in-depth study is necessary to make definitive conclusions.

2.3.8 Liquid drainage from foam

The liquid drainage from foam may play a crucial role in vaporization of LNG especially when the boil-off effect is significant, immediately after the foam is applied. The liquid drainage from the foam predicted by these experiments can be compared with a theoretical model made by Conroy *et al.* which predicts the height of the drained liquid from HEX foam [32]. The height of the liquid drained from foam in the case of free drainage is given by the following equation:

$$h_w = \alpha_f H - \frac{H}{\frac{1}{\alpha(\infty)} + \left[\frac{1}{\alpha_f} - \frac{1}{\alpha(\infty)}\right] * \exp\left[\frac{(-B\sqrt{\alpha_w}\,[t - t_{ind}])}{H^2}\right]}$$

where,

α_f = liquid volume fraction of the injected foam

$$\alpha(\infty) = \frac{B\sqrt{\alpha_w}}{AH}$$

$$A = \frac{\zeta L^2 \rho g}{\mu}$$

$$B = 0.458\frac{\zeta L \gamma}{\mu}$$

α_w=Liquid volume fraction at the foam-liquid interface

$$t_{ind} = \frac{B\left[\sqrt{0.26} - \sqrt{\alpha_f}\right]^2}{A^2 \alpha_f^2 \sqrt{0.26}}$$

$$\zeta = \text{Permeability coefficient} = \frac{k}{\alpha^2 L^2}$$

k= Permeability

$L = \text{Channel length} = 0.41\ D_b$, where, D_b=Bubble diameter

The following values were assumed for the model:

$\alpha_f = 3.3 \times 10^{-3}$

$\zeta = 5.1 \times 10^{-3}$

$D_b = 8 \times 10^{-3}\text{m}$

$H = 0.95\ \text{m}$

$L = 0.41 * 8 \times 10^{-3} = 3.3 \times 10^{-3}\text{m}$

$\gamma = 0.0225\ \text{N/m}$

$\mu = 8.93 \times 10^{-4}\ \text{Pas}$

ρ=997 kg/m^3

$A = 0.60\ \text{m/s}$

$B = 1.93 \times 10^{-4}\ \text{m}^2/\text{s}$

$\alpha_w = 0.26$

$$\alpha(\infty) = \frac{B\sqrt{\alpha_w}}{AH} = \frac{1.9 \times 10^{-4} \times \sqrt{0.26}}{0.59 \times 0.95} = 1.73 \times 10^{-4}$$

$$t_{ind} = \frac{1.9 \times 10^{-4} \times \left(\sqrt{0.26} - \sqrt{8.3 \times 10^{-3}}\right)^2}{0.6^2 \times (8.3 \times 10^{-3})^2 \times \sqrt{0.26}} = 19.7\ \text{s}$$

From Equation 1,

$$h_w = \alpha_f H - \left[\frac{H}{\left(\frac{1}{\alpha(\infty)} + \left[\frac{1}{\alpha_f} - \frac{1}{\alpha(\infty)}\right] \exp\left[\frac{\left(-B\sqrt{\alpha_w}\,[t - t_{ind}]\right)}{H^2}\right]\right)}\right]$$

$$h_w = 3.1 \times 10^{-3} - \left[\frac{0.95}{5794.1 - 5491 \times \exp(-1.09 \times 10^{-4}(t - 19.7))}\right]$$

The plot of h_w as a function of time can then be obtained.

A comparison of the model to the experimental result without forced convection and thermal radiation is shown in Figure 26. The model seems to agree with the experimental result and shows similar trends. Possible differences between the results may be due to approximation of bubble size and differences in surfactant properties.

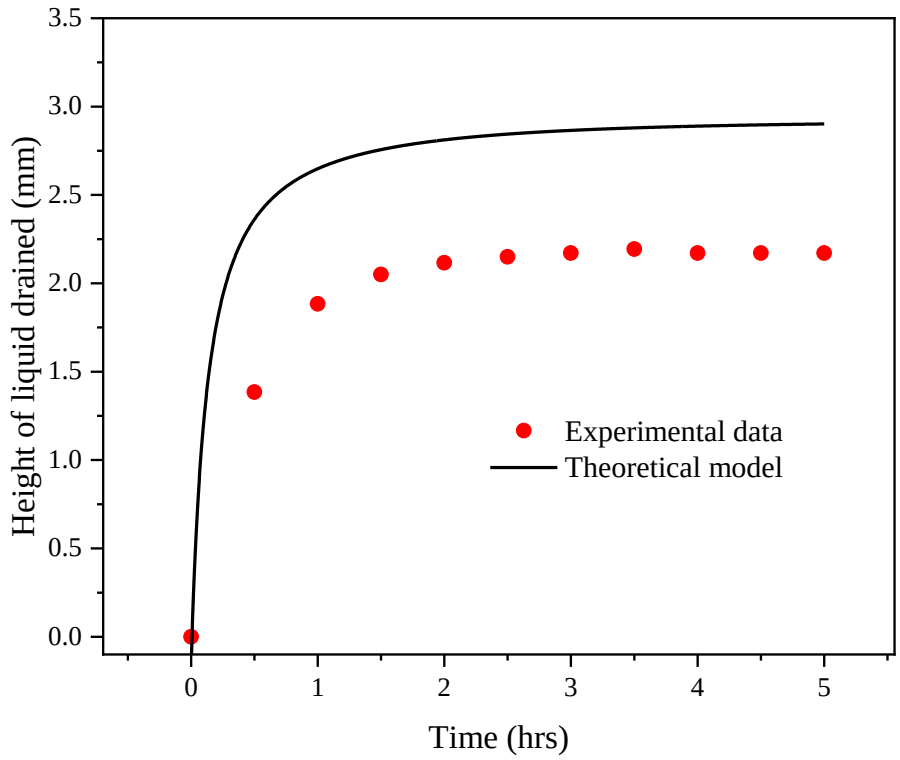

Figure 26: Height of liquid drained as a function of time without forced convection or thermal radiation obtained experimentally compared to that obtained from the theoretical model (Error bars on experimental data too small to be observed) (Reprinted with permission from [6])

2.3.9 Warming effect of the foam

The temperature of the outgoing vapors through the foam are measured experimentally and shown in Figure 24 and Figure 25. As long as the foam height is maintained sufficiently high, the vapors should be heated to a point where its density is lower than that of surrounding air (1.225 kg/m^3 at 15 ^oC, 1 atm pressure) and can be dispersed easily. Figure 27 shows the temperature at which density of methane (a major component of LNG vapor) becomes equal to that of the surrounding air at 15 ^oC. This occurs at nearly -105.7 ^oC. Therefore, as long as the vapor temperature is above this, it should be reasonable to assume sufficient dispersal. Takeno *et al.* explain that the latent heat of vaporization is lower for liquid nitrogen than LNG [9].

Therefore, if the heat flux to the pool is same, a pool of liquid nitrogen will have a higher gas velocity than that for LNG. In addition, the gas heat capacity ($\rho_g C_p$) is similar but slightly lower for nitrogen than LNG. This would determine how the temperature profile of the vapor would be as the vaporized gas passes through the foam layer, exchanging heat and reducing their density. They conclude that based on these factors, it is likely that the data provided from experiments with liquid nitrogen would be more conservative immediately after HEX foam dispersion.

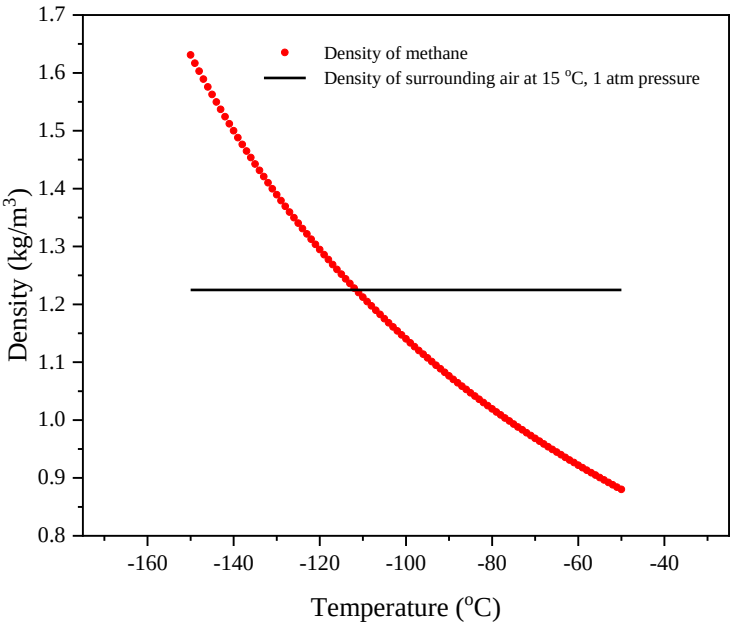

Figure 27: Density of methane as a function of temperature, methane density is equal to air density (at 15 ºC, 1 atm pressure) at about -105.7 ºC [83] (Reprinted with permission from [6])

2.4 Summary

In summary, the experiments demonstrate that foam breakage rate increases with increase in wind velocity and radiation intensity. Application of HEX foam could help reduce the vaporization of the cryogenic liquid. Liquid drainage from the foam may affect vaporization rate of cryogenic liquid, when liquid drainage is high (>2 kg/hr). As HEX foam breakage can be influenced by factors such as forced convection and thermal radiation, it must be accounted for when estimating how much foam needs to be applied for effective vapor risk mitigation.

3 IMPROVING THE STABILITY OF HEX FOAM USING EXFOLIATED ZIRCONIUM PHOSPHATE NANOPLATES*

3.1 Introduction

In case of a liquefied natural gas (LNG) spill, as LNG is a cryogenic liquid, it absorbs heat from the surroundings and forms a vapor cloud. There are multiple heat transfer mechanisms involved including conduction from the ground, convection due to wind and radiation from the sun or potential fires, which can affect the rate of LNG vaporization. Application of high expansion (HEX) foam helps block the heat due to convection and thermal radiation [34] . In addition, as the vapors of LNG pass through the foam layers, they become warmer and their density decreases. Therefore, it is important to have stable foam while maintaining its heat transfer properties.

Some experiments performed previously showed the ability of exfoliated zirconium phosphate (ZrP) nanoplates in stabilizing HEX foam. These small-scale benchtop experiments involve shaking of test tubes to form foam, which may introduce significant variability between experiments, producing foam of varying expansion ratios and also introduce non-uniformity in bubble size [33, 71].

---

*Parts of this section have been reprinted with permission from: "Improving the stability of HEX foam used for LNG vapor risk mitigation using exfoliated zirconium phosphate nanoplates", Krishnan, P., Al-Rabbat, A., Zhang, B., Huang, D., Zhang, L., Zeng, M., Mannan, M.S., Cheng, Z., 2019, Process Safety and Environmental Protection, 123, 48-58, Copyright 2019 by Krishnan *et al.* [5]

In this study, a foam generator that builds on the existing NFPA foam generator model, constructed by Harding *et al.* (2015) is used to overcome these problems and produce foam of uniform quality [65]. Some advantages of the improved foam generator include an adjusted foam application rate suitable for lab use, more mobility due to reliance only on electric utility. The use of a foam generator allows the production of uniform bubbles whose size may be controlled by passing the foam produced through a screen. This larger scale set up allows the investigation of the effects of scale up and ensure that the foam has a high expansion ratio.

In this study, foam breakage rate and liquid drainage rate was measured from experiments with a mesh setup involving commercially available C2 HEX foam stabilized by a specified concentration of zirconium phosphate(ZrP) exfoliated using TBA and compared with results from experiments without exfoliated ZrP stabilized foam under similar conditions of forced convection and solar thermal radiation [6]. In addition, the effect of liquid drainage rate on vaporization rate in the case of exfoliated ZrP nanoplates stabilized foam was evaluated and the temperature profile through the foam was studied to observe the warming effect through the foam.

3.2 Materials and methods

Chemguard C2 HEX foam was purchased from Chemguard Inc. Zirconium Phosphate ((Zr(HPO4)2·H2O or ZrP) was purchased from Sunshine Factory Co. Ltd., Chengdu, China. Tetrabutylammonium hydroxide (C16H37NO - TBA) was purchased from Sigma-Aldrich. Liquid nitrogen (> 99.998%) was used as a safe substitute for LNG, as it is a cryogenic liquid with similar properties and due to its non-flammable nature for lab safety. It was purchased from Praxair.

3.2.1 Exfoliation of ZrP with TBA

For a typical synthesis, 20 g of ZrP was first dispersed in 200 mL of water, followed by the addition of 32 mL of TBA (40 wt%, aq.). The resulting solution was then homogenized under sonication for 30 min, before additional 200 mL of water and 15 mL TBA solution were introduced. The resulting dispersion was left for overnight to ensure full intercalation of the TBA and complete exfoliation of ZrP crystals.

3.2.2 Characterization of ZrP nanoplates

A field-emission scanning electron microscope (SEM, JEOL JSM-7500F, Japan) was used to obtain SEM images of samples. Figure 8 (a) shows unexfoliated ZrP nanoplates, which showed a

well-defined hexagonal crystalline structure, similar to previous work [84]. Figure 8 (b) shows the image from transmission electron microscopy (TEM, JEM 2010, JEOL) performed to characterize the exfoliated ZrP, revealing the characteristic thin nanoplates, which are similar to other exfoliated nanomaterials such as graphene[85].

3.2.3 Preparation of foam solution

Experiments with HEX foam involved preparing a 2% foam solution using the foam concentrate based on the manufacturer's recommendation. For the experiments with HEX foam with exfoliated ZrP nanoplates, a 2% foam solution was prepared along with 2% v/v concentration of the exfoliated ZrP nanoplate solution.

Before running an experiment, the entire setup is washed with water through it to ensure that any residual foam or particles are removed. The foam solution was prepared depending on the experiment performed. The foam solution tank was mixed gently after preparing the foam solution.

3.3 Results

3.3.1 Expansion ratio of foam

The expansion ratio of the foam is defined as the ratio of foam volume to liquid volume. Foam is filled in the foam container and the volume occupied is measured. The liquid volume is estimated from the weight of the foam in the container, assuming that the liquid density is much larger than gas density. The average expansion ratio for ZrP stabilized HEX foam was 394 ± 40. This expansion ratio is slightly lower, but close to the expansion ratio obtained for foam without exfoliated ZrP nanoplates.

3.3.2 Measured wind speeds for experiments with forced convection

The average wind speed for different experiments was measured using an anemometer and reported in Table 10. There were some fluctuations in wind speeds depending on the position in which the fan was placed. A transformer was used to control the wind speed and obtain similar values for all experiments. The results from experiments with similar wind speeds were compared. It should be noted that additional turbulence may be introduced when the wind comes in contact with the foam container which acts as an obstacle. Therefore, the anemometer measurements at lower wind speeds tend to be more accurate than at higher values of wind.

Table 10: Average wind speed measurement for experiments with ZrP stabilized foam (Reprinted with permission from [5])

Experiment	Measured average wind speed (m/s)			
	without LN_2		with LN_2	
	without ZrP	with ZrP	without ZrP	with ZrP
1	0.9 ± 0.1	0.8 ± 0.1	0.8 ± 0.1	0.8 ± 0.1
2	1.9 ± 0.5	1.7 ± 0.2	1.7 ± 0.2	1.8 ± 0.2
3	2.5 ± 0.4	2.8 ± 0.2	2.8 ± 0.2	2.8 ± 0.2

3.3.3 Measured radiation intensities for experiments with thermal radiation

The thermal radiation intensity was measured using a radiation sensor and was the same in all cases as the bulb panel setup was placed at the same location and the intensity was varied using a transformer which changed the input voltage. The values for average radiation intensity are reported in Table 11.

Table 11: Average radiation intensity measurement for experiments with ZrP stabilized foam (Reprinted with permission from [5])

Experiment	Measured average radiation intensity (W/m^2)
1	60 ± 12
2	140 ± 25
3	200 ± 33
4	270 ± 50

3.3.4 Foam breakage rate measurement

Foam breakage rate is the rate at which foam breaks and is crucial to estimate the duration after which foam needs to be replenished to ensure effective vapor risk mitigation. Previous experiments illustrated the effect of forced convection and thermal radiation on HEX foam breakage rate. The current study explores these effects on HEX foam stabilized by exfoliated ZrP nanoplates. For all experiments, the foam breakage rate was estimated from the slope of a linear fit to the experimental data of change in foam height with time (Figure 28). Foam breakage rates for HEX foam stabilized by exfoliated ZrP nanoplates were measured for experiments with and without liquid nitrogen and compared with the foam breakage rates for HEX foam without exfoliated ZrP nanoplates.

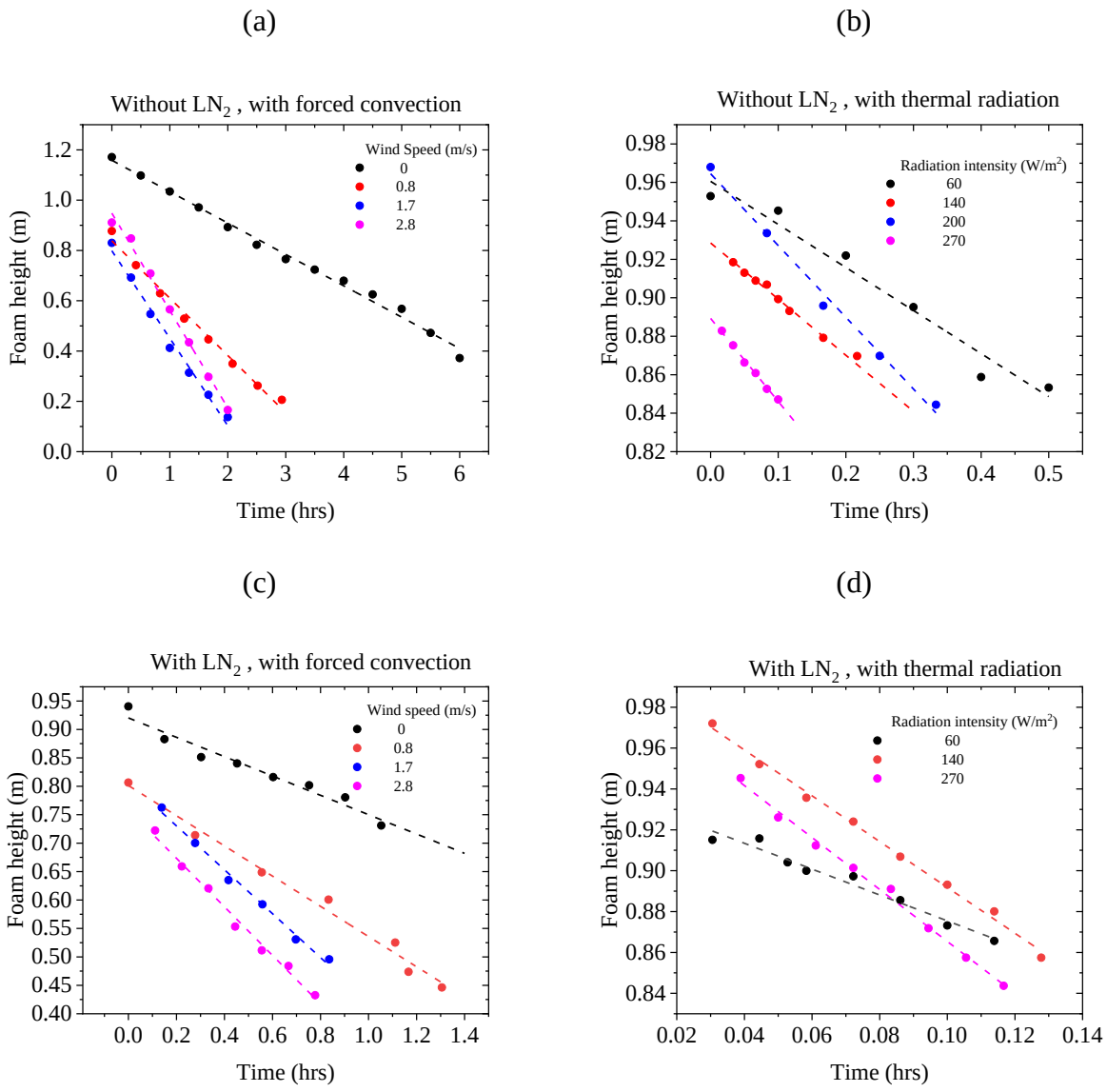

Figure 28: Foam height vs time for experiments with HEX foam stabilized by exfoliated ZrP nanoplates (Reprinted with permission from [5])

3.3.5 Experiments without liquid nitrogen

Figure 29 (a) and (b) show the results for experiments without liquid nitrogen.

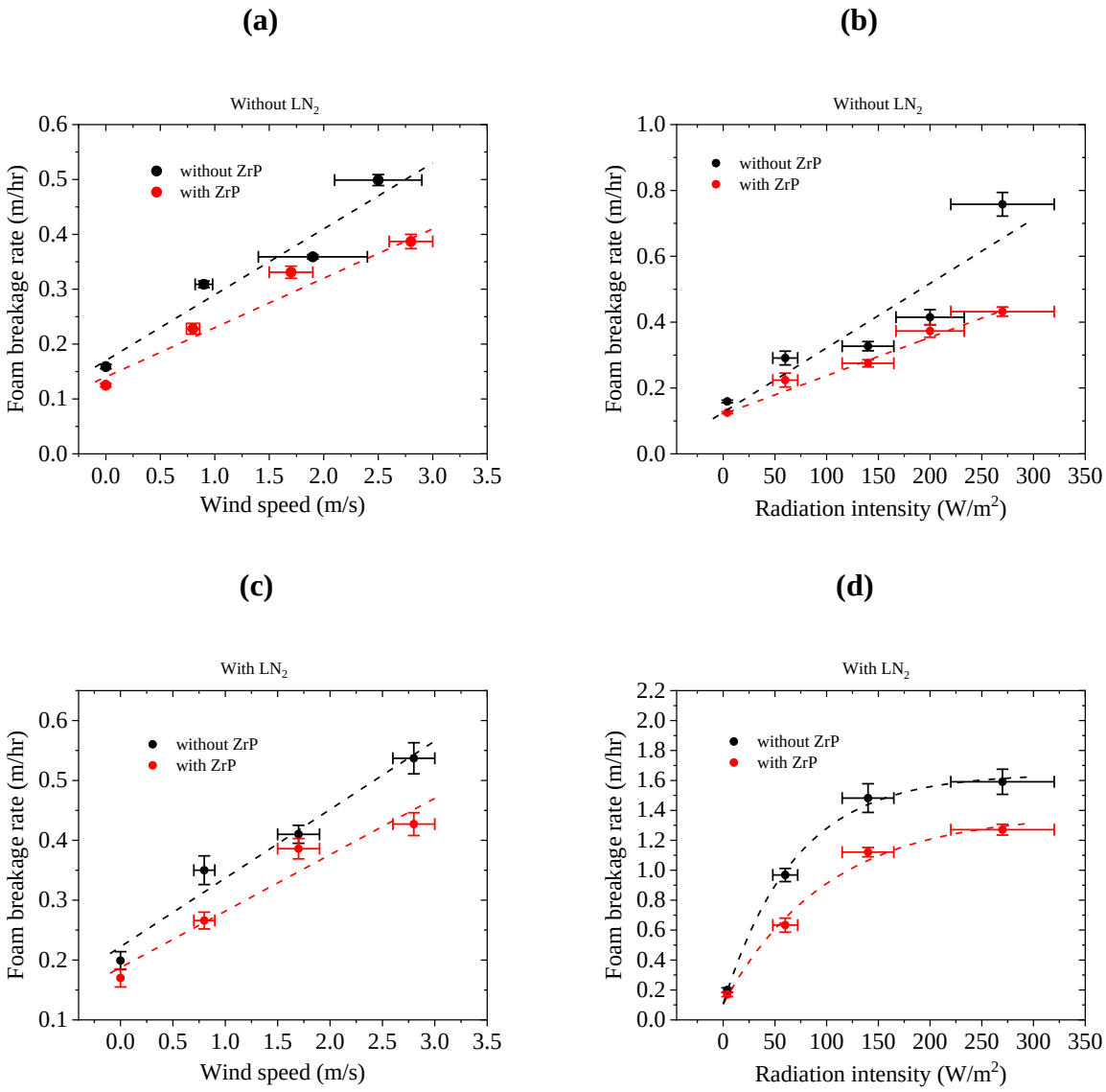

Figure 29: Foam breakage rates under forced convection and thermal radiation for HEX foam with and without exfoliated ZrP nanoplates (Reprinted with permission from [5])

Figure 29 (a) shows the effect of wind induced forced convection on foam breakage rate. It can be seen that the foam breakage rate is lower for the exfoliated ZrP nanoplate stabilized HEX foam in all cases. An increase in the wind speed seems to increase the foam breakage rate, which is similar to previous observations made from experiments without ZrP. At the highest wind speeds measured, the foam breakage rate for the foam stabilized with exfoliated ZrP nanoplates is nearly 20% lower than foam without ZrP. The magnitudes of foam breakage rates are always lower for HEX foam stabilized with exfoliated ZrP nanoplates and a linear fit through the experimental data shows a slightly lower slope for exfoliated ZrP stabilized HEX foam (Table 12).

Table 12: Equations of linear fit for foam breakage rates as a function of wind speed (Reprinted with permission from [5])

Equations of fit					
Experimental condition			**Intercept**	**Slope**	**R^2**
Forced convection	without LN_2	without ZrP	0.17 ± 0.04	0.12 ± 0.02	0.943
		with ZrP	0.14 ± 0.02	0.09 ± 0.01	0.961
	with LN_2	without ZrP	0.22 ± 0.03	0.11 ± 0.03	0.967
		with ZrP	0.19 ± 0.03	0.09 ± 0.02	0.942

Figure 29 (b) shows the effect of thermal radiation on foam breakage rate. In this case, it must be noted that the foam breakage rates are the initial foam breakage rates as the duration over which the data was collected is short. This may be attributed to the limited height over which uniform

radiation intensity is obtained within which all data is recorded. These results seem to indicate that the effect of exfoliated ZrP nanoplate addition is more pronounced at the highest radiation intensity tested (~40% reduction in foam breakage rate). A linear fit was added to this plot and there seemed to be some deviation from linear behavior for HEX foam without ZrP (Table 13). Again, the foam breakage rates were found to be lower for all cases with HEX foam stabilized with exfoliated ZrP nanoplates.

Table 13: Equations of fit for foam breakage rates as a function of radiation intensity (Reprinted with permission from [5])

Equations of fit							
Experimental condition			**Fitting Type**	**Fitting parameters**			**R^2**
Thermal Radiation	without LN_2			**Intercept**	**Slope**		
		without ZrP	Linear	0.13 ± 0.08	$2.0\times10^{-3} \pm 5\times10^{-4}$		0.855
		with ZrP	Linear	0.13 ± 0.02	$1.12\times10^{-3} \pm 9\times10^{-5}$		0.980
	with LN_2			**a**	**b**	**c**	
		without ZrP	y=a-b*exp(-c*x)	1.64 ± 0.07	1.54 ± 0.08	0.014 ± 0.002	0.999
		with ZrP	y=a-b*exp(-c*x)	1.4 ± 0.1	1.3± 0.1	0.010 ± 0.003	0.992

These results show a statistically significant reduction in foam breakage rates when foam is stabilized with exfoliated ZrP nanoplates, both with forced convection and thermal radiation.

3.3.6 Experiments with liquid nitrogen

Experiments with liquid nitrogen were performed after removing the mesh setup and placing the foam container directly on the aluminum container. Figure 29 (c) shows the effect of wind induced forced convection on foam breakage. Again, increasing the wind speed increases the foam breakage rate. The foam breakage rate for exfoliated ZrP stabilized foam seems to be nearly 20% lower than the HEX foam without ZrP at the highest wind speed tested. A linear fit shows a slightly lower slope for exfoliated ZrP stabilized HEX foam (Table 12).

Figure 29 (d) shows the effects of thermal radiation on the initial foam breakage rate. At higher radiation intensities, the foam breakage rate is higher. It can also be seen that the variation of foam breakage rate with radiation intensity is not linear (Table 13). Exfoliated ZrP nanoplate stabilized foam also has a lower foam breakage rate when compared with HEX foam without ZrP, with a 20% reduction in foam breakage rate at the highest intensity tested.

Therefore, there is a significant difference between the foam breakage rates for experiments with and without ZrP, with the exfoliated ZrP stabilized foam having a lower foam breakage rate under both forced convection and thermal radiation. This implies that it is likely that in both cases, the exfoliated ZrP stabilized foam has improved foam properties which allow it to break slowly.

The values of foam breakage rates for all experiments under forced convection and thermal radiation, are summarized in Table 14 and Table 15 respectively.

Table 14: Foam breakage rates under different wind speeds for experiments with and without ZrP stabilized foam (Reprinted with permission from [5])

Wind speed (m/s)	without LN_2		with LN_2	
	without ZrP	**with ZrP**	**without ZrP**	**with ZrP**
0	0.159 ± 0.004	0.125 ± 0.003	0.199 ± 0.015	0.170 ± 0.015
0.8	0.343 ± 0.006	0.228 ± 0.010	0.350 ± 0.024	0.266 ± 0.014
1.7	0.359 ± 0.004	0.331 ± 0.011	0.410 ± 0.015	0.386 ± 0.017
2.8	0.499 ± 0.010	0.387 ± 0.013	0.537 ± 0.026	0.427 ± 0. 019

Table 15: Foam breakage rates under different radiation intensities for experiments with and without ZrP stabilized foam (Reprinted with permission from [5])

Radiation intensity (W/m^2)	without LN_2		with LN_2	
	without ZrP	**with ZrP**	**without ZrP**	**with ZrP**
4	0.159 ± 0.004	0.125 ± 0.003	0.199 ± 0.015	0.170 ± 0.015
60	0.291 ± 0.021	0.224 ± 0.021	0.968 ± 0.044	0.633 ± 0.047
140	0.327 ± 0.014	0.275 ± 0.011	1.482 ± 0.096	1.121 ± 0.031
200	0.415 ± 0.023	0.373 ± 0.019	-	-
270	0.758 ± 0.036	0.432 ± 0.014	1.591 ± 0.084	1.271 ± 0.036

3.3.7 Vaporization rate and liquid drainage measurement

Experiments without liquid nitrogen, using the mesh setup, allowed the estimation of liquid drainage rate as a function of time with HEX foam stabilized with exfoliated ZrP nanoplates. The change in the weight of the aluminum container was the amount of liquid drained. Similarly, for

experiments with liquid nitrogen, the foam container was placed directly on the aluminum container and the change in the weight of the container allowed the estimation of the vaporization rate of liquid nitrogen. Figure 30 shows the vaporization rate and liquid drainage rates for different experiments. Figure 30 (a) shows the effect of liquid drainage on vaporization rate without forced convection or thermal radiation. Figure 30 (b) shows a similar effect under forced convection. While there is some fluctuation in the vaporization rates and liquid drainage rates, an overall trend seems to be clear from the plots. For most cases, there appears to be a trend at higher liquid drainage rates, there may not be one when the liquid drainage rate is lower. It can be seen that below a liquid drainage rate of nearly 2 kg/hr, the vaporization rates tend to be steady. This behavior is comparable with previous experiments using HEX foam without ZrP.

For the experiments with thermal radiation, steady-state could not be reached due to the duration of the experiment being limited to obtain uniform radiation intensity (Figure 31 (a)). In addition, the average liquid drainage rate is reported as there were only a limited number of points over this interval. As the standard error was high on this data, no quantitative conclusions may be made, but a possible increasing trend of liquid drainage with radiation intensity may be seen in Figure 31 (b).

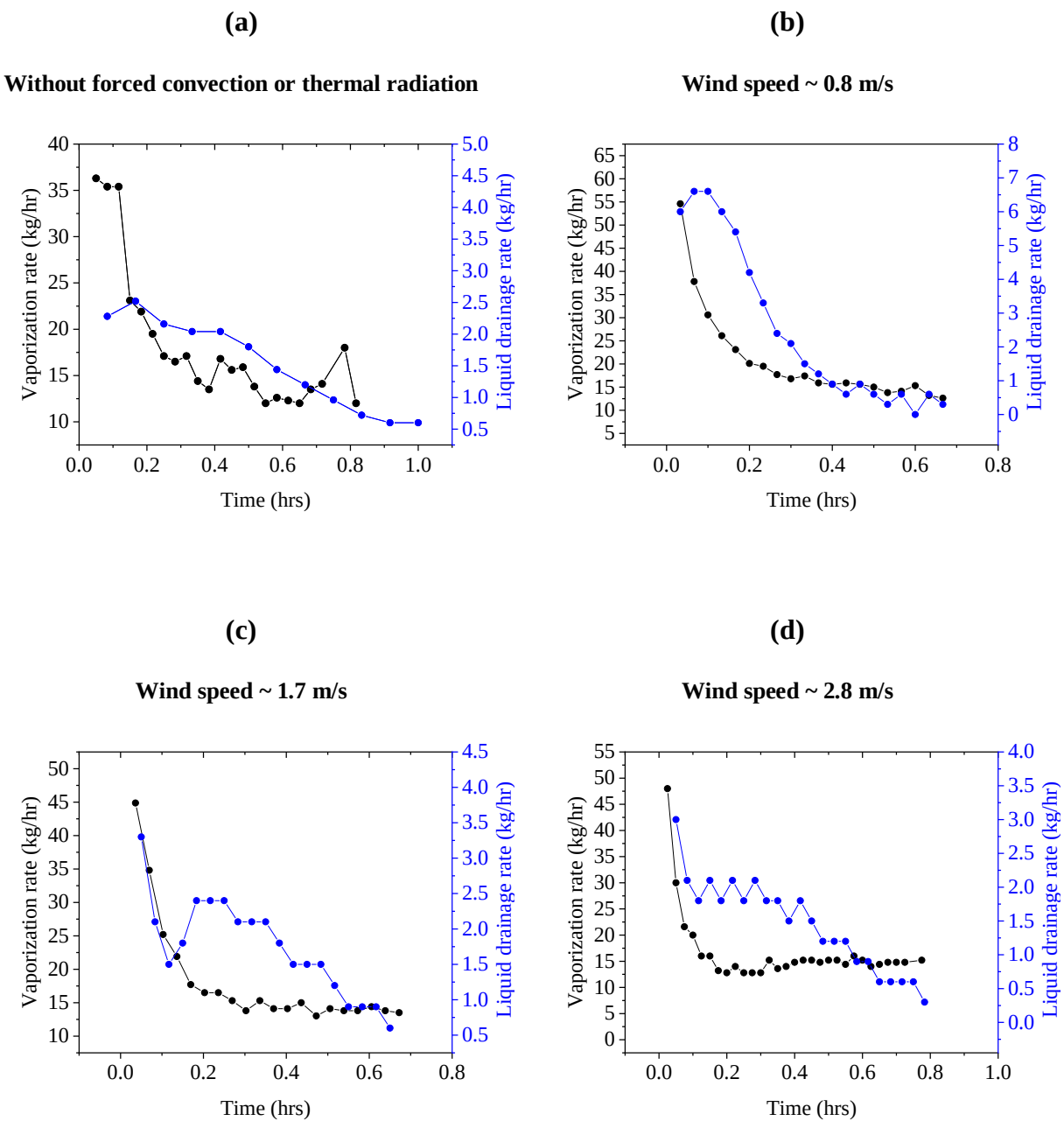

Figure 30: Vaporization rate of liquid nitrogen and liquid drainage rates for experiments with HEX foam stabilized with exfoliated ZrP nanoplates (Reprinted with permission from [5]) Exact values of measured wind speeds are reported in Table 14.

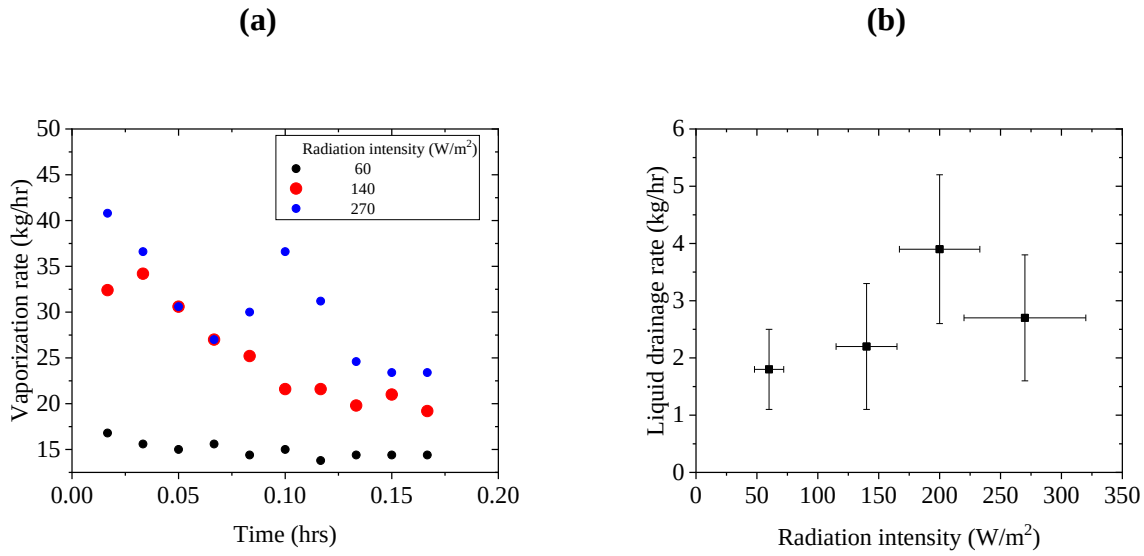

Figure 31: a) Vaporization rate under different radiation intensities for ZrP stabilized foam b) Liquid drainage rate under different radiation intensities for ZrP stabilized foam (Reprinted with permission from [5])

3.3.8 Temperature profile under forced convection and thermal radiation

The temperature profile through the foam for experiments involving HEX foam stabilized by exfoliated ZrP nanoplates were obtained using the thermocouple setup and were compared with HEX foam without ZrP. Figure 32 and Figure 33 show the temperature profile through the foam layers for one experiment with forced convection and thermal radiation respectively. These experimental results indicate that the temperatures through the foam layer seems to be either similar or slightly higher in the case of HEX foam stabilized with ZrP. This shows that exfoliated

ZrP stabilized foam continues to maintain the capability of the foam to ensure effective vapor dispersion and does not compromise on its quality.

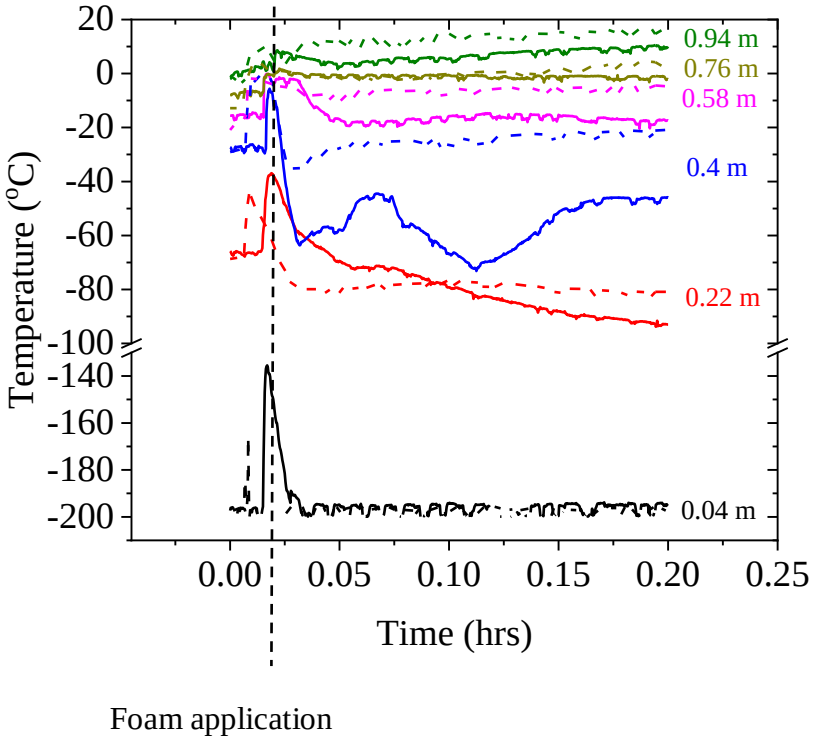

Figure 32: Temperature profile under forced convection with and without ZrP (Wind speed ~ 1.7 m/s) (Reprinted with permission from [5])
No ZrP foam shown with solid line. Exfoliated ZrP stabilized foam shown with dashed line.

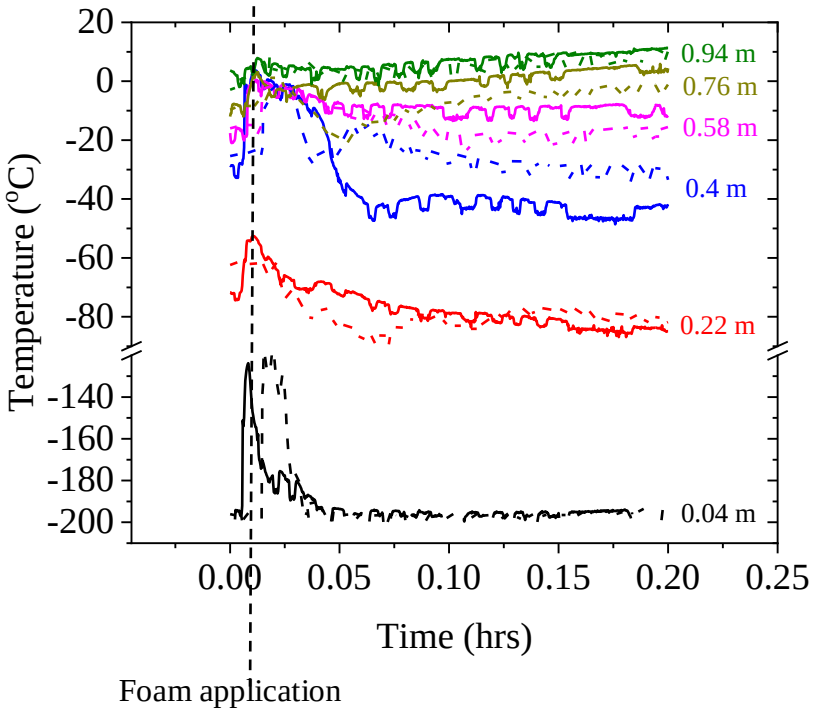

Figure 33: Temperature profile under thermal radiation with and without ZrP (Radiation intensity ~ 140 W/m^2) (Reprinted with permission from [5])
No ZrP foam shown with solid line. Exfoliated ZrP stabilized foam shown with dashed line.

3.3.9 Improvement of foam stability using exfoliated ZrP nanoplates

Foams are considered to be metastable systems due to their high interfacial energy [72]. There are several foam destabilization mechanisms, including liquid drainage from the foam over time due to gravity, diffusion of gas causing coarsening of foam, coalescence of foam due to rupture of film between bubbles, evaporation of liquid from foam which may be affected by surrounding humidity and temperature, as well as other external factors, including forced convection and thermal radiation. While these mechanisms contribute to foam instability, it is crucial to ensure high foam stability for its application on LNG. This ensures that the foam blanket over spilled LNG is effective for a long duration, allowing sufficient heat exchange between the foam layers and rising vapors.

There have been several previous efforts to improve the stability of foam using nanoparticles [33, 71, 75, 76]. Guevara *et al.* and Zhang found that these particles may be contributing to enhanced foam stability due to the particles controlling Ostwald ripening and also potentially lower liquid drainage by acting as an obstacle to liquid flow [33, 71]. This phenomenon is illustrated in Figure 9.

Zhang studied the effect of application of exfoliated ZrP nanoplate stabilized foam on cryogenic liquids, to understand its ability in mitigating the vapor risk of LNG spills [71]. However, these experiments involved small-scale tests, with foam production by shaking test tubes, which introduces the possibility of non-uniformity in foam properties, especially its expansion ratio. This work focused on overcoming some of these issues by carrying out experiments on a larger

scale and the use of a foam generator for uniform foam properties. The results from these experiments corroborate the results obtained previously from small benchtop tests by Zhang, indicating that exfoliated ZrP nanoplates can contribute to enhancing foam stability when added to surfactant solutions to produce HEX foam. For all experiments, with and without liquid nitrogen, the foam breakage rate was found to be lower for exfoliated ZrP nanoplate stabilized foam.

For experiments with forced convection, there appears to be a linear increase in foam breakage rate with wind speeds for experiments with and without ZrP. From Table 12, the slopes of fits to the data appear to be similar with and without liquid nitrogen but the intercepts are higher for the experiments with liquid nitrogen. This may be because of the interaction of the cryogenic liquid with the foam which results in the foam breaking faster, mainly as soon as it is applied.

For experiments with thermal radiation, there is an increase in foam breakage rate with increasing radiation intensity for experiments without liquid nitrogen. However, with liquid nitrogen the trend does not appear to be linear (Table 13). The foam breakage rate increases with increasing intensity but the rate of its change seems to reduce. Possible explanations for this behavior are discussed here. Increasing the radiation intensity can increase the rates of evaporation of liquid from the foam. Once the liquid fraction falls below a critical value, the process of coalescence may be dramatically enhanced, increasing the foam breakage rate [73]. Magrabi *et al.* analyzed the evaporation rates as a function of radiation intensity for low and medium expansion foams and found that these rates level off under high radiation intensities between 30-40 kW/m^2 [86]. They attributed this behavior to the mass transfer limitations of the

foam layer, resulting in much of the heat being conducted by the foam. In addition, such behavior should be expected even in the case without liquid nitrogen, which is not the case. However, it should be noted that the type of foam used for this study has a high expansion ratio and the radiation intensities used in this work are lower. Another possible reason could be that as the foam is applied on the cryogenic liquid, vapor channels are formed, which allow the vapor to gush out. It is possible that this allows the thermal radiation from the source to be transmitted to layers below the uppermost foam layer through the vapor channels causing an increase in the evaporation rate. This is expected to increase with radiation intensity, but as the radiation intensity is not going to change uniformly with height (beyond the region under consideration), it is likely that this behavior will be non-linear. The magnitude of the foam breakage rates also seems to be significantly higher than the other cases. Some of this may be attributed to the fact that the experiments with thermal radiation record initial foam breakage rates, as there was a limited duration over which uniform radiation intensity could be maintained for the experiments and the effect of the cryogenic liquid interaction with foam is higher immediately after foam application, which occurs at the beginning of the experiment.

3.3.10 Effect of formation of vapor channels on foam breakage rates

In order to further investigate the hypothesis that the presence of the vapor channels may be influencing the foam breakage rate under radiation, a set of experiments were carried out. These experiments involved modifying the experimental apparatus to generate a vapor channel by

passing air through the foam, as shown in Figure 34. The overall goal was to simulate vapor channels without liquid nitrogen and study the effect of radiation on foam breakage.

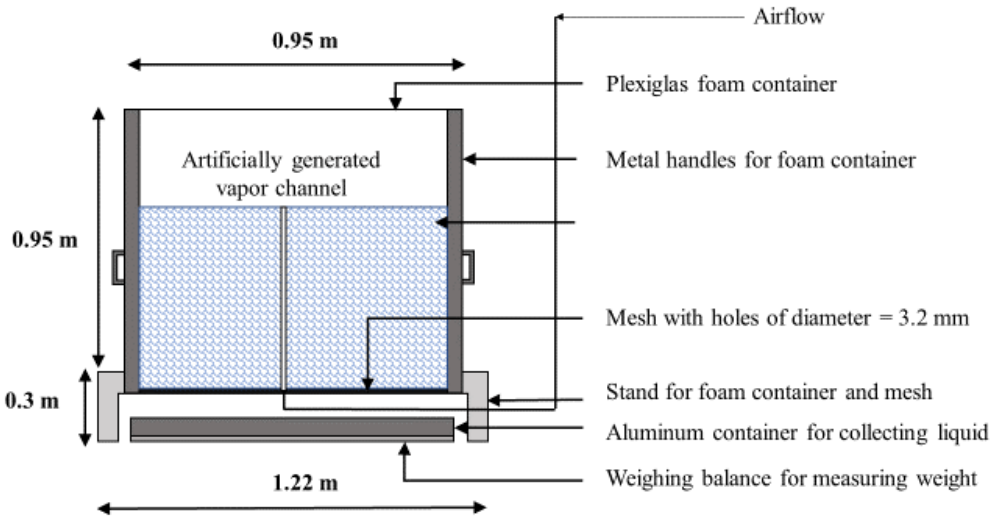

Figure 34: Experimental setup for inducing vapor channels through foam using air flow

Experiments were carried out at different radiation intensities, similar to those used previously in experiments with radiation. Figure 35 shows the variation of foam breakage rate with vapor channels and how it compares to the experiments with and without liquid nitrogen, as a function of radiation intensity (Table 16 shows equations of fit). It can be seen that, even with one vapor channel, shown in read, there is a significant increase in foam breakage rate. The overall profile is similar to the case with liquid nitrogen. The increase in foam breakage rate is however, higher

for the case with liquid nitrogen, in which case there is an effect of contact with the cryogenic liquid as well as additional vapor channels (3-5 vapor channels observed). It should also be noted that the flow rate of the air through the foam, to generate the vapor channel was adjusted such that the diameter of the vapor channel is close to that observed experimentally (~ 5 cm). However, having higher flow rates of air may induce the foam to break faster. These results show that it is likely that the presence of vapor channels may induce an increased foam breakage rate in the presence of thermal radiation.

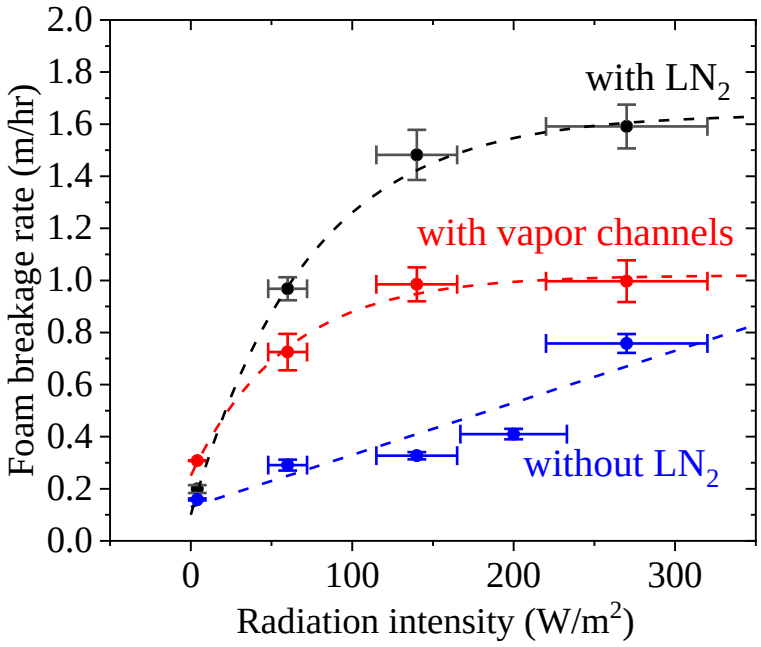

Figure 35: Foam breakage rate as a function of radiation intensity with vapor channels, when compared to the case with and without LN_2

Table 16 : Equations of fit for foam breakage rates as a function of radiation intensity for experiments verifying the effect of vapor channels

Equations of fit					
Experimental condition	**Fitting Type**	**Fitting parameters**			**R^2**
		Intercept	**Slope**		
without LN_2	Linear	0.13 ± 0.08	$2.0\times10^{-3} \pm 5\times10^{-4}$		0.855
		a	**b**	**c**	
with LN_2	y=a-b*exp(-c*x)	1.64 ± 0.07	1.54 ± 0.08	0.014 ± 0.002	0.999
with vapor channels		1.02 ± 0.04	0.77 ± 0.06	0.017 ± 0.004	0.994

3.3.11 Vaporization rate and liquid drainage for foam stabilized with ZrP nanoplates

The use of the mesh setup also allowed the study of the influence of liquid drainage rate on the vaporization rate of the cryogenic liquid. It may be concluded from Figure 30 that at higher liquid drainage rates (usually over 2 kg/hr), there may be a relationship between liquid drainage rate and vaporization rate of the cryogenic liquid. However, at lower values of liquid drainage rate, this relationship seems to be much less obvious. It is possible that when the liquid drainage rates are lower, the heat transfer is primarily through conduction from the walls of the container and is not significantly affected by boil-off due to liquid drainage.

3.3.12 Mechanism of foam stabilization using ZrP nanoplates

From Figure 36, it can be seen that for experiments with HEX foam with and without ZrP the liquid drainage rates are similar. This implies that it is possible that the stabilizing mechanism for the ZrP nanoplates may not necessarily be only by controlling the liquid drainage but also by controlling the diffusion of gas between foam bubbles, limiting Ostwald ripening. However, more experiments verifying and quantifying this observation are necessary to confirm this conclusion.

The measurement of temperature through the foam layers indicates that HEX foam stabilized with exfoliated ZrP nanoplates continue to provide the necessary heat for the rising vapors. As these vapors rise through the foam layers, they exchange heat, increasing their temperature and become lighter. This allows ease of dispersal of these vapors.

For broader industrial application, the commercial viability of exfoliated ZrP nanoplates is crucial. While some of the chemicals used in the synthesis may be expensive, research efforts to identify alternatives may be a viable option. In addition, more experiments considering different concentrations of ZrP nanoplates will allow identifying optimum conditions for maximum foam stability.

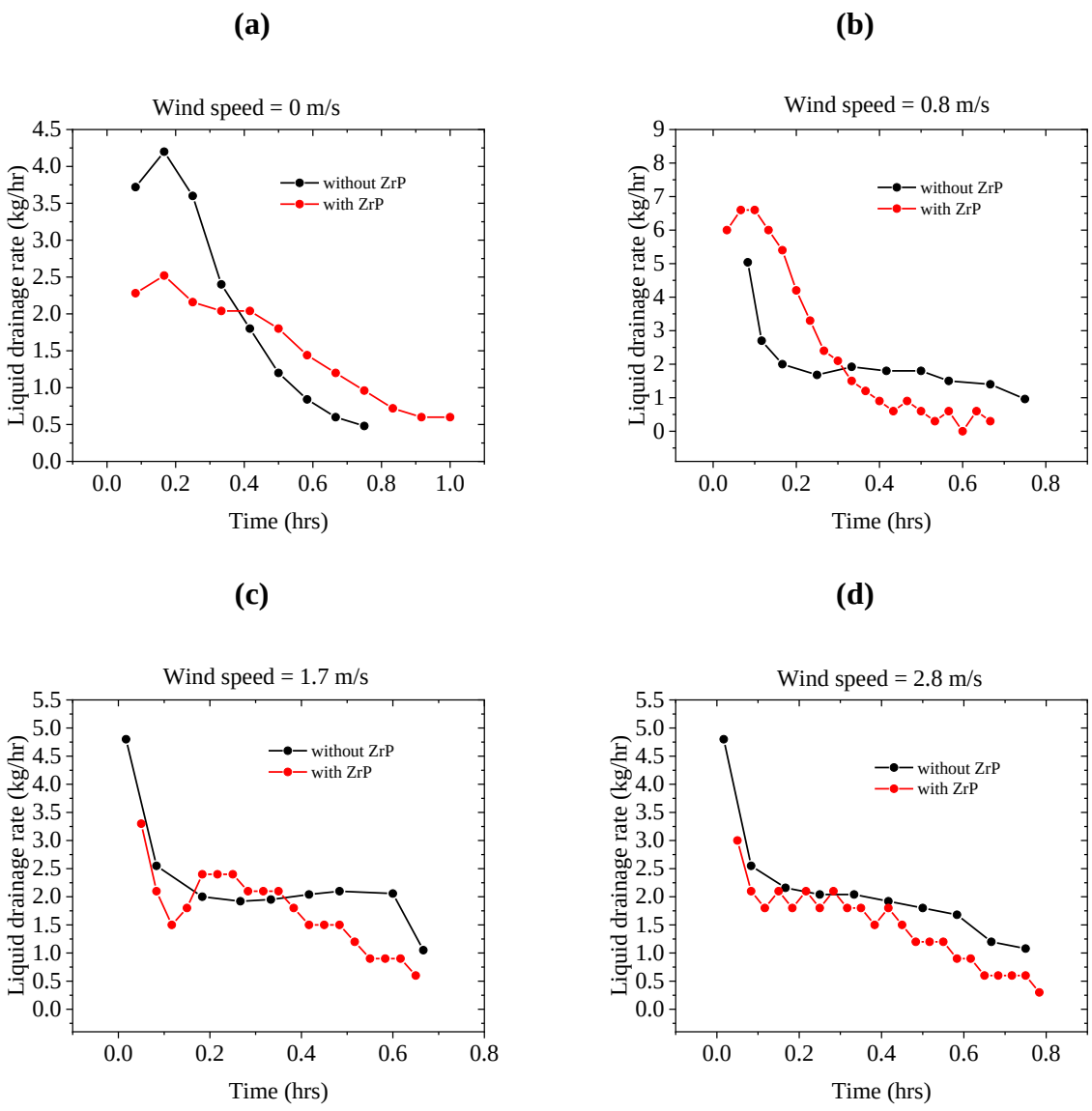

Figure 36: Liquid drainage rates comparison between experiments with HEX foam with and without exfoliated ZrP nanoplates (Reprinted with permission from [5])

3.4 Summary

In summary, exfoliated ZrP nanoplates can stabilize high expansion foam: ZrP stabilized foam reduced foam breakage rates up to 43 ± 7 %. Liquid drainage from nanoplate stabilized HEX foam may affect vaporization rate of cryogenic liquid, when liquid drainage is high (>2 kg/hr). Addition of ZrP nanoplates may not affect liquid drainage from HEX foam indicating that other mechanisms such as reduced gas diffusion or reduced coalescence may be contributing to foam stability. Foam likely maintains its ability to disperse vapor even with addition of nanoplates as the temperature profiles with and without ZrP are similar.

4 HEAT TRANSFER MODEL TO ESTIMATE HEX FOAM HEIGHT FOR LNG VAPOR RISK MITIGATION

4.1 Introduction

The National Fire Protection Association (NFPA) recommends the use of high expansion (HEX) foam for liquefied natural gas (LNG) vapor risk mitigation [30]. The role of foam application is to not only create a blanket over the LNG spill to reduce the vaporization rate, but to also transfer heat to the LNG vapors as they pass through the foam layers, making them lighter and easier to disperse in the atmosphere. The overall objective for the development of the heat transfer model is to predict the height of the foam that needs to be applied to ensure effective vapor risk mitigation. To achieve this, a simple model based on heat transfer between foam and the LNG vapors is developed to help with this prediction. A detailed explanation behind the idea for this model has been provided here.

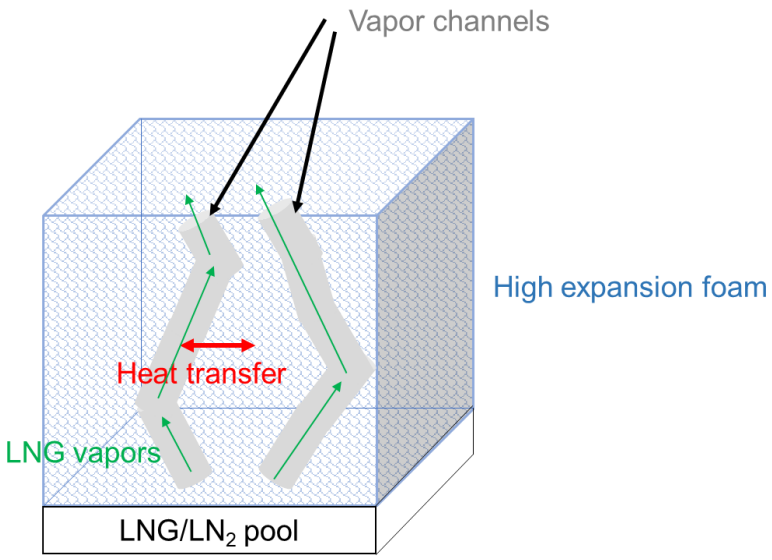

Figure 37: Schematic for the warming effect of LNG vapors by foam

The "warming effect" of the foam occurs as the LNG vapors pass through the foam layers, exchange heat, become lighter and are dispersed in the atmosphere (Figure 37). In order to mitigate the vapor risk, it is necessary to ensure that the vapor is dispersed effectively. The physical property which is most relevant in this case is the density of the LNG vapors. At room temperature, methane, which is the major constituent of LNG has density higher than air. However, at lower temperatures, closer to its boiling point, it has a density greater than air. When the density of the LNG vapors becomes less than air, it can disperse in the atmosphere. Considering methane, which is usually the major constituent of LNG, the density of methane becomes equal to air at nearly -106 ^{o}C, or 167 K (Figure 27). This is considered to be the threshold to which the average LNG vapor temperatures must be so that they can disperse in the atmosphere.

The goal of the heat transfer model is to get insight into the heat transfer behavior to predict how high the foam must be to ensure that the vapors are at least neutrally buoyant to be dispersed effectively in the atmosphere. Therefore, the height of the foam required for the outgoing vapors to have a temperature greater than 167K is considered to be the minimum height of the foam required.

4.2 Model development

A simplified heat transfer model was developed to obtain the temperature profile through the vapor channels, to estimate the minimum height of the foam for the vapors to get dispersed in the atmosphere easily (Figure 39). The criteria used was that the average temperature of the outgoing vapors of methane should be greater than 167 K, as described earlier.

Some of the main assumptions made by the model have been summarized here:

- The system has attained a steady state and the heat transfer occurs under a constant vaporization rate.
- The temperature profile through the foam is homogeneous and does not depend on the amount of foam applied.
- The vapor channel has a cylindrical geometry and is surrounded with the foam represented by the wall boundary condition.
- The outlet of the vapors is assumed to be to the atmosphere.
- The heat transfer coefficient is constant, and is equal to 10 $W/m^2/K$, a general value used for convective heat transfer coefficient for air [67].
- The vapors are nitrogen instead of LNG vapors.
- The effects of gravity are neglected.

Experiments performed show that the heat transfer occurs inside the vapor channels through which the LNG vapors escape to the atmosphere (Figure 37). These vapor channels are not necessarily straight, therefore the LNG vapors try to break through the foam through weak points

in the foam and try to find their way out. For simplicity, it is assumed that the vapor channel is a single cylinder surrounded by foam. It was also observed from the experiments that between 3 and 5 vapor channels were formed in a 1 m^2 area. In this case, we consider only one vapor channel and take the foam as a boundary condition, assuming that the interactions within the foam are negligible and the temperature profile is uniform throughout the foam.

From the experiments, through data fitting, we obtain the temperature profile through the foam (Figure 38): $T=17 - 210*e^{-3.5*x}$ ^oC (Temperature profile through the foam and frozen foam)

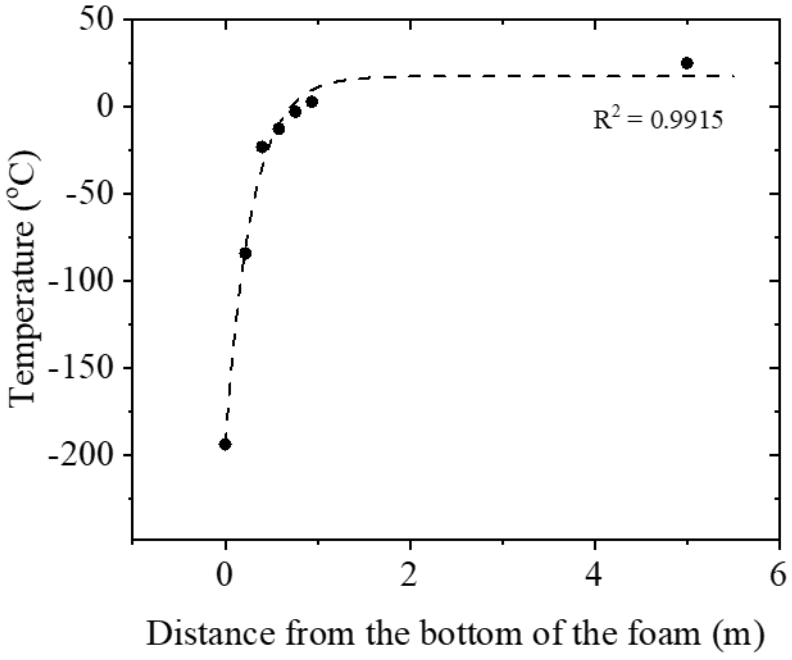

Figure 38 : Temperature profile through the foam

Table 17: Fitting parameters for the temperature profile

Equation type: y = a + b*exp(-cx)	
Parameter	**Value**
a	17 ± 6
b	-210 ± 10
c	3.5 ± 0.4
R^2	0.9915

For this fit, it is assumed that far from the foam (~5m) the temperature is close to room temperature (298 K). The goal is to run simulations to develop a steady-state hat transfer model to provide insights on the heat transfer behavior so that the outlet temperature of the vapors may be estimated.

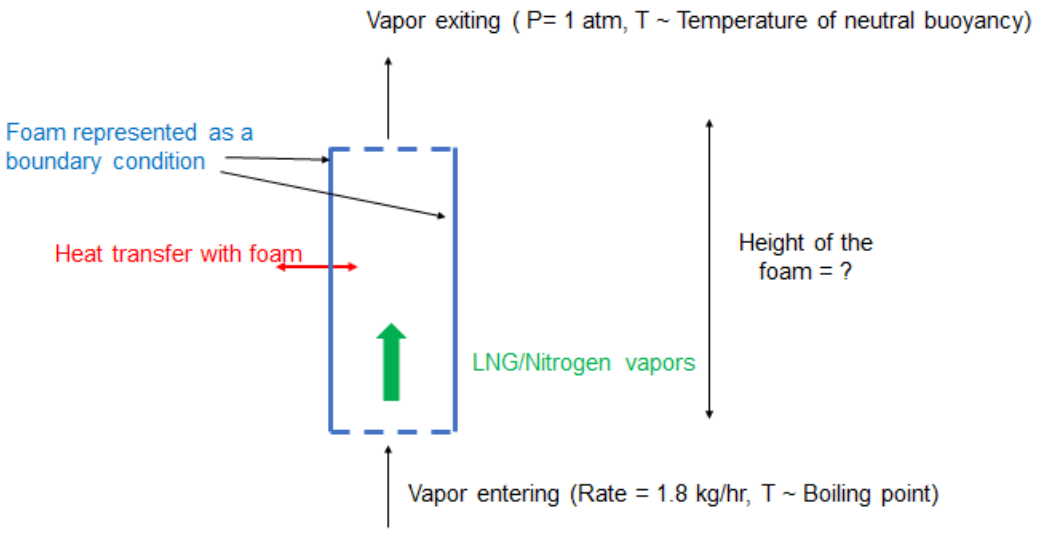

Figure 39: Schematic showing the overall model development

4.2.1 Governing equations

The governing equations of the flow under steady state were as follows (modified from ANSYS Fluent® 6.3 user guide):

The equation of continuity: $\nabla.\left(\rho\vec{V}\right) = 0$

where, ρ is the density of the fluid, $\vec{V}$ is the velocity of the fluid

The momentum equation: $\nabla.\left(\rho\vec{V}\vec{V}\right) = -\nabla p + \nabla.(\bar{\bar{\tau}})$

where, p is the static pressure, $\bar{\bar{\tau}}$ is the stress tensor

$$\bar{\bar{\tau}} = \mu\left[\left(\nabla\vec{V}+\nabla\vec{V}^{T}\right) - \frac{2}{3}\nabla.\vec{V}I\right]$$

where, μ is the molecular viscosity, I is the unit tensor

The energy equation: $\nabla.\left(\vec{V}(\rho E + p)\right) = \nabla.(k_{eff}\nabla T)$

where, $E = \int_{T_{ref}}^{T} c_p dT$

where, c_p is the specific capacity of the fluid, T is the temperature of the fluid,

T_{ref} is the reference temperature, and k_{eff} is the effective conductivity

Turbulence model - k-ϵ model:

$$\frac{\partial(\rho k u_i)}{\partial x_i} = \frac{\partial\left[\left(\mu+\frac{\mu_t}{\sigma_k}\right)\frac{\partial k}{\partial x_j}\right]}{\partial x_j} + G_k - \rho\epsilon - Y_M$$

$$\frac{\partial(\rho\epsilon u_i)}{\partial x_i} = \frac{\partial\left[\left(\mu + \frac{\mu_t}{\sigma_\epsilon}\right)\frac{\partial\epsilon}{\partial x_j}\right]}{\partial x_j} + \frac{C_{1\epsilon}\epsilon G_k - C_{2\epsilon}\rho\epsilon^2}{k}$$

where, u_i is the velocity along i direction, x_i is the distance along i direction,

x_j is the distance along j direction, k is the turbulence kinetic energy,

ϵ is the rate of dissipation of turbulence energy,

$C_{1\epsilon}$ and $C_{2\epsilon}$ are constants, σ_k and σ_ϵ are Prandtl numbers for k and ϵ

μ_t is the turbulent viscosity, $\mu_t = \frac{\rho C_\mu k^2}{\epsilon}$, C_μ is a constant

The values for the constants are taken as follows:

$C_{1\epsilon}=1.44$ $C_{2\epsilon}=1.92$ $C_\mu=0.09$ $\sigma_k=1.0$ $\sigma_\epsilon=1.3$

G_k is the turbulence kinetic energy due to mean velocity gradients

$$G_k = -\rho\overline{u_i' u_j'}\left(\frac{\partial u_j}{\partial x_i}\right)$$

where, $-\rho\overline{u_i' u_j'}$ is the apparent stress in fluctuating velocity (Reynolds stress)

Using Boussinesq hypothesis, $G_k=\mu_y S^2$

where, $S=\sqrt{2S_{ij}S_{ij}}$ is the modulus of the mean rate of strain tensor,

Y_M is the dilatation dissipation, $Y_M=2\rho\epsilon M_t^2$,

where, $M_t=\sqrt{\frac{k}{c^2}}$, $c=\sqrt{\gamma RT}$ is the speed of sound and $\gamma=c_p/c_v$

and, c_p, c_v are the specific heats at constant pressure and constant volume respectively.

4.2.2 Boundary conditions

The boundary conditions were as follows:

Inlet boundary condition

The steady state vaporization rate of liquid nitrogen from the foam is nearly 10 kg/hr. We assume that there are roughly 3-5 vapor channels that are formed and that some vapor escapes from the sides and through areas where the foam application is not complete, based on the based on experimental observation. The location of the vapor channels tends to change with time. Therefore, an approximate value of 1.8 kg/hr was chosen as the mass flow rate and the inlet temperature was set as 80 K, close to the boiling point of nitrogen.

Outlet boundary condition

The outlet is exposed to the atmosphere. Therefore, a pressure outlet boundary condition is used.

Wall boundary

A wall boundary condition is used for the outer wall with no slip boundary conditions for momentum and heat transfer through convection for the energy equation. The heat transfer

coefficient from literature for air is close to 10 $W/m^2/K$ and this is used as a reasonably acceptable value [67]. The temperature profile through the foam, obtained from experiments is used as the free stream temperature.

The governing equations and boundary conditions are then solved in a computational fluid dynamics (CFD) simulation model developed in ANSYS Fluent®.

4.3 CFD simulations

4.3.1 Design

The Design Modeler from Workbench is used to develop a simplified two dimensional, axi-symmetric model, considering the vapor channel to be of a diameter of 5 cm, height of 2 m (Figure 40). To achieve this, a rectangle of size 0.025 by 2 m is drawn which is then assumed to be symmetric about the axis. The surface is generated from the sketch and the object is generated. Please note that the surface is sketched parallel to the x-axis so that the axi-symmetric boundary condition may be used in Fluent®.

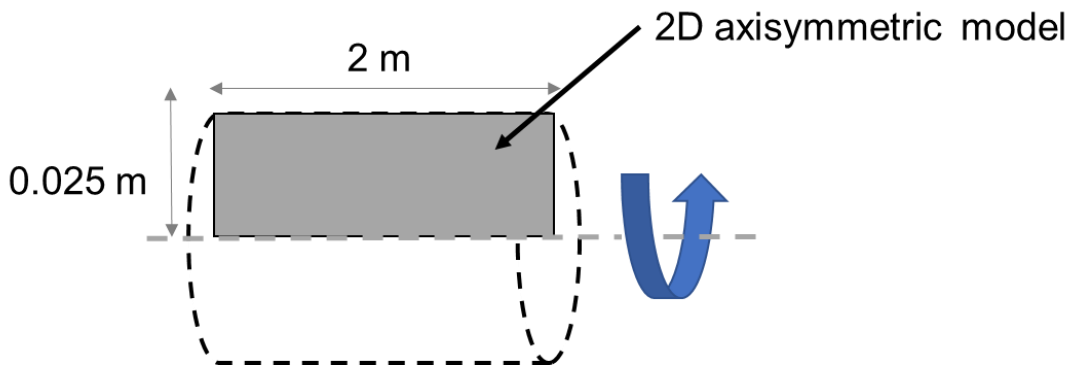

Figure 40: Schematic of the 2D axisymmetric model design

4.3.2 Meshing

Once the design was completed, an appropriate uniform mesh was added to the above object (Figure 41). A maximum face size/maximum size of 0.005 was chosen and the mesh was generated. The number of elements in the mesh were 2,000. The maximum face size/maximum size were then decreased to establish mesh independence. Each boundary (edge) was also labeled for ease of defining boundary conditions during setup. The mesh quality (0.997) and skew (0.003) are also evaluated to ensure the quality is good and skew is minimum.

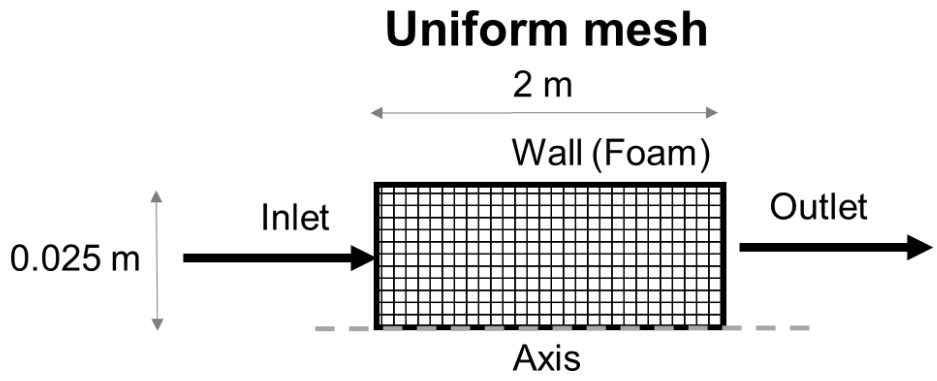

Figure 41: Schematic of the mesh in the model

4.3.3 Model setup

Once the mesh was setup, the rest of the model was setup on Fluent®. The model was setup as 2D, axi-symmetric with a pressure-based solver, under steady state. The energy equation was turned on and k-epsilon turbulence model was used. Nitrogen was used as the fluid/gas.

The following boundary conditions were used:

- Inlet– Mass Flow inlet
- Outlet– Pressure outlet
- Wall along the x axis (bottom) – Axis
  - Since the rectangular shape is used to establish a cylindrical hole (vapor channel) with foam on the side, axis boundary condition is used.
- Wall on top (Foam) – Wall
  - The temperature profile through the foam is set as a user defined function and fed as the free stream temperature:

```
#include "udf.h"
DEFINE_PROFILE(T_profile, thread, i)
 {
   real y[ND_ND];    /* this will hold the position vector */
   real x;
   face_t f;
   begin_f_loop(f,thread)
    {
```

```
    F_CENTROID(y,f,thread);
    x = -3.502495*y[0];
    F_PROFILE(f,thread,i) = 273 + 17.44632 - 211.4782 * exp(x);
   }
  end_f_loop(f,thread)
}
```

The residuals used for the model were their default values: 10^{-3} for the continuity equation, x, y velocities, k and ϵ, and 10^{-6} for the energy equation. ANSYS Fluent® uses a finite volume technique to solve the partial differential equations. A pressure-based solver was used. The scheme used to solve the equations was SIMPLE algorithm with spatial discretization involving second order upwind for the momentum and energy equations, second order for pressure and first order upwind for turbulent kinetic energy and dissipation rates. The values were initialized through hybrid initialization.

4.4 Model validation

Before using the CFD simulation model to obtain the temperature profile through the foam, the validation and mesh independency of the model was established. To validate the model, experimental results from previous work was obtained and compared with the model. The only results available were that of the outlet vapor temperature and therefore, only those were compared for a foam of height 2 m. Takeno *et al.* (1996) observed a vaporization rate close to 1.8 kg/hr (in each vapor channel) and reported the outlet temperature as a range between -5 and -20 ^{o}C [9]. Please note that the vaporization rates were calculated from the experimentally reported values while accounting for the presence of vapor channels and some loss.

The results from the simulation for the average outlet temperature were obtained and compared with the experimental result. In addition, a mesh independence analysis was also performed. Since the variable evaluated will be the outlet temperature, it was the variable analyzed for checking if the solution is mesh independent. The results obtained from the simulations are shown in Figure 42.

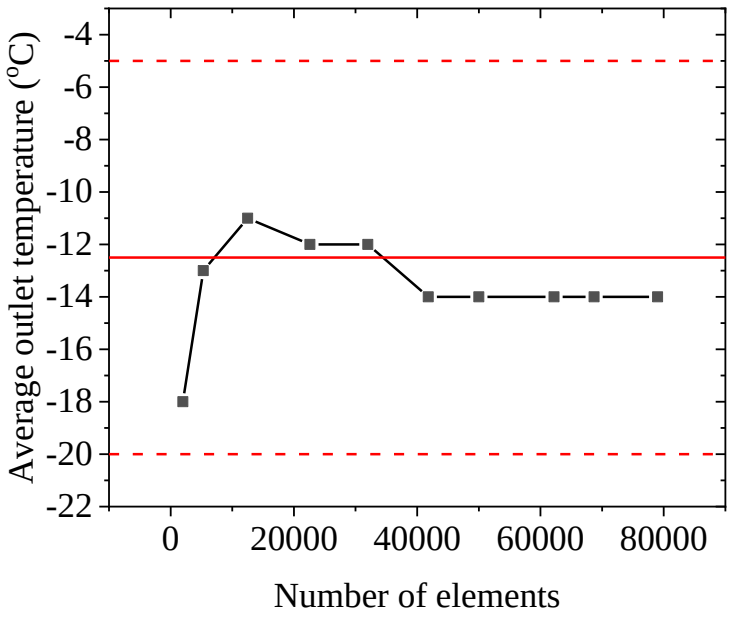

Figure 42 : The experimental result for outlet vapor temperature by Takeno *et al.* (Mass flow rate = 1.8 kg/hr) has been shown in red with the average value shown as a solid line and the dashed lines show the range of the values

From Figure 42, it is seen that the solution becomes mesh independent when the number of elements is greater than 50,000. Also, the simulation results appear to lie within the range of values for Takeno *et al.* [9].

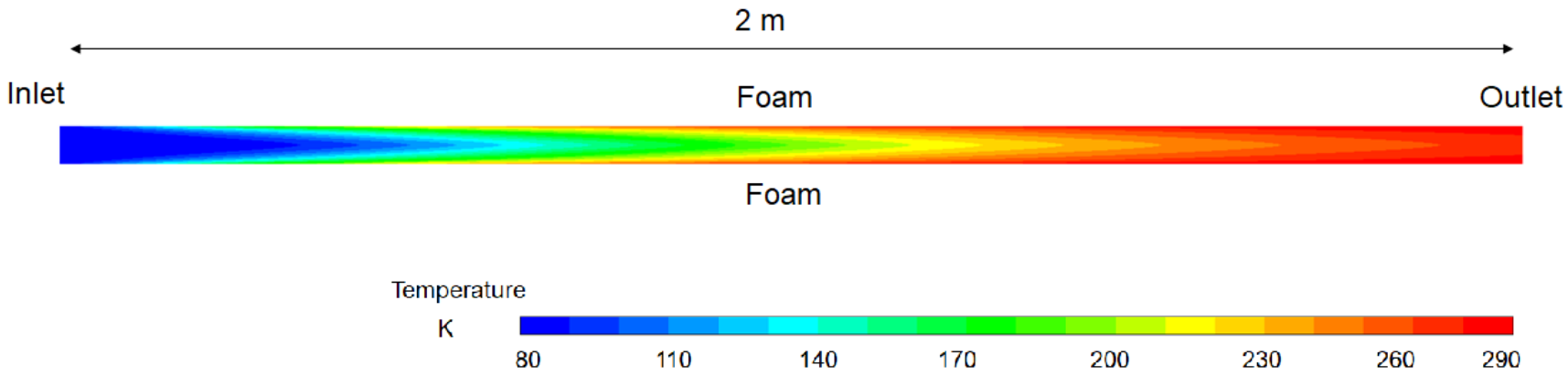

Figure 43: Overall Temperature profile through foam for LN_2

Figure 43 shows the overall temperature profile through the vapor channel. The temperature of the foam boundary changes with height and as heat is transferred to the vapors, under steady state, they get warmer.

4.5 Model results

Once mesh independence was established and the mode validation complete, multiple simulations (with max. mesh size = 10^{-3} m, which is ~50,000 elements for 2 m height) were run with methane (vapor inlet at its boiling point, T = 112 K) to identify the minimum foam height when the outlet vapor temperature is uniformly over 167K. Figure 44 shows the temperature profile at the outlet for different foam heights with an inlet temperature close to methane's boiling point and the same mass flow rate (1.8 kg/hr). It can be observed that close to 1.2 m foam height the temperature profile shows the vapors to be at least neutrally buoyant.

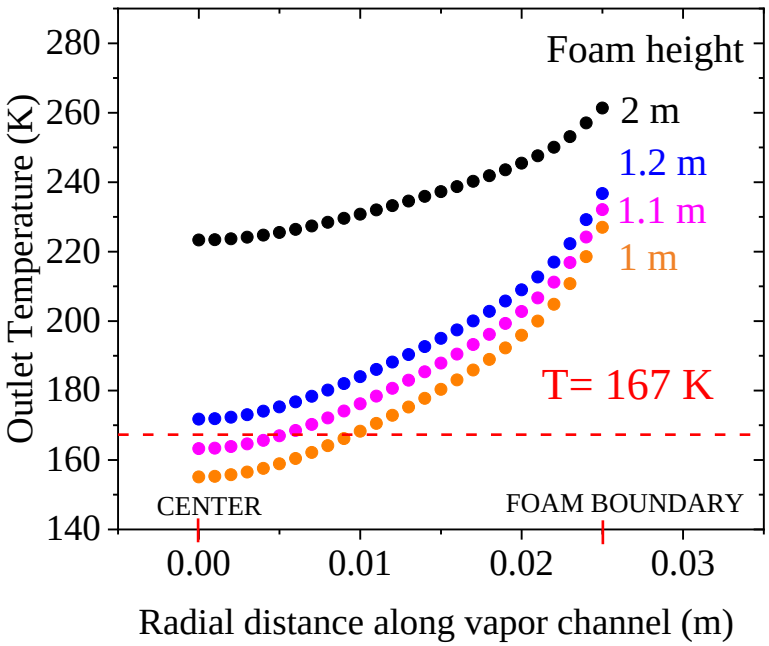

Figure 44: Different outlet temperature profiles for foam of different heights

4.6 Parametric sensitivity analysis

A parametric sensitivity analysis on the effect of vaporization rate, diameter of the vapor channel and heat transfer coefficient on the minimum height of the foam has been carried out here. This is to perform a sensitivity analysis on some of the variables assumed. We consider the effect of vaporization rate and diameter of the vapor channel on the height of the foam required. The criteria used is that the minimum outlet vapor temperature is greater than 167 K.

Figure 45 and Figure 46 show the effect of vaporization rate and diameter of the vapor channel on the height of the foam required.

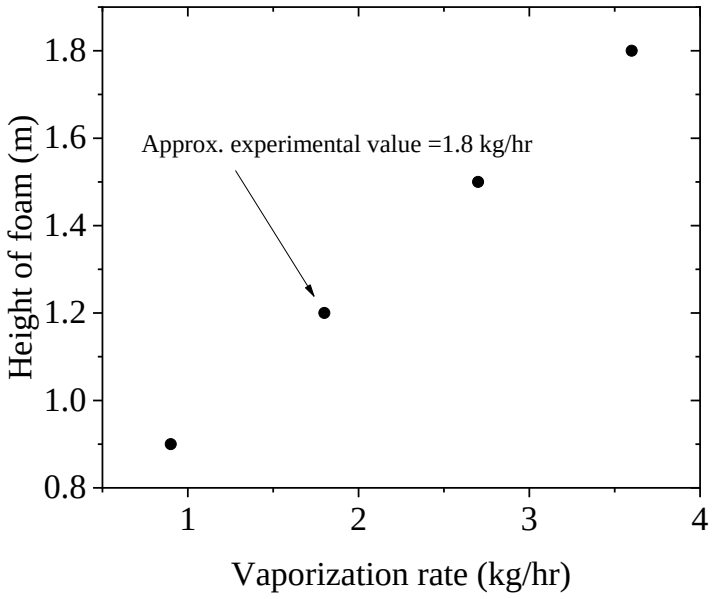

Figure 45: Effect of vaporization rate on height of foam required

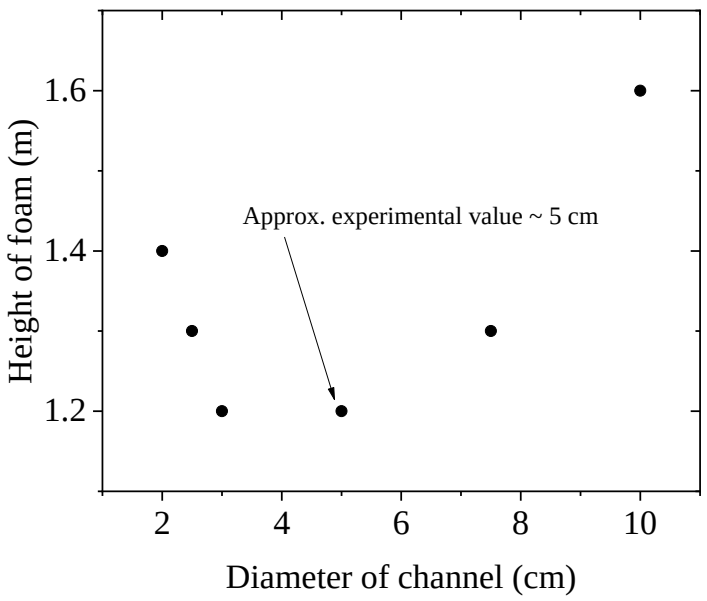

Figure 46: Effect of diameter of vapor channel on height of the foam required

From Figure 45, it is clear that increasing the vaporization rate increases the height of the foam required. This is because increasing the vaporization rate increases the velocity of the vapors flowing through the foam, which in turn reduces the time for heat transfer to occur while passing through the foam.

From Figure 46, it can be seen that increasing the diameter initially decreases the height of the foam required. This is because increasing the diameter decreases the velocity of the vapors flowing through the vapor channel and is seen in Figure 47. However, increasing it further, increases the height as well, because it increases the distance from the foam boundary, which allows the vapors in the middle to pass through without much heat transfer occurring.

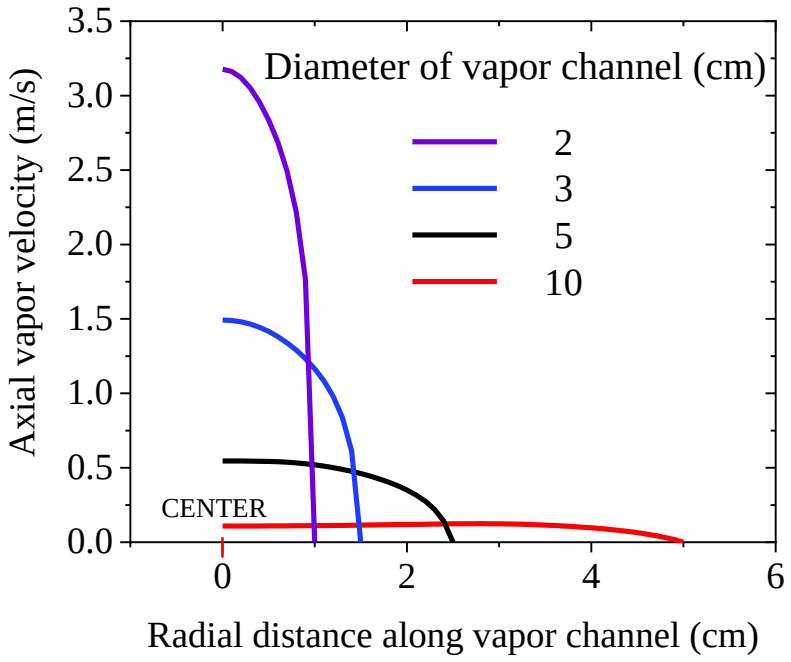

Figure 47: Change in velocity with diameter of vapor channel

From Figure 48, it is clear that increasing the heat transfer coefficient increases the height of the foam required. At lower values of the heat transfer coefficient, the height of the foam required decreases at a greater rate than at higher values. This trend can be explained by the fact that higher the heat transfer coefficient implies higher the amount of heat transfer occurs, making the vapors warmer even with a smaller height of the foam.

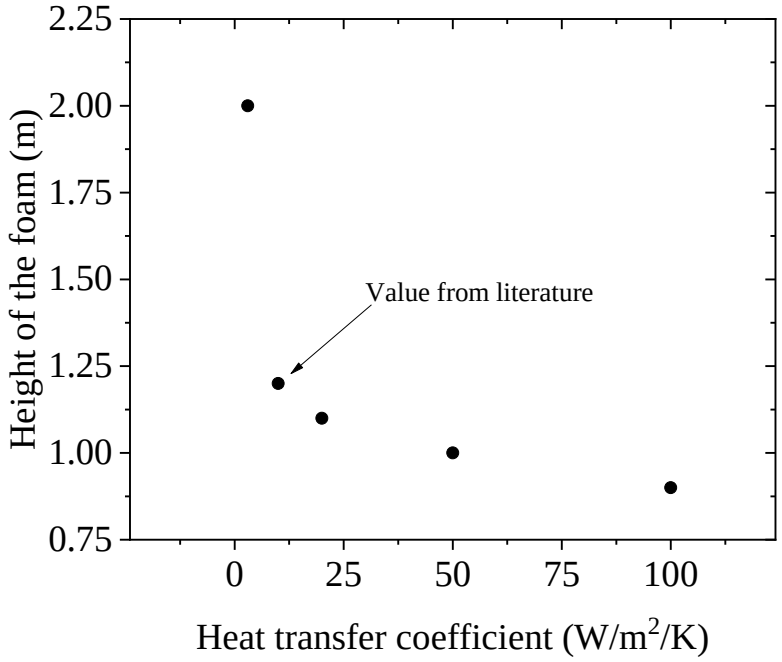

Figure 48: Effect of heat transfer coefficient on height of foam required

4.7 Summary

In summary, a simplified heat transfer model was developed to obtain the temperature profile through the vapor channels, to estimate the minimum height of the foam for the outgoing vapors to get dispersed in the atmosphere easily. CFD simulations were performed on ANSYS Fluent® to solve, continuity, momentum, energy equations along with turbulence models, based on some assumptions. The model was validated with experimental data for liquid nitrogen and a mesh independent solution was obtained. The model was then used for methane to predict the minimum height of the foam required. A sensitivity analysis for some of the important parameter values assumed was also carried out.

5 CONCLUSIONS AND FUTURE WORK*

5.1 Conclusions

High expansion (HEX) foam can not only help reduce the heat transfer to liquefied natural gas (LNG) through convection and radiation for reduced vaporization, but also heats up LNG vapor that passes through the foam layers, enabling ease of dispersal for risk mitigation. Foam also drains liquid over time, which can influence the vaporization of LNG. Therefore, it is crucial to have an experimental and theoretical study on stability of HEX foam used for LNG vapor risk mitigation.

In Section 1, a detailed introduction along with a comprehensive literature review on HEX foam application on LNG and related areas was provided.

*Parts of this section have been reprinted with permission from: "Improving the stability of HEX foam used for LNG vapor risk mitigation using exfoliated zirconium phosphate nanoplates", Krishnan, P., Al-Rabbat, A., Zhang, B., Huang, D., Zhang, L., Zeng, M., Mannan, M.S., Cheng, Z., 2019, Process Safety and Environmental Protection, 123, 48-58, Copyright 2019 by Krishnan *et al.* [5] and "Effects of forced convection and thermal radiation on HEX foam used for LNG vapor risk mitigation", Krishnan, P., Zhang, B., Al-Rabbat, A., Cheng Z., Mannan, M.S., Journal of Loss Prevention in Process Industries, 2018, 55, 423-436, Copyright 2018 by Krishnan *et al.* [6]

In Section 2, experiments studying the effects of forced convection and thermal radiation on foam breakage were carried out. A lab-scale foam generator was used to produce HEX foam and study foam breakage and liquid drainage with time. A mesh setup was used for measuring liquid drainage, a wind tunnel setup was used to study foam breakage in the presence of forced convection and a bulb-panel setup was used to study the effect of thermal radiation on foam breakage. It was found that both forced convection and thermal radiation can increase the foam breakage rates by nearly 3 and 5 times at a wind speed of 2.5 m/s and radiation intensity of 270 W/m^2 respectively when compared with the control. The rate at which liquid drains from the foam was also determined under different conditions of forced convection and thermal radiation. Experiments were also conducted in the presence of liquid nitrogen, to simulate a spill of LNG in a dike. Tests with liquid nitrogen show that the foam can help lower the vaporization rate of the cryogenic liquid. It was found that external factors such as forced convection and thermal radiation could affect the rate of foam breakage and should be accounted for while estimating the amount of foam that is applied over cryogenic liquid spills.

In Section 3, experiments were conducted to explore the effects of addition of exfoliated zirconium phosphate (ZrP) nanoplates to HEX foam to improve foam stability, in the presence of forced convection and thermal radiation using a similar setup. For all experiments, it was found that the exfoliated ZrP stabilized foam performed better than the HEX foam alone and had lower foam breakage rates. At higher values of liquid drainage rates (usually over 2 kg/hr), generally near the beginning of the experiment, vaporization rate of the cryogenic liquid was found to depend on the liquid drainage rate for HEX foam stabilized with exfoliated ZrP nanoplates. The temperature profiles under forced convection and thermal radiation with exfoliated ZrP stabilized

foam seem to exhibit similar behavior to experiments without ZrP, indicating that the foam properties for vapor dispersion are still present. The exfoliated ZrP stabilized foam may allow a longer time for foam stability, reducing the duration over which foam needs to be replenished while ensuring similar vapor risk mitigation.

In Section 4, a simple heat transfer model was developed to predict the amount of foam that needs to be applied. Computational fluid dynamics (CFD) was used to simulate the heat transfer from foam to the LNG vapors to predict the height of the foam required to effectively disperse the vapors by allowing the vapors to achieve enough heat transfer to reach a temperature above which they are lighter than air. The temperature profile through the foam was obtained experimentally and introduced as a boundary condition. The diameter of the vapor channel and the mass flow rate of the vapors were taken as values close to those observed experimentally. The heat transfer coefficient was taken from literature. By solving partial differential equations describing continuity, momentum and energy balance while considering turbulence, it was possible to obtain a solution under steady state. A mesh independent solution was obtained and was validated with results from experiments with liquid nitrogen. The model was rerun for methane and the temperature profile obtained was used to estimate the minimum height of the foam required. A sensitivity analysis on the parameters assumed was also performed to check how the solution varies if the variables change.

5.2 Future Work

Some ideas for the future work have been elucidated here:

In Section 2, the effect of salinity of foam solution as well as pH of the water on the stability of high expansion foam on a large lab-scale setup remains to be explored. In addition, the temperature of the water source could also influence the "warming effect" of foam.

In Section 3, for the study with nanoparticles, more experiments considering different characteristics such as concentration, size and aspect ratio of the nanoparticles will allow identifying optimum conditions for maximum foam stability. In addition, the economic feasibility of nanoparticle addition to high expansion foam remains to be explored. The chemicals used in the synthesis of the ZrP nanoplates may be expensive on a large scale and research efforts to identify alternatives such as clay particles could be a possible option. Another approach would be to identify which properties are most important in improving foam stability and designing nanomaterials with those properties.

In Section 4, There are some limitations to the heat transfer modeled developed in this work due to some assumptions made during model development. For a more robust model:

- Validation for different foam heights needed

  Temperature profile may vary for different heights. Therefore, experiments measuring the temperature profiles through the foam for different foam heights will enable the

validation of the model for varying foam heights and test whether the assumption of uniform temperature profile for different foam heights is valid.

- Interactions between vapor channels need to be accounted for

  We assume that the vapor channels are far enough that there is no interaction between them. However, this might not be the case. There may be non-homogenous temperature profiles through foam and the presence of two vapor channels in close proximity could alter the height of the foam required.

- Different channel geometries need to be studied

  We assume the channel geometry to be a vertical cylinder. However, this might not always be true. Therefore, variation in model geometries could be studied.

REFERENCES

[1] US EIA, Natural Gas Volumes, 2015.

[2] US EIA, International Energy Outlook 2017, 2017.

[3] US EIA, Annual Electric Generator Report, 2015.

[4] US EIA, Where Our Natural Gas Comes From, 2016.

[5] P. Krishnan, A. Al-Rabbat, B. Zhang, D. Huang, L. Zhang, M. Zeng, M.S. Mannan, Z. Cheng, Improving the stability of high expansion foam used for LNG vapor risk mitigation using exfoliated zirconium phosphate nanoplates, Process Safety and Environmental Protection, 123, 2019.

[6] P. Krishnan, B. Zhang, A. Al-Rabbat, Z. Cheng, M.S. Mannan, Effects of forced convection and thermal radiation on high expansion foam used for LNG vapor risk mitigation, Journal of Loss Prevention in the Process Industries, 55, 2018.

[7] J.L. Woodward, R. Pitblado, LNG risk based safety : modeling and consequence analysis. John L. Woodward and Robin M. Pitblado, [New York] : AIChE ; Hoboken, N.J. : Wiley, 2010.

[8] S. Mannan (Ed.), Liquefied Natural Gas, Lees' Loss Prevention in the Process Industries (Fourth Edition), Butterworth-Heinemann, Oxford, 2012.

[9] K. Takeno, T. Ichinose, K. Tokuda, R. Ohba, K. Yoshida, K. Ogura, Effects of high expansion foam dispersed onto leaked LNG on the atmospheric diffusion of vaporized gas, Journal of Loss Prevention in the Process Industries, 9, 1996.

[10] J.A. Suardin, The application of expansion foam on Liquefied Natural Gas (LNG) to suppress LNG vapor and LNG pool fire thermal radiation, Chemical Engineering, Texas A&M University, College Station, TX, 2008.

[11] S. Rathnayaka, F. Khan, P. Amyotte, Accident modeling approach for safety assessment in an LNG processing facility, Journal of Loss Prevention in the Process Industries, 25, 2012.

[12] United States National Institutes of Health, Haz-Map, 2017.

[13] S. Dan, C.J. Lee, J. Park, D. Shin, E.S. Yoon, Quantitative risk analysis of fire and explosion on the top-side LNG-liquefaction process of LNG-FPSO, Process Safety and Environmental Protection, 92, 2014.

[14] R.M. Pitblado, J. Baik, G.J. Hughes, C. Ferro, S.J. Shaw, Consequences of liquefied natural gas marine incidents, Process Safety Progress, 24, 2005.

[15] P.K. Raj, LNG fires: A review of experimental results, models and hazard prediction challenges, Journal of Hazardous Materials, 140, 2007.

[16] T. Kletz (Ed.), Chapter 8 - Liquefied Flammable Gases, What Went Wrong? (Fifth Edition), Butterworth-Heinemann, Boston, 2009.

[17] H.C. Hardee, D.O. Lee, W.B. Benedick, Thermal Hazard from LNG Fireballs, Combustion Science and Technology, 17, 1978.

[18] D.A. Crowl, J.F. Louvar, Chemical process safety : fundamentals with applications. 3rd ed., Upper Saddle River, NJ : Prentice Hall, 2011.

[19] Guidelines for vapor cloud explosion, pressure vessel burst, BLEVE, and flash fire hazards. 2nd ed, Hoboken, N.J. : Wiley, 2010.

[20] G.A. Melhem, H. Ozog, S. Saraf, C. Iomosaic, Understanding LNG Rapid Phase Transitions, Hydrocarbon Processing, 85, 2006.

[21] Y. Li, Z. Li, W. Wang, Simulating on rollover phenomenon in LNG storage tanks and determination of the rollover threshold, Journal of Loss Prevention in the Process Industries, 37, 2015.

[22] L. Hamutuk, History of accidents in the LNG industry, 2008.

[23] T. Powell, How industry and regulators kept public in the dark after 2014 LNG explosion in Washington, 2016.

[24] Department of Transportation, Cabrillo Port Liquefied Natural Gas Deepwater Port Final EIS, 2007.

[25] P. Weinberg, Cargo of Fire: A Call for Stricter Regulation of Liquefied Natural Gas Shipment and Storage, Fordham Urban Law Journal, 4, 1975.

[26] M.S. Mannan, H.H. West, K. Krishna, A.A. Aldeeb, N. Keren, S.R. Saraf, Y.-S. Liu, M. Gentile, The legacy of Bhopal: The impact over the last 20 years and future direction, Journal of Loss Prevention in the Process Industries, 18, 2005, 218-224.

[27] S. Romero, Algerian Explosion Stirs Foes of U.S. Gas Projects, The New York Times, 2004.

[28] J. Schneyer, T. Gardner, R. Valdmanis, Blast at U.S. LNG site casts spotlight on natural gas safety, Reuters, 2014.

[29] S. Anand, N. Keren, M.J. Tretter, Y. Wang, T.M. O'Connor, M.S. Mannan, Harnessing data mining to explore incident databases, Journal of Hazardous Materials, 130, 2006, 33-41.

[30] National Fire Protection Association, NFPA 11: Standard for Low, Medium and High-Expansion Foam, National Fire Protection Association, 2016.

[31] Chemguard, Vee Foam High-X, 2017.

[32] M.W. Conroy, J.C. Taylor, J.P. Farley, J.W. Fleming, R. Ananth, Liquid drainage from high-expansion (HiEx) aqueous foams during and after filling of a container, Colloids and Surfaces A: Physicochemical and Engineering Aspects, 426, 2013.

[33] J. Guevara, A. Mejia, M. Shuai, Y.-W. Chang, M.S. Mannan, Z. Cheng, Stabilization of Pickering foams by high-aspect-ratio nano-sheets, Soft Matter, 9, 2013.

[34] B. Zhang, Y. Liu, T. Olewski, L. Vechot, M.S. Mannan, Blanketing effect of expansion foam on liquefied natural gas (LNG) spillage pool, Journal of Hazardous Materials, 280, 2014.

[35] B. Zhang, B. Harding, Y. Liu, M.S. Mannan, Liquefied Natural Gas Vapor Hazard Mitigation with Expansion Foam Using a Research-Scale Foam Generator, Industrial & Engineering Chemistry Research, 55, 2016.

[36] Dow's chemical exposure index guide. 1st ed, New York, NY : American Institute of Chemical Engineers, 1994.

[37] V.M. Fthenakis, Prevention and Control of Accidental Releases of Hazardous Gases, Wiley, 1993.

[38] Y. Qiao, H.H. West, M.S. Mannan, D.W. Johnson, J.B. Cornwell, Assessment of the effects of release variables on the consequences of LNG spillage onto water using FERC models, Journal of Hazardous Materials, 130, 2006.

[39] R. Qi, P.K. Raj, M.S. Mannan, Underwater LNG release test findings: Experimental data and model results, Journal of Loss Prevention in the Process Industries, 24, 2011.

[40] O. Basha, T. Olewski, L. Véchot, M. Castier, S. Mannan, Modeling of pool spreading of LNG on land, Journal of Loss Prevention in the Process Industries, 30, 2014.

[41] N. Gopalaswami, R.A. Mentzer, M. Sam Mannan, Investigation of pool spreading and vaporization behavior in medium-scale LNG tests, Journal of Loss Prevention in the Process Industries, 35, 2015.

[42] T. Olewski, L. Vechot, S. Mannan, Study of the Vaporization Rate of Liquid Nitrogen by Small and Medium-Scale Experiments Chemical Engineering Transactions, 31, 2013.

[43] L. Véchot, T. Olewski, C. Osorio, O. Basha, Y. Liu, S. Mannan, Laboratory scale analysis of the influence of different heat transfer mechanisms on liquid nitrogen vaporization rate, Journal of Loss Prevention in the Process Industries, 26, 2013.

[44] N. Gopalaswami, L. Vechot, T. Olewski, M.S. Mannan, Small-scale experimental study of vaporization flux of liquid nitrogen released on ice, Journal of Loss Prevention in the Process Industries, 37, 2015.

[45] M. Ahammad, Y. Liu, T. Olewski, L.N. Véchot, M.S. Mannan, Application of Computational Fluid Dynamics in Simulating Film Boiling of Cryogens, Industrial & Engineering Chemistry Research, 55, 2016.

[46] D. Siuta, A.S. Markowski, M.S. Mannan, Uncertainty techniques in liquefied natural gas (LNG) dispersion calculations, Journal of Loss Prevention in the Process Industries, 26, 2013.

[47] R. Qi, D. Ng, B.R. Cormier, M.S. Mannan, Numerical simulations of LNG vapor dispersion in Brayton Fire Training Field tests with ANSYS CFX, Journal of Hazardous Materials, 183, 2010.

[48] B.R. Cormier, R. Qi, G. Yun, Y. Zhang, M. Sam Mannan, Application of computational fluid dynamics for LNG vapor dispersion modeling: A study of key parameters, Journal of Loss Prevention in the Process Industries, 22, 2009.

[49] G. Yun, D. Ng, M.S. Mannan, Key Observations of Liquefied Natural Gas Vapor Dispersion Field Test with Expansion Foam Application, Industrial & Engineering Chemistry Research, 50, 2011.

[50] R.E.R. Vasquez, Study of the effects of obstacles in liquefied natural gas (LNG) vapor dispersion using CFD modeling, Safety Engineering, Texas A&M University, College Station,TX, 2012.

[51] G. Yun, D. Ng, M.S. Mannan, Key Findings of Liquefied Natural Gas Pool Fire Outdoor Tests with Expansion Foam Application, Industrial & Engineering Chemistry Research, 50, 2011.

[52] L.C.H. Gomez, Experiments for the measurement of LNG mass burning rates, in: Chemical Engineering, Texas A&M University, College Station, TX, 2011.

[53] J.A. Suardin, Y. Wang, M. Willson, M.S. Mannan, Field experiments on high expansion (HEX) foam application for controlling LNG pool fire, Journal of Hazardous Materials, 165, 2009.

[54] J.A. Suardin, R. Qi, B.R. Cormier, M. Rana, Y. Zhang, M.S. Mannan, Application of fire suppression materials on suppression of LNG pool fires, Journal of Loss Prevention in the Process Industries, 24, 2011.

[55] M.A. Rana, Y. Guo, M.S. Mannan, Use of water spray curtain to disperse LNG vapor clouds, Journal of Loss Prevention in the Process Industries, 23, 2010.

[56] M.A. Rana, Forced dispersion of Liquefied Natural Gas vapor clouds with water spray curtain application, Chemical Engineering, Texas A&M University, College Station, TX, 2009.

[57] M.A. Rana, B.R. Cormier, J.A. Suardin, Y. Zhang, M.S. Mannan, Experimental study of effective water spray curtain application in dispersing liquefied natural gas vapor clouds, Process Safety Progress, 27, 2008.

[58] G. Yun, W.J. Rogers, M.S. Mannan, Risk assessment of LNG importation terminals using the Bayesian–LOPA methodology, Journal of Loss Prevention in the Process Industries, 22, 2009.

[59] B. Islam, Risk Management Strategy for Road Transportation of LNG, Safety Engineering, Texas A&M University, College Station, TX, 2015.

[60] G. Lamus, Comparative Analysis Between LNG Import and Export Terminals, Safety Engineering Texas A&M University, College Station, TX, 2016.

[61] H.R. Wesson, J.R. Welker, L.E.Brown, Control LNG spill fires, Hydrocarbon Processing, 51, 1972.

[62] K. Zuber, LNG Facilities - Engineered Fire Protection Systems, 79th Annual Meeting of the National Fire Protection Association, Chicago, IL, 1975.

[63] S.M. Mitchell, M.S. Mannan, Designing Resilient Engineered Systems, Chemical Engineering Progress, 2006.

[64] G.W. Yun, Control of vapor dispersion and pool fire of Liquefied Natural Gas (LNG) with expansion foam, Chemical Engineering Texas A&M University, College Station, TX, 2010.

[65] B. Harding, B. Zhang, H. Chen, S. Mannan, Improved research-scale foam generator design and performance characterization, 39, 2015.

[66] B.Z. Harding, B. Zhang, H. Chen, M.S. Mannan, Efficacy of decontamination foam on a non-polar hazardous chemical surrogate, Journal of Loss Prevention in the Process Industries, 43, 2016.

[67] C. Ye, M. Hua, X. Pan, B. He, J. Jiang, Development of heat transfer and evaporation model of LNG covered by Hi-Ex foam, Journal of Loss Prevention in the Process Industries, 44, 2016.

[68] J. Yang, Y. Li, J. Zhu, H. Han, Quantitative study of the factors of LNG liquid foam stability: Operating parameters and collection containers and time, Process Safety and Environmental Protection, 117, 2018.

[69] P. Walstra, Principles of Foam Formation and Stability, Foams: Physics, Chemistry and Structure, Springer London, 1989.

[70] P. Stevenson, Foam Engineering: Fundamentals and Applications, Wiley, 2012.

[71] L. Zhang, LNG suppression foam stabilized by Zirconium Phosphate, Chemical Engineering, Texas A&M University, College Station, TX, 2015.

[72] R.J. Pugh, Bubble and Foam Chemistry, Cambridge University Press, 2016.

[73] V. Carrier, A. Colin, Coalescence in Draining Foams, Langmuir, 19, 2003.

[74] X. Li, S.I. Karakashev, G.M. Evans, P. Stevenson, Effect of Environmental Humidity on Static Foam Stability, Langmuir, 28, 2012.

[75] B.P. Binks, T.S. Horozov, Aqueous Foams Stabilized Solely by Silica Nanoparticles, Angewandte Chemie International Edition, 44, 2005.

[76] S. Zhang, D. Sun, X. Dong, C. Li, J. Xu, Aqueous foams stabilized with particles and nonionic surfactants, Colloids and Surfaces A: Physicochemical and Engineering Aspects, 324, 2008.

[77] P. Armento, M. Casciola, M. Pica, F. Marmottini, R. Palombari, F. Ziarelli, Silica–zirconium phosphate–phosphoric acid composites: preparation, proton conductivity and use in gas sensors, Solid State Ionics, 166, 2004.

[78] F. Bauer, M. Willert-Porada, Comparison between Nafion® and a Nafion® Zirconium Phosphate Nano-Composite in Fuel Cell Applications, Fuel Cells, 6, 2006.

[79] X. He, H. Xiao, H. Choi, A. Díaz, B. Mosby, A. Clearfield, H. Liang, α-Zirconium phosphate nanoplatelets as lubricant additives, Colloids and Surfaces A: Physicochemical and Engineering Aspects, 452, 2014.

[80] N. Wang, Flame Retardancy of Polymer Nanocomposites based on Layered Aluminum Phosphate and Computational Study of Intercalation of Amines into α-Zirconium Phosphate and Adsorption of a Model Organic Pollutant, Milwaukee, WI, Marquette University, 2011.

[81] X. Wang, D. Zhao, I.B.N. Medina, A. Diaz, H. Wang, A. Clearfield, M.S. Mannan, Z. Cheng, Surface modification of layered zirconium phosphate with PNIPAM, Chemical Communications, 52, 2016.

[82] R.D. Mehta, P. Bradshaw, Design rules for small low speed wind tunnels, The Aeronautical Journal, 83, 1968.

[83] U. Setzmann, W. Wagner, A New Equation of State and Tables of Thermodynamic Properties for Methane Covering the Range from the Melting Line to 625 K at Pressures up to 1000 MPa, in in NIST Chemistry WebBook, NIST Standard Reference Database Number 69, J. Phys. Chem. Ref. Data, 20, 1991.

[84] M. Zeng, P. Wang, J. Luo, B. Peng, B. Ding, L. Zhang, L. Wang, D. Huang, I. Echols, E. Abo Deeb, E. Bordovsky, C.-H. Choi, C. Ybanez, P. Meras, E. Situ, M.S. Mannan, Z. Cheng, Hierarchical, Self-Healing and Superhydrophobic Zirconium Phosphate Hybrid Membrane Based on the Interfacial Crystal Growth of Lyotropic Two-Dimensional Nanoplatelets, ACS Appl Mater Inter, 10, 2018.

[85] M. Zeng, S.A. Shah, D. Huang, D. Parviz, Y.-H. Yu, X. Wang, M.J. Green, Z. Cheng, Aqueous Exfoliation of Graphite into Graphene Assisted by Sulfonyl Graphene Quantum Dots for Photonic Crystal Applications, ACS Applied Materials and Interfaces, 9, 2017.

[86] S.A. Magrabi, B.Z. Dlugogorski, G.J. Jameson, The Performance of Aged Aqueous Foams for Mitigation of Thermal Radiation, Developments in Chemical Engineering and Mineral Processing, 8, 2000.